学位申請論文

磯部博志

主論文

EVOLUTION OF THE HED (howardite-eucrite-diogenite) PARENT BODY
-PARTIAL MELT EXPERIMENTS ON DIFFERENTIATION PROCESSES-

Hiroshi ISOBE

Department of Environmental Safety Research
Japan Atomic Energy Research Institute
Tokai, Ibaraki, 319-11, JAPAN

CONTENTS

Abstract

Three series of melting experiments with a chondritic material, a eucrite-diogenite mixture, and a eucritic material were carried out using a one atmosphere gas mixing furnace to illustrate liquidus phase relation and chemical compositions of the phases. Locations of an olivine control line, olivine-pyroxene phase boundary and olivine-pyroxene-plagioclase peritectic point in the 'pseudo-liquidus' diagrams of the system silica-olivine-anorthite (SiO_2-Ol-An) and silica-forsterite-fayalite (SiO_2-Fo-Fa) were determined. Based on the melting relations and the chemical compositions of crystals and melts obtained in the experiments, it is revealed that a eucrite-diogenite-pallasite parent body evolved from the chondritic material by two successive stages of solid-liquid separations; the first stage is the separation between pallasite and its coexisting melt with the composition of eucrite-diogenite mixture in equilibrium at around 1400°C, and the second is that between diogenite and its coexisting melt with the composition of eucrite in equilibrium at around 1200°C in the eucrite-diogenite mixture portion. Maximum fractionation processes in both stages are excluded, because the association of eucrite-diogenite-pallasite cannot be explained without a significant change of redox conditions in the interior of the parent body.

Density difference between crystals and its coexisting melt and viscosity of the melt in the temperature range of the two stages of the solid-liquid separations were calculated using the experimental data. Then, sinking velocity of crystals and effective velocity of natural convection in magma oceans on the parent body were calculated. It is suggested from the calculations that the first stage fractionation took place by partial melting of the chondritic material. The coexistence of olivine and Fe-Ni metal in pallasite cannot be explain by crystallization.

The second stage can be explained by the separation of diogenitic solid as a cumulate in a magma ocean of the first stage melt. Diogenitic pyroxene is considered to be suspended by natural convection in the magma ocean before the separation at 1200°C.

1 Introduction

Evolution history of the planets in the solar system such as the Earth is one of major themes of the planetary science. The Earth has a complex history and its evolution is still proceeding. Since no Earth's materials have the age of the beginning of the solar system and since only the evolved materials in the crust and upper mantle of the Earth can be obtained, it has been limited to study the evolution at the earliest stage of the history of the Earth from the view point of material sciences.

On the other hand, meteorites has been considered to be fragments of asteroids, and varieties of the meteorites inherited heterogeneity in and among their parent bodies. Since most of the meteorites have the age of the birth of the solar system, the meteorites give an information of the evolution of the early solar system.

Chondrites among meteorites preserve similar composition to the solar abundance except for volatile elements, and are considered to the material that represents the composition of the solar system. Then, their parent bodies have been considered to experience no differentiation in a planetary scale.

If differentiation activities occurred on the parent body which has chondritic bulk composition, homogeneity in the parent body must be lost and compositions of any part of the parent body altered from the chondritic composition. Differentiated meteorites have the chemical composition far from the solar abundance. Achondrites among the differentiated meteorites have been considered to be rocks formed by an igneous process and assigned to layers in their parent bodies. The parent bodies of some achondrites have been assigned to some of

asteroids in the solar system (e.g. Gaffey and McCord, 1977). Evolutional activities in the parent bodies of achondrites went on only in the early history of the solar system, because achondrites have the age of the early solar system. Therefore, achondrites will give an information on igneous process like the formation of a magma ocean on the planets in the early solar system.

The most established association of achondrites is that of eucrite (a pigeonite-plagioclase achondrite), diogenite (an almost wholly orthopyroxene achondrite), and howardite (a polymict breccia of eucrite and diogenite, see Appendix 1). These three achondrites are called as HED meteorites by using their first letters. This association was constructed based on the fact that howardite can be explained as the mixture of brecciated eucrite and diogenite (e.g. McCarthy *et al.*, 1972, 1973). Furthermore, the association is also supported by the fact that these three meteorites are on one fractionation line in a three isotope plot of oxygen (e.g. Clayton *et al.*, 1976, Clayton and Mayeda, 1978). These HED meteorites have been considered to originate from one parent body. And then, the parent body is assigned to asteroid Vesta, based on the similarity of reflectance spectra of Vesta and HED meteorites (e.g. McCord and Gaffey, 1974).

Two kinds of stony-iron meteorites are also assigned to the parent body of HED meteorites. One is mesosiderite, which is similar to howardites and has been interpreted as the mixture of howarditic silicates and Fe-Ni metal formed by collisions of HED parent body with iron asteroids (e.g. Floran, 1978). Another type of the stony-iron meteorites is pallasite, which consists only of olivine and Fe-Ni metal (see Appendix 1). Origin of pallasite has been discussed in relation to the formation of HED meteorites as described below.

[Models for origin of HED meteorites]

On the origin of HED meteorites and the evolution of the parent body, Mason (1967) first proposed a model. He treated pallasite as one of the members of the HED association based on the assumption that the bulk composition of the parent body is chondritic, because the average composition of HED meteorites is significantly depleted in Mg and concentrated in Si, Al and Ca, compared with that of CI chondrites. Then, he assigned eucrite, diogenite and pallasite to three layers in the parent body (Figure 1-1). Since the parent body by Mason includes pallasite other than HED meteorites, it will be called a HED meteorite-pallasite parent body (HEDP-PB) hereafter. Mason's assumption that pallasite is a member of the parent body of HED meteorites is supported by a subsequent study where pallasite is plotted on the fractionation line of HED meteorites in the three isotope plot of oxygen (Clayton and Mayeda, 1978).

Radius of Mason's HEDP-PB was estimated to be about 300km based on the assumption that the exsolution texture of Fe-Ni metal in pallasite was formed during the cooling of the core of HEDP-PB. Mason first suggested a fractional crystallization process to form these igneous rocks in HEDP-PB, with no detailed discussion. In his model, howardites were also considered to be a product of the fractional crystallization process.

Mason pointed out that Mg/Fe ratio of his HEDP-PB calculated as that of the mixture of HED meteorites and pallasite became similar to that of H chondrites. However, alkali content of his HEDP-PB was depleted and sulfur was almost lacking from the chondrite composition. He noted that the consistencies of this model with chondritic material far

outweigh the inconsistency in sodium content.

On the basis of the HEDP-PB model by Mason (1967) (Figure 1-1), Dreibus and Wänke (1980) estimated the bulk composition of HEDP-PB from new data of the chemical compositions of HED meteorites and pallasites (Table 1-1). In their calculation, the ratio of eucrite and diogenite in HEDP-PB was decided to be similar to Al/Sc ratio in a CI chondrite (Orgueil). Then, in order to set the bulk major composition equal to that of the CI chondrite, they added pallasitic olivine to the eucrite-diogenite mixture. Metal/silicate ratio of the bulk composition and Mg/Fe ratio of the silicate portion were decided from Mn/Fe and W/La ratios of HED meteorites and pallasites. Then, Mg# (100·MgO/(MgO+FeO) in mol%) of the silicate portion of their HEDP-PB became 79, which is close to those of H chondrites.

Ringwood (1989) preferred Mason's model, but suggested that the Mg/Si atomic ratio of the parent body should be similar to 1.27 of the Earth's upper mantle, rather than 1.05 of a chondritic composition. However, his argument is considered to come only from his misreading of Mg# of the bulk composition of HEDP-PB in the paper by Dreibus and Wänke (1980). He noted that Dreibus and Wänke (1980) showed that the Mg# of HEDP-PB was 83-85 (p5, Ringwood, 1989). This value is not in agreement with Mg#79, the result of Dreibus and Wänke (1980).

After about a decade from the proposal of HEDP-PB by Mason (1967), Stolper (1975, 1977) first carried out melting experiments of natural eucrites to clarify igneous process in the formation of eucrite. The experimental results show that the bulk compositions of noncumulate eucrites, which is considered to represent eucrite magma itself, are close to the Ol-Px-Pl peritectic point of the system of SiO_2-Ol-An. He pointed out that the melt of the peritectic point cannot be generated by

fractional crystallization. He also thought that chemical equilibrium among phases during crystallization in a natural igneous process is hardly achieved. Then, he suggested that the eucritic melt is a primary magma by a partial melting of the source region which consists of olivine, pyroxene, plagioclase, chromite and metallic iron. Cumulate eucrites and diogenites as well as variation among noncumulate eucrites were explained by variation in degrees of partial melting and the following fractional crystallization processes.

On the basis of the Stolper's model, Consolmagno and Drake (1977), Hertogen *et al.* (1977), Morgan *et al.* (1978) and Jones (1984) estimated the bulk composition of the parent body for eucritic magma using partitioning of minor and trace elements (Table 1-1). These compositions are fundamentally chondritic in major and minor elements. However, Mg# of 65-70 of the compositions is significantly lower than that of 79 in the HEDP-PB model (Dreibus and Wänke, 1980).

Ikeda and Takeda (1985) studied details of lithic clasts and mineral fragments in an Antarctic howardite, Y-7308. They proposed a model on the evolutional process of magma ocean on the parent body, where primary magma in the ocean was produced under reducing condition by partial or batch melting of a carbonaceous or LL chondritic material. Then, fractional crystallization of the primary magma took place more or less in an open system. This fractionation process was introduced in this model to explain the continuum of chemical composition of minerals in lithic clasts and fragments. In this model, a dunite layer as the cumulates with the composition different from pallasitic olivine is produced. Then, the parent body is not HEDP-PB, and will be called a HED meteorites - dunite parent body (HEDD-PB).

Hewins and Newsom (1988) pointed out that the Ol-Px phase

boundary in the system of SiO_2-Ol-An can shift toward Ol side as pressure becomes high, and then it changes from a reaction to cotectic lines. They suggested a possibility that even a maximum fractionation process can generate the eucritic magma on the Ol-Px-An peritectic point by assuming a 'small' pressure drop of 1kb, rather than the equilibrium process in Stolper's model.

Ikeda (1989) modified the model by Ikeda and Takeda (1985) with the bulk composition of the parent body given by Dreibus and Wänke (1980). In the formation process of diogenite and eucrites from the fractionated magma, he suggested a chemical equilibrium process rather than maximum fractionation in the model of Ikeda and Takeda (1985), because the bulk compositions of eucrites are around the peritectic point of Ol-Px-An as pointed out by Stolper (1977).

Several different models have been proposed on the igneous process in the parent body of HED meteorites as mentioned above. One of the reasons why the process was not well-understood is the lack of the knowledge on the phase relations among crystals and coexisting melt phase and their chemical compositions in the system of a chondritic material and the related systems. Only partial melting experiments of natural eucrites have been carried out in the relation to the generation of HED meteorites by Stolper (1977).

As for the phase relation of a chondritic material, Seitz and Kushiro (1974) and Takahashi (1983) conducted melting experiments under one atmosphere to high pressures for application to the evolution of the Earth's mantle. However, their experiments were not concerned with compositional changes of melt and mineral phases. Furthermore, the phase relation at high pressure is not applicable to the study of the

evolution of the HED parent body, because mineral assemblages at high pressure is not observed in HED meteorites and pallasites.

Longhi and Pan (1988) conducted melting experiments of low-alkali basaltic materials at the atmospheric pressure for application to lunar petrogenesis. They illustrated phase boundaries in the system of SiO_2–Ol–An, as a function of Mg/Fe ratio and wollastonite component of the melt. The starting material of their experiments is not similar to chondritic material. Thus, their phase diagram can not also be applied directly to the igneous process in the HED parent body. Consequently, for quantitative discussion of the igneous process in the HED parent body, it is necessary to carry out melting experiments to determine the phase relation and compositional changes of melt and minerals in the system of a chondritic material at normal pressure.

[The present study and its assumptions]

In the present study, partial melting experiments of a chondritic and its related materials were conducted using a one atmosphere gas mixing furnace. Since melting relation of a chondritic material should be explained in a multi component system, the experiments must be carried out on various starting materials with different bulk compositions. However, a small number of the experiments is enough to study the igneous process, if a model on the evolution of the HED parent body is established. Therefore, a working hypothesis was first constructed, and then, three experimental systems were chosen according to it. This working hypothesis will be reexamined after the experiments.

In the working hypothesis, we adopt that the parent body of HED meteorites should include pallasite in HEDP-PB model or dunite (+metallic iron) in HEDD-PB model for the body to have a chondritic composition.

And then, we try to reconstruct the evolution processes of the HEDP-PB from a chondritic material. We prefer the HEDP-PB model rather than the HEDD-PB model simply because we have pallasite samples but there are no samples of dunite meteorite except fragments in a few howardite.

In order to study the igneous process in the parent body, three kinds of igneous rocks, eucrite, diogenite and one of the olivine-bearing rocks (pallasite or dunite), should at least be taken into considerations. Then, solid-liquid separation to produce three kinds of the igneous rocks must occur at least in two distinct stages.

At the first stage of the solid-liquid separation, there are three cases to produce one of the three meteorites as shown in Figure 1-2 (case A: pallasite, case B: diogenite, case C: eucrite). Among these three cases, we adopted the case A as the working hypothesis, simply because olivine in pallasite has the largest Mg#. The sequence of the formation of the meteorites in the case A is essentially the same as those in the models by Mason (1967), Ikeda and Takeda (1985) and Ikeda (1989). According to the sequence of case A, the bulk compositions of starting materials in three series of the experiments are chosen to be a chondritic material, a mixture of diogenite and eucrite, and a eucritic material. The details of the compositions will be given in the following chapter.

Solid-liquid separation by igneous activities is strongly affected by gravity. Therefore, gravitational separation should be taken into considerations in discussions on igneous processes on planets, as well as melting relation. Role of the gravitational separation in the evolution of the HED parent body has not been estimated, except for a few calculations of density difference between crystals and liquid in a

magma ocean (e.g. Ikeda, 1989). Solid-liquid separation process by partial melting must be controlled mainly by density difference between crystals and partial melt, and viscosity of melt, as well as degree of the partial melting. On the other hand, in a case of solid-liquid separation by crystallization, the process should be discussed based on data of sinking velocities of crystals and effective velocity of natural convection in a magma ocean. In the present study, physical parameters to describe an effect of gravity to the solid-liquid separation on HEDP-PB were calculated using the results of the partial melting experiments.

Based on the phase relations obtained by the partial melting experiments and the effect of gravity to the solid-liquid separation, a new model on the evolution of HEDP-PB will be constructed.

Table 1-1 Compositions of the HED-pallasite parent body and eucrite parent body models (Wt.% and Mol%).

Weight Fractions

	Jones	Morgan	Hertogen	C & D	Stolper	D & W
Na_2O	0.11	0.05	0.05	0.04	0.03	0.11
MgO	27.7	28.5	29.5	29.7	27.9	31.5
Al_2O_3	3.2	2.5	2.4	1.8	1.8	3.27
SiO_2	40.3	39.8	41.4	39	42.6	46.2
K_2O	0.01	0.004	0.004	0	0	0.0092
CaO	2.6	2.1	2.0	1.2	1.7	2.57
TiO_2	0.16	0.1	0.12	0	0	0.16
Cr_2O_3	0.34	0	0.5	0	0	0.87
MnO	0.63	0	0.46	0	0	0.42
FeO	25.2	26.6	24.2	28.3	26	14.8
Total	100.3	99.7	100.6	100.0	100.0	99.9

Mol Fractions

Na_2O	0.10	0.04	0.04	0.04	0.03	0.10
MgO	38.15	39.20	40.01	40.50	38.21	42.25
Al_2O_3	1.74	1.36	1.29	0.97	0.97	1.73
SiO_2	37.23	36.72	37.67	35.67	39.14	41.57
K_2O	0.01	0.00	0.00	0.00	0.00	0.01
CaO	2.57	2.08	1.95	1.18	1.67	2.48
TiO_2	0.11	0.07	0.08	0.00	0.00	0.11
Cr_2O_3	0.12	0.00	0.18	0.00	0.00	0.31
MnO	0.49	0.00	0.35	0.00	0.00	0.32
FeO	19.47	20.53	18.42	21.65	19.98	11.14
Mg#	66.21	65.63	68.48	65.16	65.67	79.14

Jones: Jones (1984), Morgan: Morgan *et al.*, (1977), Hertogen: Hertogen *et al.*, (1977), C & D: Consolmagno and Drake (1977), Stolper: Stolper (1977) from Dodd (1981), D & W: Dreibus and Wänke (1980)

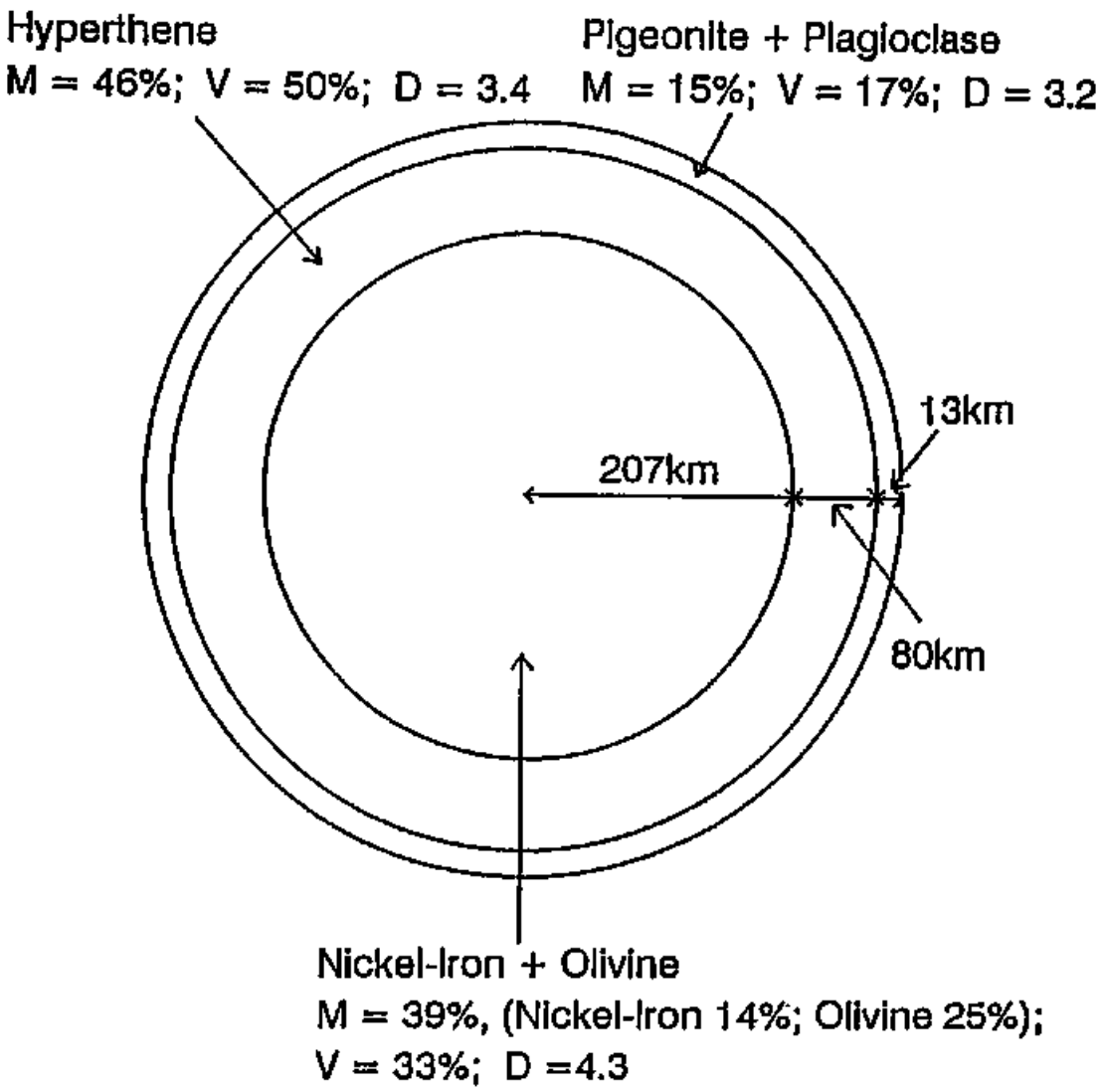

Figure 1-1
A model of a pallasite-diogenite-eucrite parent body by Mason (1967). Volume and mass fraction of each layer are calculated based on the bulk composition data of HED meteorites at that time.

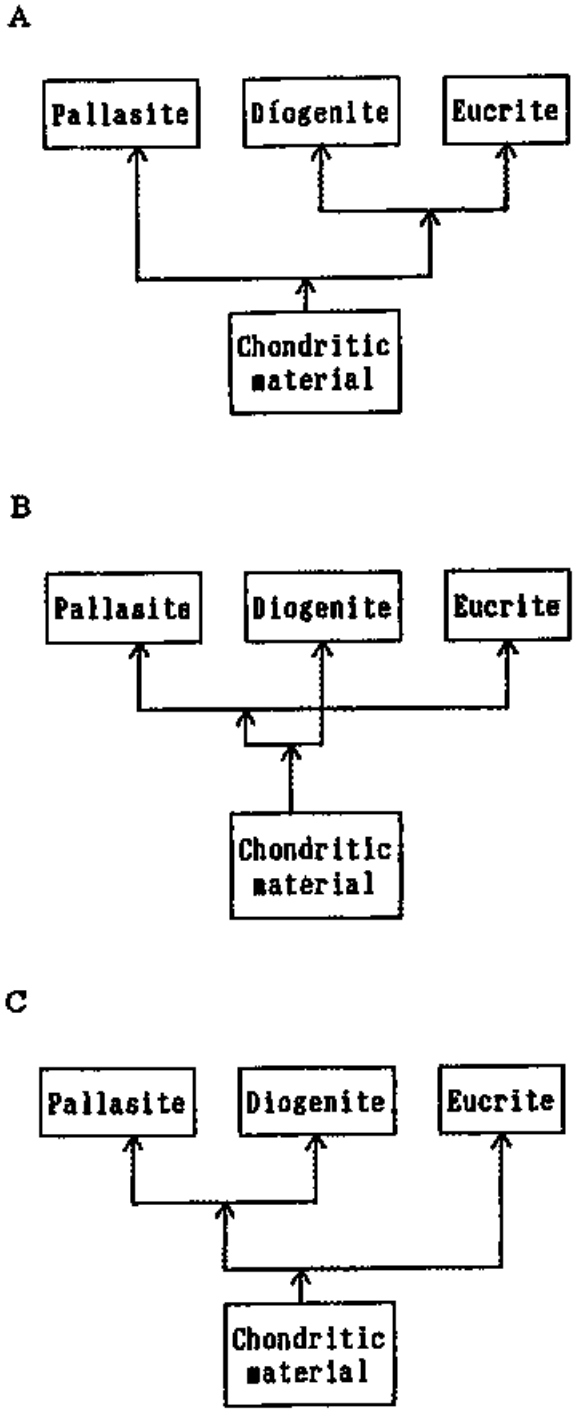

Figure 1-2
Schematic flow diagrams of formation processes of pallasite, diogenite and eucrite from a chondritic material. The three kinds of rocks should be formed through at least two steps. Then, there are three different assortments.

2 Experiments — starting materials and procedures

2-1 Composition of the starting materials

As described in Chapter 1, three series of partial melting experiments with different starting materials were conducted. These three series with a chondritic material, a eucrite-diogenite mixture and a eucritic material are called CH, ED and EU experiments, respectively.

A chondritic material was used as a starting material because the bulk composition of HEDP-PB is assumed to be basically chondritic. The bulk composition of the starting material adopted here is given in Table 2-1, with the solar abundance and the bulk composition of HEDP-PB by Dreibus and Wänke (1980). The present composition was determined by the following three processes. First, ten major cation elements with the ratios of the solar abundance (Matsui, 1979) were taken into consideration. The bulk composition of HEDP-PB proposed by Dreibus and Wänke (1980) was not adopted here, because their composition was calculated based on the composition of a specific CI meteorite rather than the solar abundance.

Second, metallic iron and iron sulfide phases were removed to represent the silicate portion of the bulk composition of HEDP-PB. The FeO content was determined as Mg# of about 79, according to that of the silicate portion of HEDP-PB of Dreibus and Wänke (1980). This value is similar to those of H-group chondrites. Metallic phase is present more or less in HED meteorites and pallasite and may affect equilibrium in the silicate portion with the condition of oxygen fugacity. However, the present experiments without metallic iron can be essentially applied to discussions on the formation of HED and related meteorites, as long as elements participating redox reaction, such as oxygen, are closed in

a system concerned. In fact, this condition would be held in HEDP-PB.

Sulfur content of HED and the related meteorites are much less than that of chondrites. The reason why the sulfur contents of the differentiated meteorites are depleted from the chondritic composition is still obscure. In the present study, sulfur was omitted from the starting material, simply because of the depletion, in addition to difficulty of the experiments with sulfur phases.

Third, the contents of Na_2O and K_2O were chosen as 0.14 and 0.01 wt.%, respectively, which are less than those of the solar abundance to represent the depletion of these elements in HEDP-PB.

The second series of the experiments (ED experiments) were conducted to elucidate a differentiation process of eucrites and diogenites. The chemical composition of the starting material of the ED experiments was determined to be that of the mixture of average diogenite (55 wt.%) and average noncumulate eucrite (45 wt.%) (Dodd, 1981), based on the results of CH experiments. The bulk composition of the starting material in ED experiments is given in Table 2-2, with the average compositions of diogenites and noncumulate eucrites (Dodd, 1981).

The third series of the melting experiments (EU experiments) were done to investigate a crystallization path of a eucritic magma. Therefore, the chemical composition of the starting material was chosen to represent typical noncumulate eucrites (Table 2-2).

Melt fraction of run products decrease with the temperature of the partial melt experiments decreasing. It is difficult to analyze melt composition of small area without affects of surrounding crystals. To obtain accurate composition of the partial melts, fraction of melts must

be as large as possible. Consequently, partial melt experiments of modified materials of CH and ED starting materials were also carried out (CH-HM and ED-HM, High Melt fraction). Composition of starting materials (Table 2-3) were determined from the results of CH and ED experiments to melt 70% of the starting material and to be 30% of olivine or olivine + pyroxene.

Table 2-1 Compositions (wt. %) of the starting material of the melting experiments of a chondritic material (CH), the solar abundance (Matsui, 1979), solar abundance with Mg/(Mg+Fe) mol ratio of 0.79 and the eucrite parent body (HEDP-PB) by Dreibus and Wänke (1980). The solar abundance of elements is recalculated as oxides. Metallic iron and iron sulfides are excluded from the system in the experiments (see the text for more details). C.I.P.W. norms are calculated for the compositions except for the solar abundance. An and Or are anorthite and orthoclase components in plagioclase (mol %), respectively.

	Solar Abundance	Solar abun. (Metal free)	CH	HEDP-PB
Na_2O	1.03	1.36	0.14	0.11
MgO	23.85	31.47	31.90	31.5
Al_2O_3	2.41	3.18	3.23	3.27
SiO_2	33.86	44.68	45.29	46.2
K_2O	0.10	0.13	0.01	0.0092
CaO	2.23	2.94	2.98	2.57
TiO_2	0.11	0.14	0.14	0.16
Cr_2O_3	0.53	0.70	0.70	0.87
MnO	0.37	0.49	0.49	0.42
FeO	35.52	14.91	15.11	14.8
Total	100	100	100	99.91
Mg	54	79	79	79
Fe		24.84*		
Ni		2.04*		
C.I.P.W. Norm				
ilmenite		0.3	0.3	0.3
chromite		1.1	1.1	1.3
plagioclase		14.3 ($An_{15}Or_4$)	9.5 ($An_{88}Or_1$)	9.5 ($An_{88}Or_1$)
diopside		9.8	5.1	3.6
hypersthene		6.3	31.5	38.4
olivine		68.2	52.7	47.0

*These are weight ratios of the elements subtracted from the solar abundance. The values are ratios to the total weight of silicate portion as 100.

Table 2-2 Compositions (wt. %) of the starting materials of ED and EU experiments, average diogenite, average noncumulate eucrite (Dodd, 1981). Composition of ED starting material is the mixture of 55 wt.% of average diogenite and 45 wt.% of average noncumulate eucrite.

	Average Diogenite	ED	Average Noncum. Eucrite	EU
Na_2O	0.05	0.25	0.50	0.5
MgO	26.71	17.99	7.20	7.3
Al_2O_3	0.81	6.12	12.58	12.5
SiO_2	52.82	51.17	48.86	50.0
K_2O	0.00	0.02	0.04	0.1
CaO	0.94	5.17	10.33	10.4
TiO_2	0.07	0.35	0.70	0.7
Cr_2O_3	1.48	0.97	0.34	0.2
MnO	0.53	0.54	0.55	0.5
FeO	16.24	17.41	18.75	17.7
Total	99.65	100	99.85	100
Mg#	75	65	41	42
C.I.P.W. Norm				
ilmenite	0.1	0.7	1.3	1.3
chromite	2.2	1.4	0.5	0.3
plagioclase	2.4 ($An_{83}Or_0$)	17.8 ($An_{88}Or_1$)	36.4 ($An_{88}Or_1$)	36.4 ($An_{87}Or_2$)
quartz			1.6	3.2
diopside	2.2	8.3	16.3	16.9
hypersthene	87.2	70.6	43.7	41.8
olivine	5.6	1.3		

Table 2-3 Compositions of starting materials (Wt.%) and temperature (°C) of HM experiments. Starting material for ED-2HM to ED-6HM is same to that of ED experiments (Table 2-2).

No.	CH-7HM	CH-8HM	CH-9HM	CH-11HM	CH-12HM	CH-13HM
T(°C)	1450	1430	1410	1380	1350	1330
Na_2O	0.1	0.1	0.1	0.1	0.1	0.1
MgO	28.4	27.8	27.0	25.8	24.9	21.9
Al_2O_3	3.7	4.0	4.2	4.6	4.8	5.3
SiO_2	46.7	47.0	47.3	48.2	49.0	51.2
CaO	3.7	3.8	4.0	4.4	4.6	5.1
TiO_2	0.1	0.1	0.2	0.2	0.2	0.3
Cr_2O_3	0.6	0.6	0.5	0.5	0.4	0.3
MnO	0.5	0.4	0.4	0.4	0.4	0.4
FeO	16.2	16.2	16.3	15.9	15.6	15.2
Total	100.0	100.0	100.0	100.0	100.0	100.0

No.	CH-14HM	CH-15HM	CH-16HM	CH-17HM
T(°C)	1300	1280	1250	1200
Na_2O	0.1	0.3	0.3	0.3
MgO	20.9	19.9	19.2	17.6
Al_2O_3	6.2	6.8	8.0	9.6
SiO_2	51.2	51.0	50.4	50.2
CaO	5.9	6.4	7.0	8.0
TiO_2	0.3	0.3	0.3	0.3
Cr_2O_3	0.3	0.2	0.1	0.0
MnO	0.4	0.3	0.3	0.3
FeO	14.8	14.7	14.4	13.5
Total	100.0	100.0	100.0	100.0

No.	ED-7HM	ED-8HM	ED-9HM	ED-10HM
T(°C)	1250	1220	1200	1180
Na_2O	0.4	0.4	0.4	0.4
MgO	16.7	15.9	14.9	14.4
Al_2O_3	7.1	7.6	8.4	8.8
SiO_2	49.3	49.6	49.3	49.0
CaO	6.3	6.9	7.2	7.6
TiO_2	0.4	0.4	0.4	0.5
Cr_2O_3	0.0	0.1	0.1	0.1
MnO	0.4	0.4	0.4	0.4
FeO	19.5	18.8	19.0	18.9
Total	100.0	100.0	100.0	100.0

2-2 Experimental procedures

The starting materials were prepared from mixtures of oxides (MgO, Al_2O_3, SiO_2, TiO_2, Cr_2O_3, MnO_2 and Fe_2O_3) and carbonates (Na_2CO_3, K_2CO_3 and $CaCO_3$). After weighing and mixing them in an agate mortar, the reagents were reduced from Fe_2O_3 and MnO_2 and decarbonated by heating at 1150°C for 2 hours in an 1 atm. vertical furnace with a H_2/CO_2 gas flow at oxygen fugacity, fO_2, of $10^{-10.8}$ atm. Major crystalline phases in the starting materials after the heating were determined to be cristobalite, olivine and/or pyroxene by a powder X-ray diffraction method.

Partial melting experiments were carried out at 1 atm. total pressure using the Pt wire loop method for experiments with silicate melts (Donaldson *et al.*, 1975). Before the experiments, Pt or Pt/Rh alloy wires (0.3mm in diameter) were saturated with Fe to prevent a loss of Fe from the charges to Pt during the experiments (Donaldson, 1979; Grove, 1981). This method is generally adopted to the melting experiments of materials with Fe at 1 atm. For the HM series experiments, Fe saturated Pt wires of 0.1mm in diameter were used to minimize a change of Fe content of the charges.

In the present experiments, the wires were immersed in a dummy material with similar composition to the starting material, and heated at 1400°C for 15 to 18 hours under the same fO_2 condition as that of the experiments. After the heating, the wires were leached out from the dummy material with hydrofluoric acid. Fe soaked Pt/Rh_{40} wires instead of the Fe-soaked Pt wires were used in the experiments at temperatures higher than the Pt-Fe solidus (1570°C).

About 100mg of the starting materials were formed into pellets and

held in a vertical furnace. Oxygen fugacity was controlled by a H_2/CO_2 gas mixture. The fO_2 value adopted in the experiments was the average of the fO_2 values of the IW and FMQ buffer curves in a log scale. Under this fO_2 condition, it is considered that most of the iron are present as Fe^{2+} and the change in the FeO content of the charge is minimum during the experiments. Temperature was measured before and after the experiments with a Pt-$PtRh_{13}$ thermocouple, calibrated against the melting points of Au and Ni.

Melting experiments were carried out at temperatures between 1120°C and 1600°C in CH, 1070°C and 1420°C in ED, and 1060°C and 1250°C in EU experiments, for durations between 0.2 and 74.5 hours (Table 2-4). CH-HM experiments were carried out from 1450°C to 1200°C and ED-HM were from 1400°C to 1180°C. Starting material of ED-HM experiments from 1400°C to 1280°C (ED-2HM to ED-6HM) was same to that of ED experiments. To ascertain invariability of the melt composition during the experiments, at 1400°C of ED-HM experiments, three runs of different duration (10 minutes, 5 and 11.5 hours) were carried out.

After the heating, run products were quenched into water and resinified. Vertical cross sections of the products were polished (Figure 2-1) and observed under scanning electron microscopes (SEM's, HITACHI S-530 and S-650) with back-scattered electron imaging (BEI). Quantitative chemical analyses of the products were done by EDX systems (HORIBA EMAX-2200, Kevex delta and KEVEX-7000Q) with the accelerating voltage of 20kV and the beam current of 0.1nA, with a focused beam. The X-ray intensities were corrected with the ZAF method.

Table 2-4 Temperatures, run durations and oxygen fugacities of experiments. Observed phases of run products are also tabulated. CH, ED and EU are the same as those in Table 1-1.

Gl: Glass, Crm: Chromite, Ol: Olivine, Opx; Orthopyroxene,
Pig: Pigeonite, Px: Pyroxene, Pl: Plagioclase, Silica: SiO_2 mineral,
?: uncertain phases.
*Chromites are included in olivine crystals.

CH

No.	T (°C)	t (hour)	-log(fO_2) (bar)	Phases
1	1600	0.2	6.31	Gl, Ol
2	1570	0.3	6.53	Gl, Ol, Crm*
3	1540	0.7	6.76	Gl, Ol, Crm*
4	1510	1.0	7.00	Gl, Ol, Crm*
5	1490	1.5	7.16	Gl, Ol, Crm*
6	1470	2.0	7.33	Gl, Ol, Crm
7	1450	2.5	7.50	Gl, Ol, Crm
8	1430	5.8	7.67	Gl, Ol, Crm
9	1410	8.0	7.85	Gl, Ol, Crm
10	1400	14.0	7.94	Gl, Ol, Crm
11	1380	13.0	8.13	Gl, Ol, Crm
12	1350	13.5	8.42	Gl, Ol, Crm
13	1330	9.8	8.61	Gl, Ol, Opx, Crm
14	1300	21.7	8.92	Gl, Ol, Opx, Crm
15	1280	14.3	9.13	Gl, Ol, Opx, Crm
16	1250	18.5	9.45	Gl, Ol, Opx, Crm
17	1200	23.5	10.03	Gl, Ol, Opx, Crm
18	1160	31.4	10.51	Gl?, Ol?, Px?, Crm?, Silica?
19	1140	41.5	10.76	?
20	1120	48.5	11.02	?

Table 2-4 (continued)

ED

No.	T (°C)	t (hour)	-log(fO_2) (bar)	Phases
1	1420	1.0	7.76	Gl
2	1400	14.0	7.94	Gl, Crm
3	1370	8.0	8.22	Gl, Ol, Crm
4	1330	9.8	8.61	Gl, Ol, Opx, Crm
5	1300	14.0	8.92	Gl, Ol, Opx, Crm
6	1280	14.3	9.13	Gl, Ol, Opx, Crm
7	1250	18.5	9.45	Gl, Ol, Opx, Crm
8	1220	21.0	9.79	Gl, Ol, Opx, Crm
9	1200	23.5	10.03	Gl, Opx, Crm
10	1180	29.3	10.26	Gl, Ol, Opx, Crm
11	1160	31.4	10.51	Gl, Pig, Crm, Pl
12	1140	41.5	10.76	Gl, Pig, Crm, Pl
13	1120	48.5	11.02	Gl?, Pig, Crm, Pl
14	1100	48.8	11.29	Pig, Crm, Pl?, Silica
15	1070	74.5	11.71	Pig?, Silica?

EU

No.	T (°C)	t (hour)	-log(fO_2) (bar)	
1	1250	19.4	9.45	Gl, Crm
2	1220	21.1	9.79	Gl, Crm
3	1200	23.0	10.03	Gl, Crm
4	1180	27.1	10.26	Gl, Crm
5	1160	40.8	10.51	Gl, Ol, Pig, Pl, Crm
6	1140	44.2	10.76	Gl, Pig, Pl, Crm
7	1120	50.3	11.02	Gl, Pig, Pl, Crm
8	1100	64.8	11.29	Gl?, Ol?, Pig, Pl, Crm, Silica
9	1080	72.0	11.57	Ol?, Pig, Pl, Crm, Silica
10	1060	72.0	11.85	Pig?, Pl?, Crm?, Silica?

Table 2-4 (continued)

CH-HM experiments

No.	T (°C)	t (hour)	-log(fO_2) (bar)	Phases
7HM	1450	2.7	7.50	Gl, Ol, Crn
8HM	1430	5.7	7.67	Gl, Ol, Crn
9HM	1410	9.0	7.85	Gl, Ol, Crn
11HM	1380	11.7	8.13	Gl, Ol, Crn
12HM	1350	11.5	8.42	Gl, Ol, Crn
13HM	1330	11.7	8.61	Gl, Ol, Opx, Crn
14HM	1300	14.1	8.92	Gl, Ol, Opx, Crn
15HM	1280	16.9	9.13	Gl, Ol, Opx, Crn
16HM	1250	20.0	9.45	Gl, Ol, Opx, Crn
17HM	1200	23.7	10.03	Gl, Ol, Opx, Crn

ED-HM experiments

No.	T (°C)	t (hour)	-log(fO_2) (bar)	Phases
2HM1	1400	10min	7.94	Gl, Crn
2HM2	1400	5.0	7.94	Gl, Crn
2HM3	1400	11.5	7.94	Gl, Crn
3HM	1370	12.0	8.22	Gl, Ol, Crn
3HM'	1350	9.8	8.42	Gl, Ol, Crn
4HM	1330	11.8	8.61	Gl, Ol, Opx, Crn
5HM	1300	12.8	8.92	Gl, Ol, Opx, Crn
6HM	1280	16.3	9.13	Gl, Ol, Opx, Crn
7HM	1250	20.1	9.45	Gl, Ol, Opx, Crn
8HM	1220	22.3	9.79	Gl, Ol, Opx, Crn
9HM	1200	24.0	10.03	Gl, Ol, Opx, Crn
10HM	1180	28.1	10.26	Gl, Ol, Pig?, Crn

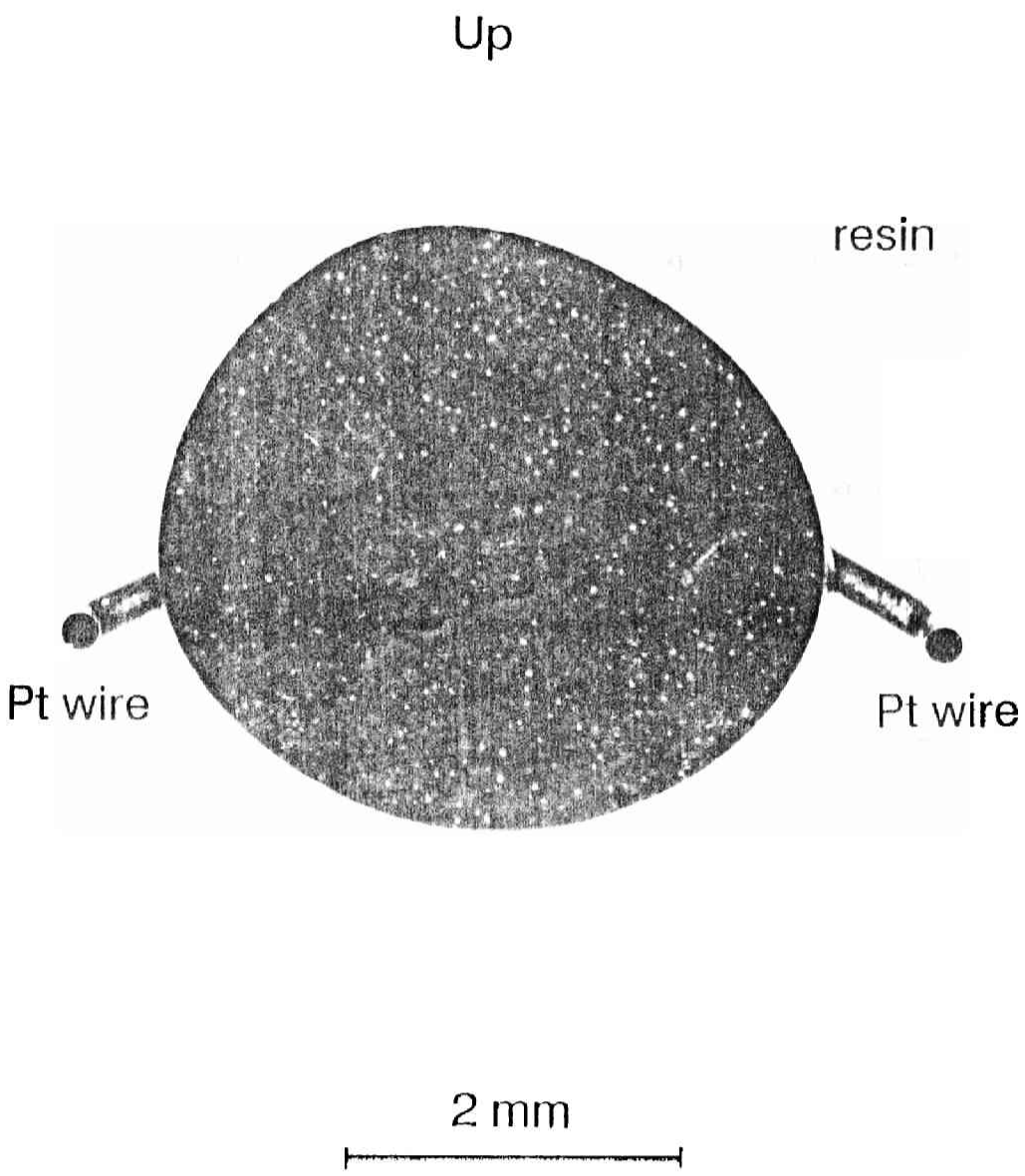

Figure 2-1
A close-up photograph of the polished surface of the run product (Run# CH10, 1400°C, 14hours)after fixed in a resin. Scale bar is 2mm. "Up" indicates a upside of the charge in the furnace during the heating.

3 Results and interpretation

3-1 Mineral assemblages of the run products

In the temperature range between 1120°C and 1600°C of the CH experiments, main crystalline phases of the run products are olivine and orthopyroxene in quenched glass which was originally melt phase during the experiments (Table 2-4). Back-scattered electron images of typical charges are shown in Figures 3-1a, 1b and 1c. The melting relations of this system is shown in Figure 3-2. The liquidus phase of this starting material is olivine, and the liquidus temperature is above 1600°C. Any experiments above 1600°C were not done due to a limitation of the furnace. Chromite appears as inclusions in olivine crystals at 1570°C and in the melt at 1470°C. The chromite inclusions might be relicts of the starting material. Orthopyroxene joins at 1330°C. In runs at temperatures less than 1160°C, glass was not be identified clearly.

In the series of the ED experiments, main crystalline phases are olivine, pyroxene (orthopyroxene and pigeonite) and plagioclase in the temperature range between 1070°C and 1370°C. Quenched glass is distinguished in the run products from 1140°C to 1420°C. The phase relation of this system is also shown in Figure 3-2. Olivine and chromite start to crystallize at temperatures between 1370°C and 1400°C. Orthopyroxene joins with minor amount of olivine and chromite at 1330°C. Pigeonite and plagioclase join at 1160°C. At temperatures below 1120°C, each phase in the run products was too small to be analyze quantitatively. At 1070°C, identification of phases could not be done. Back-scattered electron images of typical charges are shown in Figures 3-1d and 1e.

Main crystalline phases of the run products of the EU experiments

are pigeonite and plagioclase in the temperature range from 1060°C to 1160°C. Temperature difference of the liquidus and solidus of this material for the main phases (1060°C to 1250°C) is smaller than those of other two starting materials. Phase relation of this system is shown in Figure 3-2. Chromite is a liquidus phase. Liquidus temperature of chromite is higher than 1250°C, the highest temperature of EU experiments. Olivine, pigeonite and plagioclase join at 1160°C. Olivine disappears at 1140°C. Below 1160°C, pigeonites and plagioclases are major solid phases. Below 1100°C, quenched melt was not observed in the run products and minerals might not be in equilibrium. A back-scattered electron image of a typical charge is shown in Figure 3-1f.

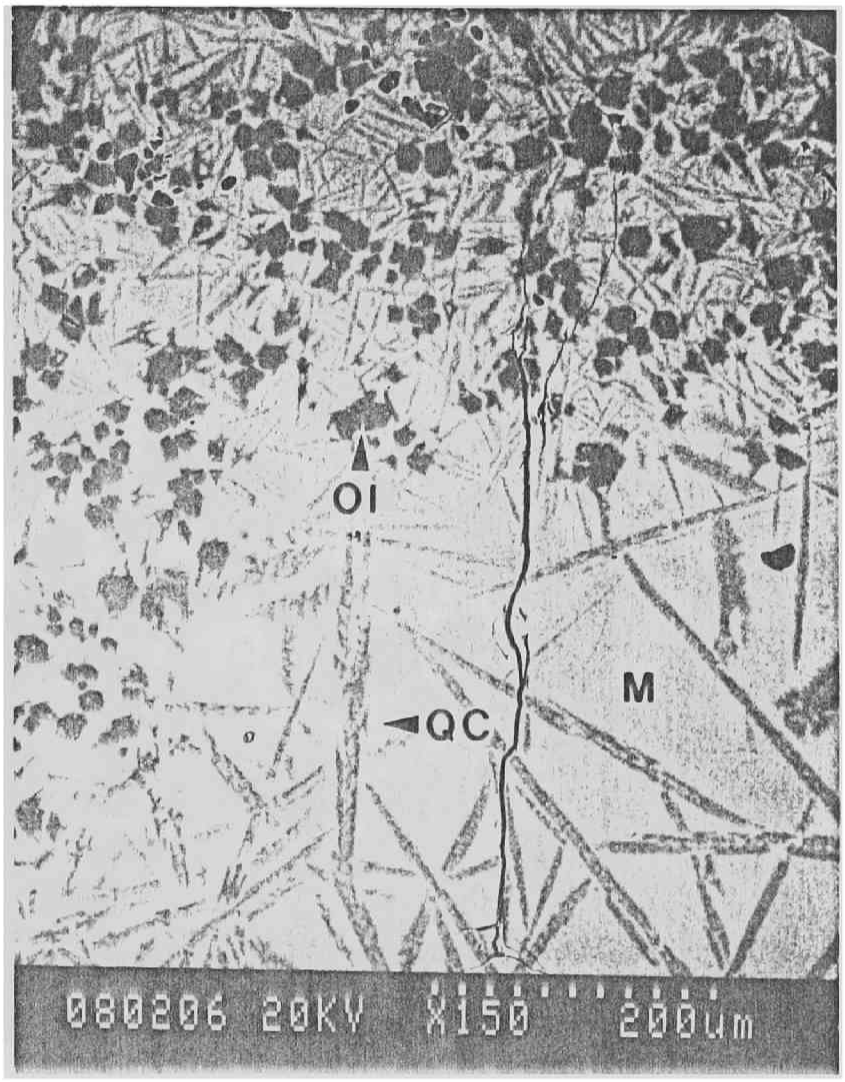

Figure 3-1
Back-scattered electron images (BEI) of the run products. Contrast of plain surface in BEI is reflect average atomic number of the material.

Figure 3-1a
Run No. CH-3, 1540°C, 0.7hours. Large quench crystals are observed but melt regions without quenching effect are also observed.
Ol: Olivine, M: Melt, QC: Quench crystals.

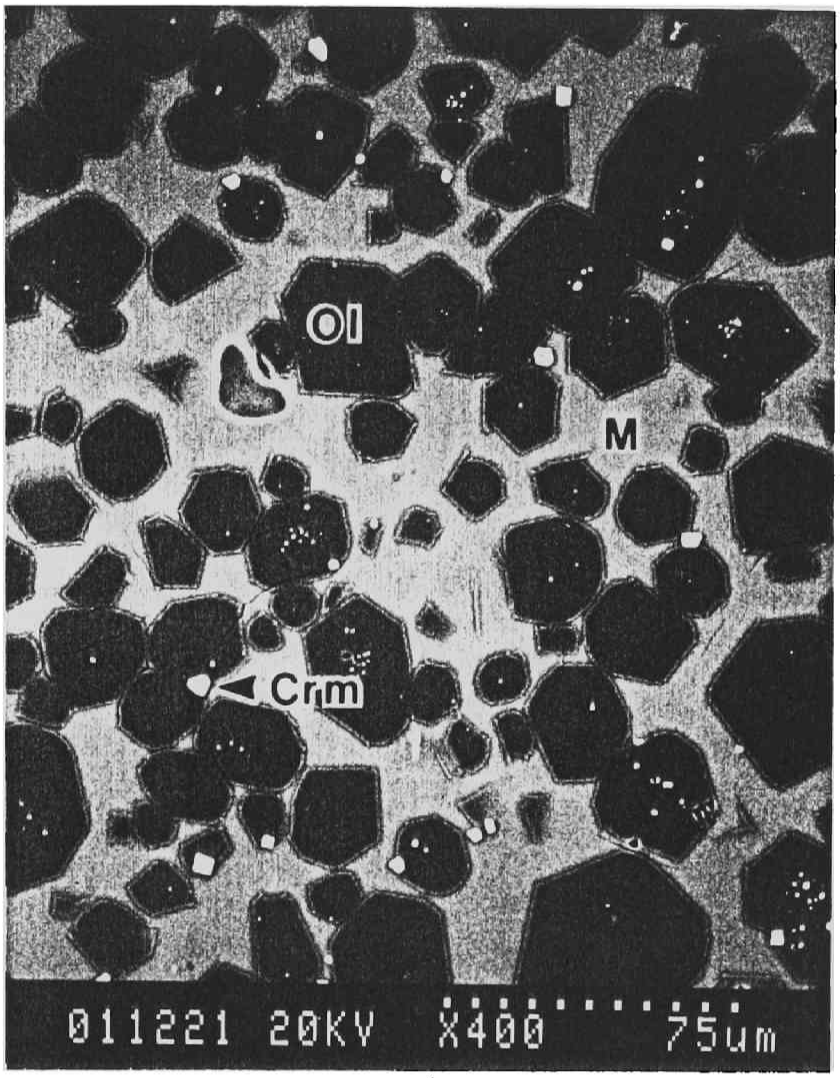

Figure 3-1b

Run No. CH-10, 1400°C, 14hours. Olivine crystals are granular and several to several tens μm in size and have no zoning contrast under BEI except for thin olivine-melt boundaries. This contrast may be caused by the geometric edge effect and/or quench growth of olivines. Crm: Chromite.

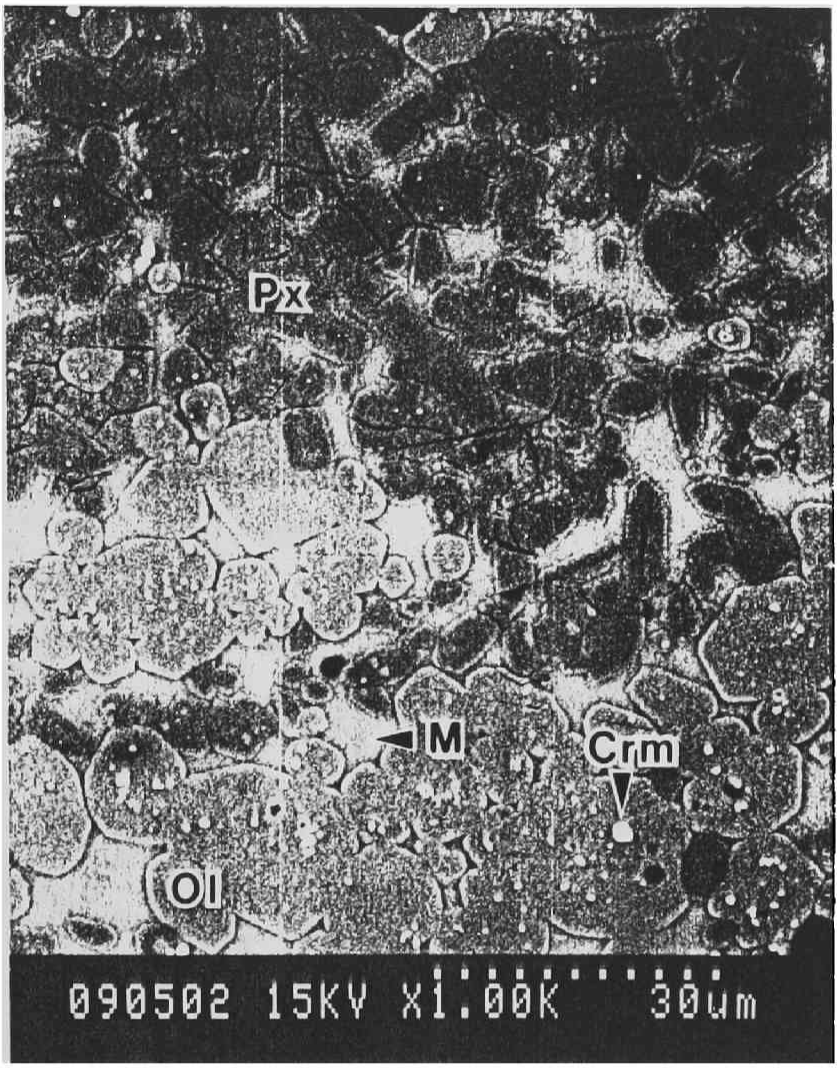

Figure 3-1c

Run No. CH-17, 1200°C, 23.5hours. Pyroxene crystallized in this temperature and melt fraction is quite small. In this BEI, there are olivine dominant area and pyroxene dominant area apparently. However, magnification of this BEI is larger than those of others and those area is not much larger than the crystals of olivine or pyroxene in the other run products. Px: Pyroxene.

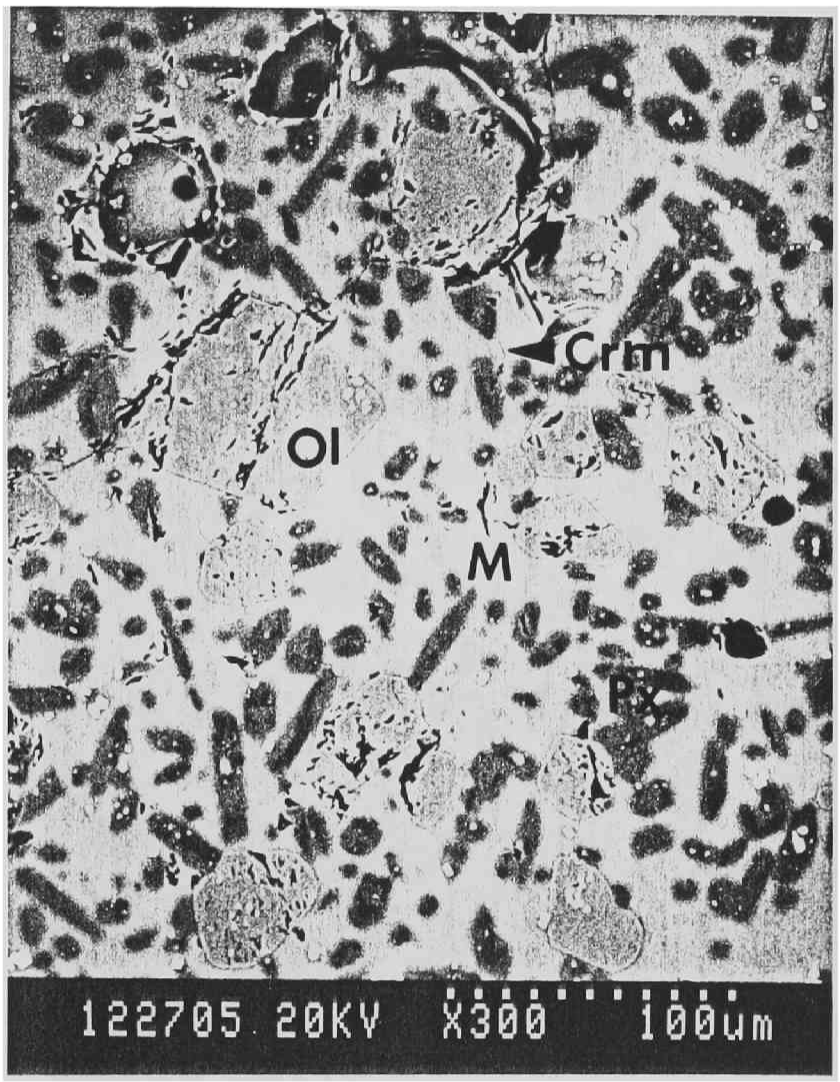

Figure 3-1d

Run No. ED-7, 1250°C, 18.5hours. Pyroxene crystals are smaller than olivines. Volume fraction of olivines in this BEI photograph are larger than the other area of this run product. Contrasts same as Figure 3-1b can be seen in the pyroxene-melt and olivine-melt boundaries.

Figure 3-1e
Run No.12, 1140°C, 41.5hours. Plagioclase is one of major crystalline phases. It is difficult to analyze the melts because those have only a small fraction. Pl: Plagioclase.

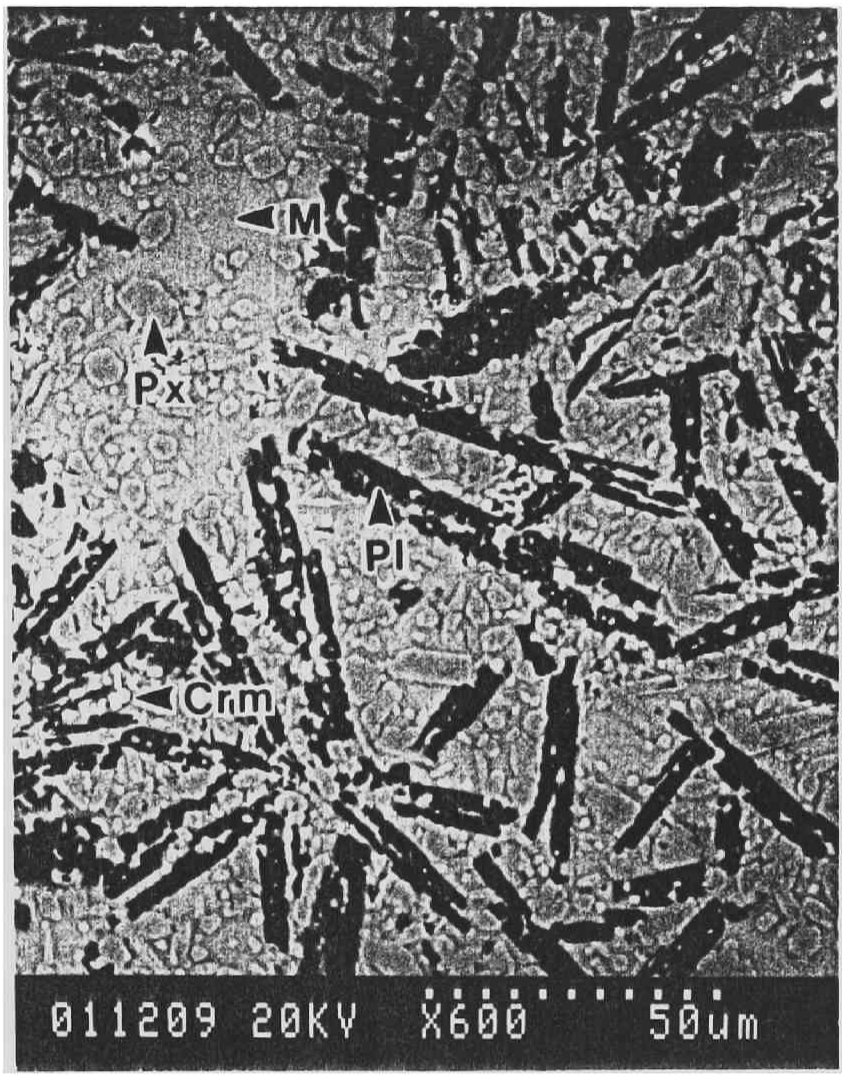

Figure 3-1f
Run No. EU-5, 1160°C, 40.8hours. Pyroxene crystals are smaller than plagioclases. Plagioclase crystals elongate up to 100μm. Areas of crystals and melt are almost the small limits of quantitative analysis by EPMA.

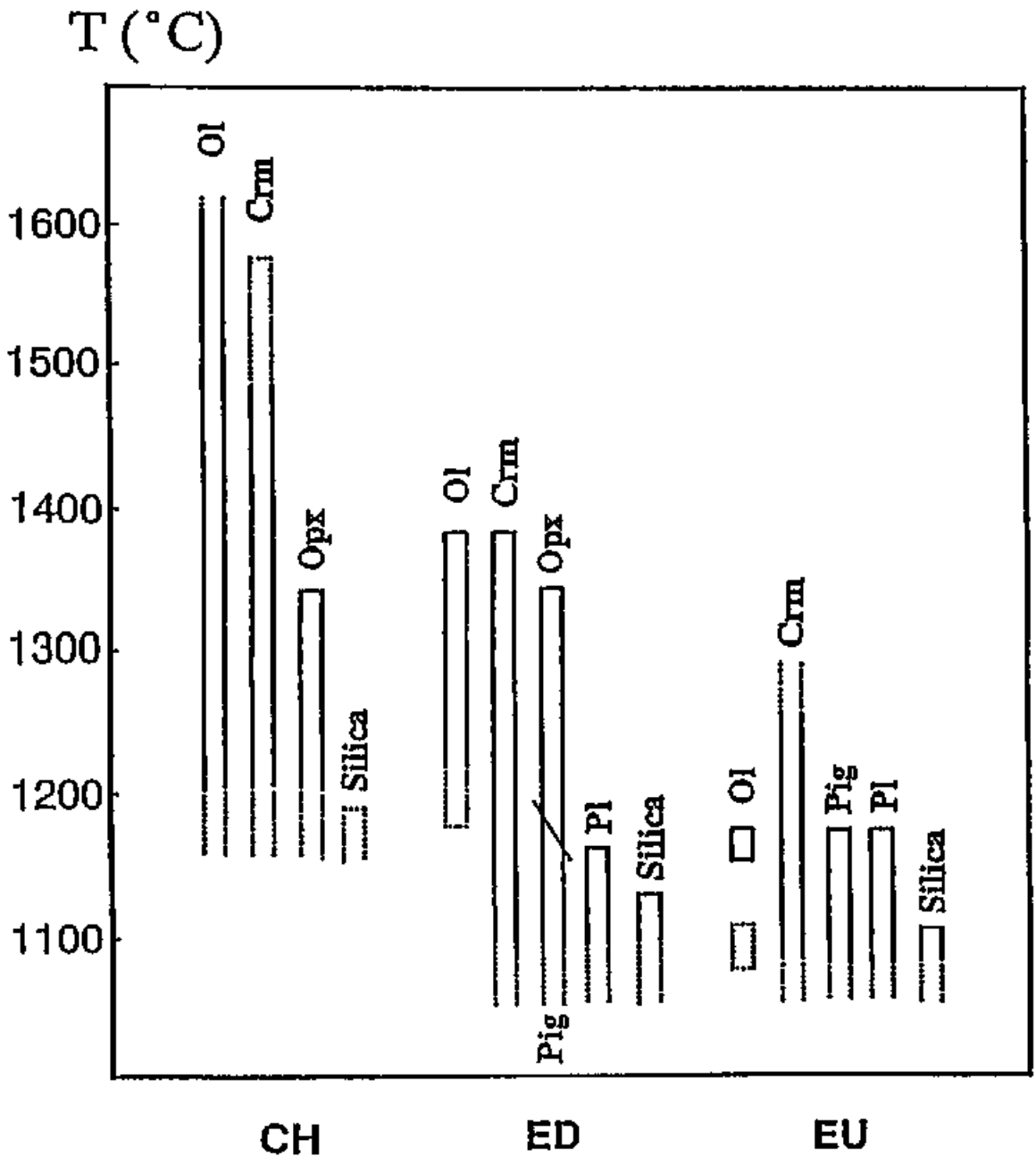

Figure 3-2

Summary of CH, ED and EU partial melting experiments. Dotted areas represent unequilibrium phases (lower temperature) or uncertain temperature range (higher temperature). At the temperature range where the melt fraction is too small to be analyzed, crystal phases are not to in equilibrium with the melt within run durations. Pyroxene phase of the ED experiments is orthopyroxene at high temperatures and pigeonite at low temperatures. Appearance of olivine under 1100°C in the EU experiments may due to unequilibrium mineral assemblage or Fe-rich olivine composition. Abbreviations; Ol: Olivine, Crm: Chromite, Opx: Orthopyroxenes, Silica: SiO_2 mineral, Pig: Pigeonite, Pl, Plagioclase.

3-2 Composition of the melts and minerals

The crystals coexisting with the melt are almost homogeneous and show no zoning pattern except for the quenched rims observed in the back-scattered electron images (Figures 3-1b and c). Typical standard deviations of Fo content of olivines and En content of pyroxenes in each run product are 0.2% at above 1250°C and increase with the temperature decreasing. The Fo content of olivine, and the En and Wo contents of orthopyroxene are shown in Table 3-1 and Appendix 2. Chromite crystals were too small to be analyzed quantitatively.

In the melt portion, quench crystals are dispersed in the run products at temperatures higher than 1490°C (Figure 3-1a). At temperatures lower than 1490°C, quenching effects can be seen as rims with the width of a few μm (Figures 3-1b and 1c). The chemical compositions of the melts are changed near the quench crystals and the rims. Therefore, analysis points of the melts were chosen to avoid the effects from the quench crystals and the rims as much as possible. Standard deviations of major elements compositions in analyzed points are less than 1.0 wt.% except the run products with quench crystals (above 1490°C) and below 1200°C. The melt composition of each run product is determined by averaging the values of about 5 analyses. They are listed in Tables 3-1, 3-2, 3-3 and Appendix 2.

Equilibrium in the phases of the run products can be examined by Mg-Fe exchange between olivines and melts. Mg-Fe partition coefficients between olivines and melts (Kdol) calculated from the analyzed values of the run products are 0.29 to 0.34 (Table 3-4). Typical standard deviation of Kdol from the deviations of olivines and melts is 0.02. Equilibrium value of Kdol depends on the composition of the melt (Ford

et al., 1983). From 94 data of the compositions of olivines and melts by Pt wire loop experiments (Weill and McKay, 1975, Rhodes *et al.*, 1979, Longhi and Pan, 1988, Colson *et al.*, 1988 and Ulmer, 1989), composition dependence of an equilibrium value of Kdol for a composition of a melt is calculated on the formula of Ford *et al.*, (1983). Temperature dependence is neglected because temperature and composition of the melt in this study is not independent. Calculated values of Kdol (KdCalc) for the melt compositions of the present experiments are 0.30 to 0.33 and its standard deviation is 0.02 (Table 3-4).

Table 3-4 shows that Kdol of CH experiments are apparently smaller than those of ED experiments at the same temperature range. And Kdol and KdCalc do not agree within 0.02 from CH-6 to CH-13 and from ED-3 to ED-5. Values of these CH runs are lower than those of KdCalc and those of ED runs are higher than KdCalc. This difference in CH experiments must be caused by quench growth of olivines when volume fraction of melt is relatively small. Quench growth of olivines decreases Kd value apparently. In ED experiments, runs above liquidus temperature (ED-1 and 2) show Fe loss from charges about 5 to 10 %. Fe loss from the melt portion increases Kd apparently.

It is difficult to estimate these effects quantitatively. To minimize the difference between CH and ED experiments, melt compositions from CH-6 to CH-13 are corrected on the assumption of quench growth of olivine that has 3% of mass of melt portion and its Fo content 10% smaller than that of core region of olivine crystals (columns labeled [q] in Table 3-4). To correct Fe loss of ED experiments, Fe content of melts in cation fraction from ED-1 to ED-6 are gained 5% except ED-2 that gained 10% (columns labeled [i] in Table 3-4). Quench effect in ED experiments is neglected because of large volume fraction of melt in those experiments.

And Fe loss in CH experiments is also neglected because of relatively short run durations and small Fe content. Runs below 1250°C are not corrected by any methods because of agreement between Kdol and KdCalc.

To avoid quench effect and Fe loss, compositions of starting materials for HM experiments are determined as mixtures of 70% of corrected melt composition and 30% of olivine or 15% of olivine + 15% of pyroxene. For ED-2 to ED-6 experiments, HM experiments were carried out from the ED starting material with Pt wires of 0.1mm in diameter to minimize Fe loss to wires.

[Results of HM experiments]

From the melt compositions of three experiments of ED-2HM, it is ascertained that Fe loss in HM experiments is negligible (Table 3-4). In the Table 3-4, agreement between Kdol and KdCalc of HM experiments show that both quench effect and Fe loss are negligible in the HM experiments. The chemical compositions of the melts and crystals in the run products are listed in Appendix 2.

Compositions of melt and mineral phases obtained by HM experiments represent the compositions around Ol-Px phase boundary of the systems discussed in the present study. In the later chapters, melt and mineral compositions of HM experiments are used for the discussion of the Ol-Px phase boundary and properties of the melt.

[Melt and mineral compositions in CH experiments]

The chemical compositions of the melts and crystals in the run products are listed in Table 3-1 and Appendix 2. The compositions of melts vary from the starting materials with temperature. Figure 3-3 shows the five major elements of melts of CH and CH-HM experiments in cation fraction with temperature range from 1200°C to 1600°C. At the temperature below 1160°C, crystals and melt of the run products were too small to be analyzed accurately. Thus, the data below 1160°C will not be used in further discussion. In Figure 3-3, Si content increases with decreasing temperature while the major crystalline phase is solely olivine (above 1350°C). Then, it slightly decreases with decreasing temperature after pyroxene joins to the crystalline phase. Fe content has the maximum at around 1450°C and other three elements vary monotonously.

At the temperature range where the main crystalline phase is solely olivine, the contents of the major elements in the melt change in a simple manner (Figure 3-3). The molar compositions, X_{MO} (%), can be fitted by quadratic functions of the temperature, T (°C, 1350°C - 1600°C), within the standard deviation of 0.5 mol%, as follows;

$$
\begin{aligned}
X_{MgO} &= 156.7 - 2.340\cdot10^{-1}\cdot T + 1.047\cdot10^{-4}\cdot T^2 \\
X_{AlO1.5} &= 22.59 - 1.022\cdot10^{-2}\cdot T - 1.028\cdot10^{-6}\cdot T^2 \\
X_{SiO2} &= 101.8 - 4.176\cdot10^{-2}\cdot T + 1.830\cdot10^{-6}\cdot T^2 \qquad (3\text{-}1) \\
X_{CaO} &= 34.15 - 2.567\cdot10^{-2}\cdot T + 3.871\cdot10^{-6}\cdot T^2 \\
X_{FeO} &= -210.3 + 3.069\cdot10^{-1}\cdot T - 1.050\cdot10^{-4}\cdot T^2 .
\end{aligned}
$$

As seen in these diagrams, any melts in the experiments do not agree with the composition of diogenite or eucrite at the specific temperature. Especially, Mg and Fe contents of melts are never equal to

those of eucrites. However, it should be noted that the composition of the melt at around 1400°C is similar to that of the mixture of 55 wt.% of average diogenite and 45 wt.% of average noncumulate eucrite (a line labeled ED in Figure 3-3).

The compositions of olivine before the pyroxene appearance are plotted against the temperature (Figure 3-4). The Fo content, X_{Fo} (%), can be also fitted by quadratic function of the temperature, T (°C), within the standard deviation of 0.5 mol%, as follows;

$$X_{Fo} = 127.5 - 8.283 \cdot 10^{-2} \cdot T + 3.790 \cdot 10^{-5} \cdot T^2 . \qquad (3\text{-}2)$$

It should also be noted that the Fo content of olivine at 1400-1500°C ($Fo_{86\text{-}88}$) is similar to those of olivines in pallasites (Dodd, 1981; see Appendix 1).

Volume fractions of solid can be estimated as a function of the temperature before the pyroxene appearance, from the compositions of olivine and melt (Figure 3-5) because the main solid phase is solely olivine in this temperature range. The volume fraction of olivine, V_{ol}, can be expressed as follows;

$$W_{ol} = \frac{W_{ist} - W_{imelt}}{W_{iol} - W_{imelt}}$$

$$V_{ol} = \frac{W_{ol}/D_{ol}}{W_{ol}/D_{ol} + (1 - W_{ol})/D_{melt}} \qquad (3\text{-}3)$$

where W_{ist}, W_{imelt} and W_{iol} are the weight fractions of component i in the starting material, melt phases and olivines of the run products, respectively. At around 1400°C, the solid (olivine) and melt have almost the same volume fractions.

In Figure 3-5, the volume fraction of solid where Fe-Ni metal is taken into consideration is also shown. Fe/Ni ratio of the metal portion

subtracted from the solar abundance to determine the composition of the starting material is listed in Table 2-1. Volume fraction of metal portion can be calculated by equation 3-3 from weight fraction and density of silicate and metal portions. Solidus and liquidus temperatures of this Fe/Ni alloy is about 1500°C. Consequently, the volume fraction of metal portion should be added to solid phase below 1500°C and to liquid phase above that temperature.

[Melt and mineral compositions in ED experiments]

The chemical compositions of the melts and crystals in the run products are listed in Table 3-2 and Appendix 2. Standard deviations of major elements compositions in analyzed points are less than 1.0 wt.% except the below 1200°C. Figure 3-6 shows the five major elements of melts produced by ED and ED-IIM experiments in cation fraction in the temperature range from 1140°C to 1420°C. At the temperature below 1120°C, crystals and melt of the run products were too small to be analyzed accurately. Thus, the data below 1120°C will not be used in further discussion.

In Figure 3-6, Si content is almost constant in this temperature range. Fe content has the maximum at around 1250°C and other three elements vary monotonously. At the temperature range from 1180°C to 1330°C, main crystalline phase is orthopyroxene (Figure 3-2). In this range, the molar compositions of the major elements (X_{MO}, in %) in the melt can be fitted by quadratic functions (a linear function for Si) of temperature, T (°C) (Figure 3-6) as follows;

$$X_{MgO} = 100.2 - 2.087\cdot10^{-1}\cdot T + 1.120\cdot10^{-4}\cdot T^2$$

$$X_{Al_2O_{1.5}} = 227.4 - 3.026\cdot10^{-1}\cdot T + 1.032\cdot10^{-4}\cdot T^2$$

$$X_{SiO_2} = 44.75 + 3.259\cdot10^{-3}\cdot T \qquad (3\text{-}4)$$

$$X_{CaO} = 31.33 - 3.702\cdot10^{-3}\cdot T - 1.136\cdot10^{-5}\cdot T^2$$

$$X_{FeO} = -324.1 + 5.408\cdot10^{-1}\cdot T - 2.154\cdot10^{-4}\cdot T^2.$$

The standard deviations of the functions are within 0.5 mol%.

In Figure 3-6, the melt at about 1200°C has similar composition to the average of noncumulate eucrites although the SiO_2 content is slightly higher than that of the average eucrite. However, bulk compositions of some noncumulate eucrites are similar to the melt composition produced by the ED experiments at around 1200°C. The bulk compositions of three noncumulate eucrite, Y-74450, Sioux County and Stannern are also shown in Table 3-2.

Compositional trends of the pyroxenes produced in ED and ED-HM experiments are plotted in a pyroxene quadrilateral (Figure 3-7). Orthopyroxene is present in the temperature range from 1330°C to 1180°C, and pigeonites below 1160°C. The compositional range of orthopyroxenes around 1200°C ($En_{75\pm2}Wo_{3\pm1}$) is similar to that of diogenitic pyroxenes ($En_{75\text{-}80}Wo_1$; see Appendix 1). Enstatite and wollastonite mol% of each analysis are also plotted in Figure 3-8. In the temperature range where orthopyroxene crystallizes, the En and Wo components, X_{En} and X_{Wo}, can be fitted by quadratic functions of temperature as follows;

$$X_{En} = -831.1 + 1.365\cdot T - 5.105\cdot10^{-4}\cdot T^2$$

$$X_{Wo} = 406.4 - 6.168\cdot10^{-1}\cdot T + 2.346\cdot10^{-4}\cdot T^2. \qquad (3\text{-}5)$$

The standard deviations are slightly larger than those of the melt, and are several %. This inhomogeneity may be derived by local inhomogeneity of chromium content of the starting material.

Mg-Fe partitioning coefficients between pyroxenes and melts (Kdpx) calculated from the average compositions of the pyroxenes are 0.26±0.03. On the other hand, olivine crystals are homogeneous and have more Fe-rich composition than pyroxenes. The values of Kdol and average ratio of Kdol/Kdpx are 0.32±0.00 and 1.25, respectively. These values are consistent with those from the experiments that olivine and pyroxene coexist with melt by Stolper (1977) and the Mg-Fe partitioning coefficients between olivines and pyroxenes by Larimer (1968). Consequently, pyroxene compositions used in the later discussion are average value of those of each run products, and those are considered to be in equilibrium. Plagioclase crystals are heterogeneous as well as the pyroxenes. Chromite crystals were too small to be analyzed quantitatively.

Because the pyroxenes are the major solid phase including olivine and pyroxene below 1330°C, volume fraction of solid (or pyroxene) can be estimated by using the compositions of the olivine, pyroxenes and melt. As shown in Figure 3-9, the solid fraction exceeds 0.5 at about 1200°C.

[Melt and mineral compositions in EU experiments]

The compositions of the melts and crystals in the run products are listed in Table 3-3 and Appendix 2. Standard deviations of each analyses of melt phases are less than 1.0 wt.%. The Fe content in the melts becomes higher, while the Mg and Al contents become lower with decreasing temperature. The fraction of the Fe-rich melts were

relatively smaller than the crystals, and suddenly disappeared with further decreasing temperature. These results are essentially the same as those of the previous melting experiments of Juvinas and Sioux County eucrites (Stolper, 1977).

The compositions of pigeonite and fraction of crystals in the run products change widely in the narrow temperature range from 1120°C to 1160°C. The compositions of pigeonite are plotted in a pyroxene quadrilateral in Figure 3-7. This compositional range of the pyroxene coincides with that of cumulate eucritic pyroxenes (Stolper, 1977), and inverted pigeonites in cumulate eucrites (Takeda, 1979). The compositions of plagioclase, which are around An_{90-95}, do not change largely with temperature. They are similar to those of the eucritic plagioclase (An_{90-95}, see Appendix 1). Chromite crystals were too small to be analyzed quantitatively.

Table 3-1 Compositions of the melts (oxide wt. %), olivines (Fo content in mol %) and pyroxenes (En and Wo contents in mol %) of the run products of CH experiments analyzed by EPMA. Each analysis of melt is normalized to 100% as a total.

Mg#: Mg/(Mg+Fe) mol % of melt, Crm: Chromite, Silica: SiO_2 mineral, ?: uncertain phases.
*Chromites are included in olivine crystals.

Run No.		1	2	3	4	5	6	7	8	9	10
Temp. (°C)	Starting Material	1600	1570	1540	1510	1490	1470	1450	1430	1410	1400
Na_2O	0.14	0.0	0.2	0.2	0.1	0.1	0.0	0.2	0.1	0.0	0.0
MgO	31.90	31.1	28.7	26.0	23.9	22.5	21.7	19.8	19.0	18.1	17.4
Al_2O_3	3.23	3.3	3.9	4.0	4.5	5.7	5.2	5.4	5.9	6.2	6.8
SiO_2	45.29	44.7	45.4	46.5	47.6	47.7	48.6	49.6	50.1	50.6	51.9
K_2O	0.01	0.0	0.0	0.0	0.0	0.0	0.0	0.1	0.0	0.0	0.0
CaO	2.98	3.1	3.6	3.9	4.4	4.6	4.9	5.4	5.6	5.8	6.1
TiO_2	0.14	0.1	0.2	0.1	0.2	0.2	0.2	0.2	0.2	0.3	0.3
Cr_2O_3	0.70	0.7	0.7	0.8	0.8	0.8	0.8	0.9	0.9	0.8	0.8
MnO	0.49	0.5	0.6	0.6	0.6	0.6	0.6	0.7	0.6	0.6	0.6
FeO	15.11	16.4	16.7	17.9	17.8	17.8	17.9	17.8	17.5	17.5	16.1
Mg#	79	77	75	73	71	69	68	66	66	65	66
Fo		91.9	91.3	89.5	88.9	88.4	87.7	87.0	86.7	86.0	86.7
En											
Wo											
Other phases			Crm*	Crm*	Crm*	Crm*	Crm	Crm	Crm	Crm	

Table 3-1 (continued)

Run No.	11	12	13	14	15	16	17	18	19	20
Temp. (°C)	1380	1350	1330	1300	1280	1250	1200	1160	1140	1120
Na_2O	0.1	0.1	0.2	0.2	0.4	0.4	0.5			
MgO	16.5	15.4	14.2	12.8	11.8	11.0	9.0			
Al_2O_3	6.7	7.0	7.7	9.0	10.0	11.7	14.1			
SiO_2	52.2	53.3	52.7	52.7	52.5	51.8	51.6			
K_2O	0.0	0.0	0.1	0.3	0.2	0.0	0.0			
CaO	6.4	6.8	7.4	8.5	9.2	9.9	11.3			
TiO_2	0.3	0.3	0.4	0.4	0.4	0.4	0.5			
Cr_2O_3	0.7	0.6	0.5	0.4	0.3	0.2	0.0			
MnO	0.6	0.6	0.6	0.6	0.5	0.5	0.5			
FeO	16.7	15.9	16.1	15.2	14.8	14.1	12.5			
Mg#	64	63	61	60	59	58	56			
Fo	85.5	84.9	83.5	82.8	82.0	81.4	81.0	?		
En			84.7	84.0	82.2	79.8	74-79	?		
Wo			1.1	1.5	2.0	3.3	4-8			
Other phases	Crm	Crm	Crm	Crm	Crm	Crm	Crm	Crm? Silica?		

Table 3-2 Compositions of the melts (oxide wt. %), olivines (Fo content in mol %) and pyroxenes (En and Wo contents in mol %) of the run products of the ED experiments. Each analysis of melt is normalized to 100% as a total. Compositions of some noncumulate eucrites (McCarthy *et al.*, 1973, Takeda *et al.*, 1978) are also tabulated.

Mg#: Mg/(Mg+Fe) mol % of melt, Crm: Chromite, Pl: Plagioclase, Silica: SiO_2 mineral, ?: uncertain phases, An: Anorthite component in plagioclase (mol %).

Run No.		1	2	3	4	5	6	7	8	9	10
Temp. (°C)	Starting Material	1420	1400	1370	1330	1300	1280	1250	1220	1200	1180
Na_2O	0.25	0.2	0.2	0.3	0.3	0.5	0.5	0.5	0.5	0.5	0.6
MgO	17.99	18.4	18.6	17.4	15.0	13.0	11.9	9.5	8.7	7.7	7.3
Al_2O_3	6.12	6.5	6.6	6.4	7.2	8.4	8.5	10.1	10.8	12.0	12.5
SiO_2	51.17	51.4	52.0	52.5	52.0	51.0	51.2	50.2	50.7	50.4	50.0
K_2O	0.02	0.0	0.0	0.0	0.1	0.0	0.1	0.0	0.1	0.0	0.1
CaO	5.17	5.1	5.3	5.3	6.2	7.1	7.7	8.8	9.5	9.9	10.4
TiO_2	0.35	0.3	0.3	0.3	0.4	0.4	0.5	0.5	0.6	0.6	0.7
Cr_2O_3	0.97	0.8	0.7	0.6	0.5	0.3	0.4	0.0	0.2	0.1	0.2
MnO	0.54	0.5	0.6	0.6	0.6	0.6	0.6	0.6	0.5	0.5	0.5
FeO	17.41	16.8	15.8	16.6	17.8	18.7	18.7	19.7	18.3	18.3	17.7
Mg#:	65	66	68	65	60	55	53	46	46	43	42
Fo				84.6	81.5	78.6	76.8	73.2	71.4		~68
En					82.8	80.1	79~84	75~81	72~80	72~81	70~79
Wo					1.0	1.4	1.5	2.0	2.5	3	4
Other phases			Crm	Crm	Crm	Crm	Crm	Crm	Crm	Crm	Crm

Table 3-2 (continued)

Run No.	11	12	13	14	15
Temp. (°C)	1160	1140	1120	1100	1070
Na_2O	0.5	0.5			
MgO	6.3	5.7			
Al_2O_3	13.3	12.8			
SiO_2	50.4	49.5			
K_2O	0.2	0.2			
CaO	10.3	10.5			
TiO_2	1.0	2.0			
Cr_2O_3	0.0	0.0			
MnO	0.5	0.4			
FeO	17.5	18.3			
Mg#:	39	36			
Fo					
En	63-67	60-64	56-62	58-62	-62?
Wo	5-8	5-7	7-11	9-13	-8?
Other phases	Crm Pl (An80-90)	Crm Pl (An75-85)	Crm Pl (An80-85)	Crm Pl? Silica	? Silica

	Y-74450	Sioux County	Stannern
Na_2O	0.51	0.45	0.62
MgO	8.06	7.11	6.97
Al_2O_3	10.82	12.84	12.33
SiO_2	49.36	49.03	49.70
K_2O	0.06	0.03	0.06
CaO	9.52	10.35	10.67
TiO_2	1.04	0.62	0.98
Cr_2O_3	0.33	0.35	0.34
MnO	0.51	0.56	0.53
FeO	18.26	18.58	17.78
Total	99.57*	99.89	99.98
Mg#	44	41	41

*Total contains the other components.

Table 3-3 Compositions of the melts (oxide wt. %), olivines (Fo content in mpl %) and pyroxenes (En and Wo contents in mol %) of the run products of the EU experiments analyzed by EPMA. Each analysis of melt is normalized to 100% as a total.

Mg#: Mg/(Mg+Fe) mol % of melt, Crm: Chromite, Pl: Plagioclase, Silica: SiO_2 mineral, ?: uncertain phases. An: Anorthite component in plagioclase (mol %).

Run No.		1	2	3	4	5	6	7	8	9	10
Temp. (°C)	Starting Material	1250	1220	1200	1180	1160	1140	1120	1100	1080	1060
Na_2O	0.5	0.1	0.4	0.0	0.3	0.1	0.2	0.1			
MgO	7.3	7.4	7.7	7.6	7.3	6.3	5.5	4.1			
Al_2O_3	12.3	12.4	12.4	12.4	12.9	12.4	11.8	10.9			
SiO_2	49.5	50.2	50.2	50.0	50.0	50.2	50.4	50.1			
K_2O	0.1	0.2	0.2	0.2	0.1	0.1	0.0	0.2			
CaO	10.4	10.4	10.3	10.5	10.5	11.0	10.9	10.7			
TiO_2	0.7	0.7	0.7	0.7	0.7	0.8	0.9	1.3			
Cr_2O_3	0.3	0.0	0.0	0.0	0.0	0.0	0.0	0.0			
MnO	0.5	0.7	0.6	0.6	0.6	0.6	0.6	0.7			
FeO	18.4	17.9	17.5	18.0	17.6	18.6	19.7	21.8			
Mg#:	41	42	44	43	43	38	33	25			
Fo						62.1			40.4?	36.7?	
En						63-67	58-62	48-51	-40	40-43	-30?
Wo						6-10	8-11	12-13	20-30	15-33	-38?
Other phases		Crm	Crm	Crm	Crm	Crm Pl (An85-95)	Crm Pl (An85-90)	Crm Pl (An80-90)	Crm Pl (An75-85) Silica	Crm Pl (An80-90) Silica	Crm? Pl? Silica?

Table 3-4 Mg-Fe partitioning coefficients between olivine and melt (Kdol) and weight % of melts of the run products. The compositions of the run products and corrected values of melt composition by quench effect or iron loss ([q] and [i], respectively).
Kd Calc represents Kd value calculated from the composition of the melt by the composition dependence of Kdol. Typical standard deviations of Kdol and KdCalc are 0.02.

CH experiments

No.	CH-1	CH-2	CH-3	CH-4	CH-5	CH-6	CH-6[q]
T(°C)	1600	1570	1540	1510	1490	1470	1470
Wt fraction (%)							
Na_2O	0.0	0.2	0.2	0.1	0.1	0.0	0.0
MgO	31.1	28.7	26.0	23.9	22.5	21.7	22.2
Al_2O_3	3.3	3.9	4.0	4.5	5.7	5.2	5.1
SiO_2	44.7	45.4	46.5	47.6	47.7	48.6	48.4
K_2O	0.0	0.0	0.0	0.0	0.0	0.0	0.0
CaO	3.1	3.6	3.9	4.4	4.6	4.9	4.8
TiO_2	0.1	0.2	0.1	0.2	0.2	0.2	0.2
Cr_2O_3	0.7	0.7	0.8	0.8	0.8	0.8	0.8
MnO	0.5	0.6	0.6	0.6	0.6	0.6	0.6
FeO	16.4	16.7	17.9	17.8	17.8	17.9	18.0
Total	100.0	100.0	100.0	100.0	100.0	100.0	100.0
Mg#	77.2	75.4	72.1	70.5	69.3	68.4	68.8
Fo	91.9	91.3	89.5	88.9	88.4	87.7	87.7
En							
Wo							
Kdol	0.30	0.29	0.30	0.30	0.30	0.30	0.31
KdCalc	0.30	0.30	0.31	0.31	0.31	0.32	0.31

Table 3-4 (continued)

No.	CH-7	CH-7q	CH-7HM	CH-8	CH-8q	CH-8HM	CH-9	CH-9q	CH-9HM
T(°C)	1450	1450	1450	1430	1430	1430	1410	1410	1410
Wt fraction (%)									
Na_2O	0.2	0.2	0.1	0.1	0.1	0.1	0.0	0.0	0.2
MgO	19.8	20.3	21.4	19.0	19.6	20.3	18.1	18.7	19.7
Al_2O_3	5.4	5.3	4.6	5.9	5.8	5.0	6.2	6.0	5.4
SiO_2	49.5	49.3	48.9	50.2	49.9	49.6	50.7	50.3	49.7
K_2O	0.1	0.1		0.0	0.0		0.0	0.0	
CaO	5.4	5.3	5.1	5.6	5.5	5.5	5.8	5.7	5.6
TiO_2	0.2	0.2	0.0	0.2	0.2	0.0	0.3	0.3	0.3
Cr_2O_3	0.9	0.9	0.8	0.9	0.9	0.8	0.8	0.8	0.7
MnO	0.7	0.7	0.5	0.6	0.6	0.6	0.6	0.6	0.5
FeO	17.8	17.9	18.7	17.5	17.6	18.1	17.5	17.6	17.9
Total	100.0	100.0	100.0	100.0	100.0	100.0	100.0	100.0	100.0
Mg#	66.5	66.9	67.1	65.9	66.4	66.7	64.8	65.4	66.2
Fo	87.0	87.0	86.9	86.7	86.7	86.6	86.0	86.0	86.2
En									
Wo									
Kdol	0.30	0.30	0.31	0.30	0.30	0.31	0.30	0.31	0.31
KdCalc	0.32	0.32	0.32	0.32	0.32	0.32	0.32	0.32	0.32

No.	CH-10	CH-10q	CH-11	CH-11q	CH-11HM	CH-12	CH-12q	CH-12HM
T(°C)	1400	1400	1380	1380	1380	1350	1350	1350
Wt fraction (%)								
Na_2O	0.0	0.0	0.1	0.1	0.1	0.1	0.1	0.2
MgO	17.4	18.0	16.5	17.1	17.9	15.4	16.0	16.6
Al_2O_3	6.8	6.6	6.7	6.5	6.1	7.0	6.8	6.5
SiO_2	51.9	51.6	52.1	51.7	51.5	53.3	52.9	52.6
K_2O	0.0	0.0	0.0	0.0		0.0	0.0	
CaO	6.1	5.9	6.4	6.2	6.1	6.8	6.6	6.6
TiO_2	0.3	0.3	0.3	0.3	0.3	0.3	0.3	0.3
Cr_2O_3	0.8	0.8	0.7	0.7	0.6	0.6	0.6	0.4
MnO	0.6	0.6	0.6	0.6	0.5	0.6	0.6	0.5
FeO	16.1	16.2	16.7	16.8	16.9	15.9	16.1	16.2
Total	100.0	100.0	100.0	100.0	100.0	100.0	100.0	100.0
Mg#	65.8	66.4	63.8	64.4	65.3	63.3	63.9	64.7
Fo	86.7	86.7	85.5	85.5	85.3	84.9	84.9	84.8
En								
Wo								
Kdol	0.30	0.30	0.30	0.31	0.32	0.31	0.32	0.33
KdCalc	0.32	0.32	0.33	0.32	0.32	0.33	0.33	0.32

Table 3-4 (continued)

No.	CH-13	CH-13q	CH-13HM	CH-14	CH-14q	CH-14HM	CH-15	CH-15q	CH-15HM
T(°C)	1330	1330	1330	1300	1300	1300	1280	1280	1280
Wt fraction (%)									
Na_2O	0.2	0.2	0.2	0.2	0.2	0.2	0.4	0.4	0.2
MgO	14.2	14.8	14.9	12.8	13.4	13.5	11.8	12.4	12.1
Al_2O_3	7.7	7.5	7.2	9.0	8.8	8.3	10.0	9.7	9.6
SiO_2	52.7	52.4	52.8	52.6	52.2	52.2	52.4	52.1	52.7
K_2O	0.1	0.1		0.4	0.4		0.2	0.2	
CaO	7.4	7.2	7.4	8.5	8.3	8.7	9.2	9.0	9.3
TiO_2	0.4	0.4	0.5	0.4	0.4	0.4	0.4	0.4	0.5
Cr_2O_3	0.5	0.5	0.4	0.4	0.4	0.3	0.3	0.3	0.2
MnO	0.6	0.6	0.5	0.6	0.6	0.5	0.5	0.5	0.4
FeO	16.1	16.3	16.3	15.2	15.4	15.9	14.8	15.1	15.1
Total	100.0	100.0	100.0	100.0	100.0	100.0	100.0	100.0	100.0
Mg#	61.1	61.8	62.0	60.0	60.8	60.3	58.7	59.5	58.8
Fo	83.5	83.5	83.4	82.8	82.8	82.1	82.0	82.0	81.9
En	84.7	84.7	84.1	84.0	84.0	82.6	82.2	82.2	81.5
Wo	1.1	1.1	1.2	1.5	1.5	1.5	2.0	2.0	2.1
Kdol	0.31	0.32	0.32	0.31	0.32	0.33	0.31	0.32	0.32
KdCalc	0.33	0.32	0.33	0.32	0.32	0.32	0.32	0.32	0.33

No.	CH-16	CH-16HM	CH-17	CH-17HM
T(°C)	1250	1250	1200	1200
Wt fraction (%)				
Na_2O	0.4	0.3	0.5	0.3
MgO	11.0	10.4	9.0	8.4
Al_2O_3	11.7	11.3	14.1	14.0
SiO_2	51.8	52.1	51.6	52.0
K_2O	0.0		0.0	
CaO	9.9	10.4	11.3	11.8
TiO_2	0.4	0.4	0.5	0.5
Cr_2O_3	0.2	0.2	0.0	0.1
MnO	0.5	0.4	0.5	0.4
FeO	14.1	14.6	12.5	12.7
Total	100.0	100.0	100.0	100.0
Mg#	58.2	55.8	56.2	54.2
Fo	81.4	80.2	81.0	79.3
En	79.8	79.3	74-79	75.7
Wo	3.3	3.4	4-8	6.0
Kdol	0.32	0.31	0.30	0.31
KdCalc	0.32	0.33	0.32	0.33

Table 3-4 (continued) ED experiments

No.	ED-1	ED-1[1]	ED-2	ED-2[1]	ED-2HM1	ED-2HM2	ED-2HM3
T(°C)	1420	1420	1400	1400	1400	1400	1400
Wt fraction (%)							
Na_2O	0.2	0.2	0.2	0.2	0.2	0.2	0.2
MgO	18.4	18.2	18.6	18.3	17.7	17.7	17.9
Al_2O_3	6.5	6.4	6.6	6.5	5.8	5.7	5.7
SiO_2	51.4	51.0	51.9	51.1	51.1	51.4	51.6
K_2O	0.0	0.0	0.0	0.0			
CaO	5.1	5.1	5.3	5.2	5.4	5.4	5.3
TiO_2	0.3	0.3	0.3	0.3	0.3	0.3	0.3
Cr_2O_3	0.8	0.8	0.7	0.7	0.8	0.8	0.8
MnO	0.5	0.5	0.6	0.6	0.6	0.6	0.6
FeO	16.8	17.5	15.8	17.1	18.1	17.8	17.7
Total	100.0	100.0	100.0	100.0	100.0	100.0	100.0
Mg#	66.1	65.0	67.7	65.6	63.6	63.9	64.4
Fo							
En							
Wo							
Kdol							
KdCalc							

No.	ED-3	ED-3[1]	ED-3HM	ED-3HM'	ED-4	ED-4[1]	ED-4HM
T(°C)	1370	1370	1370	1350	1330	1330	1330
Wt fraction (%)							
Na_2O	0.3	0.3	0.2	0.2	0.3	0.3	0.3
MgO	17.4	17.3	17.5	15.8	15.0	14.8	14.9
Al_2O_3	6.4	6.3	5.7	6.1	7.2	7.1	6.7
SiO_2	52.5	52.1	51.5	52.1	51.9	51.5	52.3
K_2O	0.0	0.0			0.1	0.1	
CaO	5.3	5.3	5.4	5.9	6.2	6.1	6.3
TiO_2	0.3	0.3	0.3	0.3	0.4	0.4	0.4
Cr_2O_3	0.6	0.6	0.7	0.6	0.5	0.5	0.5
MnO	0.6	0.6	0.7	0.6	0.6	0.6	0.7
FeO	16.6	17.3	17.9	18.2	17.8	18.5	18.0
Total	100.0	100.0	100.0	100.0	100.0	100.0	100.0
Mg#	65.1	64.0	63.5	60.7	60.0	58.9	59.6
Fo	84.6	84.6	84.5	82.7	81.5	81.5	81.9
En					82.8	82.8	82.7
Wo					1.0	1.0	0.9
Kdol	0.34	0.34	0.32	0.32	0.34	0.34	0.33
KdCalc	0.32	0.32	0.32	0.33	0.33	0.33	0.33

Table 3-4 (continued)

No.	ED-5	ED-5[1]	ED-5HM	ED-6	ED-6[1]	ED-6HM	ED-7	ED-7HM
T(°C)	1300	1300	1300	1280	1280	1280	1250	1250
Wt fraction (%)								
Na_2O	0.5	0.5	0.2	0.5	0.5	0.3	0.5	0.3
MgO	13.0	12.9	12.9	11.9	11.8	11.3	9.5	10.4
Al_2O_3	8.4	8.3	7.7	8.5	8.4	8.4	10.1	9.2
SiO_2	51.0	50.5	51.7	51.1	50.7	50.9	50.3	51.6
K_2O	0.0	0.0		0.1	0.1		0.0	
CaO	7.1	7.0	7.2	7.7	7.6	8.1	8.8	8.5
TiO_2	0.4	0.4	0.5	0.5	0.5	0.5	0.5	0.4
Cr_2O_3	0.3	0.3	0.4	0.4	0.4	0.4	0.0	0.1
MnO	0.6	0.6	0.7	0.6	0.6	0.6	0.6	0.5
FeO	18.7	19.5	18.8	18.7	19.4	19.6	19.7	19.0
Total	100.0	100.0	100.0	100.0	100.0	100.0	100.0	100.0
Mg#	55.3	54.1	55.0	53.1	51.9	50.7	46.2	49.4
Fo	78.6	78.6	78.9	76.8	76.8	76.1	73.2	75.4
En	80.1	80.1	80.5	79-84	79-84	78.5	75-81	79.4
Wo	1.4	1.4	1.1	1.5	1.6	1.8	2.0	1.7
Kdol	0.34	0.34	0.33	0.34	0.34	0.32	0.31	0.32
KdCalc	0.32	0.32	0.33	0.33	0.32	0.33	0.33	0.33

No.	ED-8	ED-8HM	ED-9	ED-9HM	ED-10	ED-10HM	ED-11	ED-12
T(°C)	1220	1220	1200	1200	1180	1180	1160	1140
Wt fraction (%)								
Na_2O	0.5	0.3	0.5	0.3	0.6	0.4	0.5	0.5
MgO	8.7	8.7	7.7	7.6	7.3	6.9	6.3	5.7
Al_2O_3	10.8	10.5	12.0	11.3	12.5	12.6	13.3	12.8
SiO_2	50.7	51.1	50.4	50.5	50.0	50.6	50.4	49.5
K_2O	0.1		0.0		0.1		0.2	0.2
CaO	9.5	9.8	9.9	10.2	10.4	10.8	10.3	10.5
TiO_2	0.6	0.6	0.6	0.6	0.7	0.7	1.0	2.0
Cr_2O_3	0.2	0.2	0.1	0.1	0.2	0.1	0.0	0.0
MnO	0.5	0.4	0.5	0.4	0.5	0.4	0.5	0.4
FeO	18.3	18.4	18.3	19.0	17.7	17.4	17.5	18.3
Total	100.0	100.0	100.0	100.0	100.0	100.0	100.0	100.0
Mg#	45.9	45.6	42.9	41.6	42.4	41.4	39.1	35.7
Fo	71.4	72.2		69.5	68.4	68.7		
En	72-80	74.2	72-81	74.2	70-79	67.4	63-67	60-64
Wo	2.5	3.0	3	4.0	4	5.6	5-8	5-7
Kdol	0.34	0.32		0.31	0.34	0.32		
KdCalc	0.33	0.33	0.33	0.33	0.33	0.33		

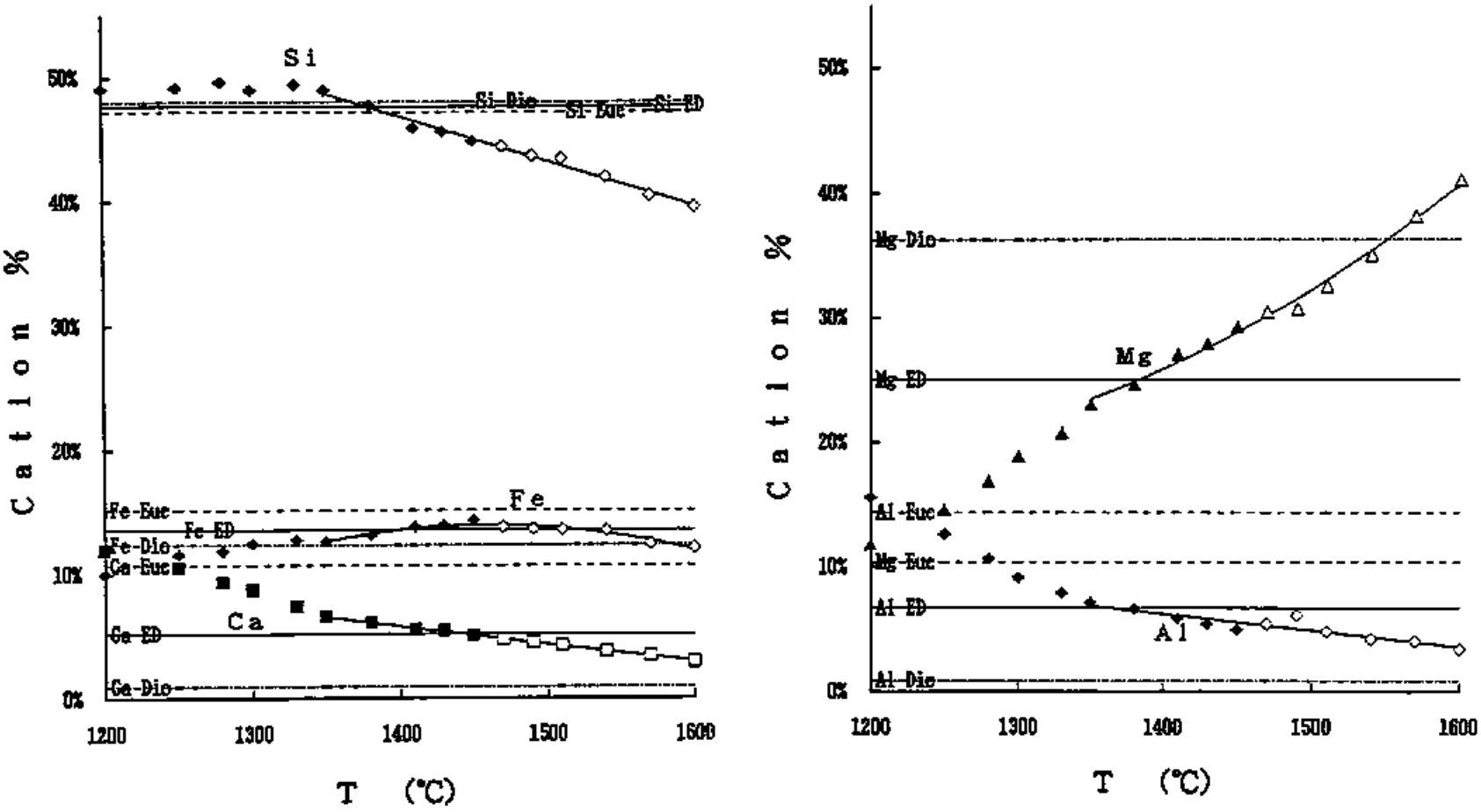

Figure 3-3
Si, Mg, Fe, Al and Ca cation contents of the melt in CH experiments (open symbols) and CH-HM experiments (solid symbols) from 1200°C to 1600°C. Fitting curves as quadratic function of the temperature from 1350°C to 1600°C are also shown. The Al and Ca contents decrease monotonously with increase of temperature and Mg monotonously increases. Si content has a maximum at around 1350°C and the Fe content has a maximum due to increasing of the Al and Ca contents with decreasing temperature. Contents of average diogenite (Dio), average noncumulate eucrite (Euc) and starting material of ED experiments (ED) are also shown.

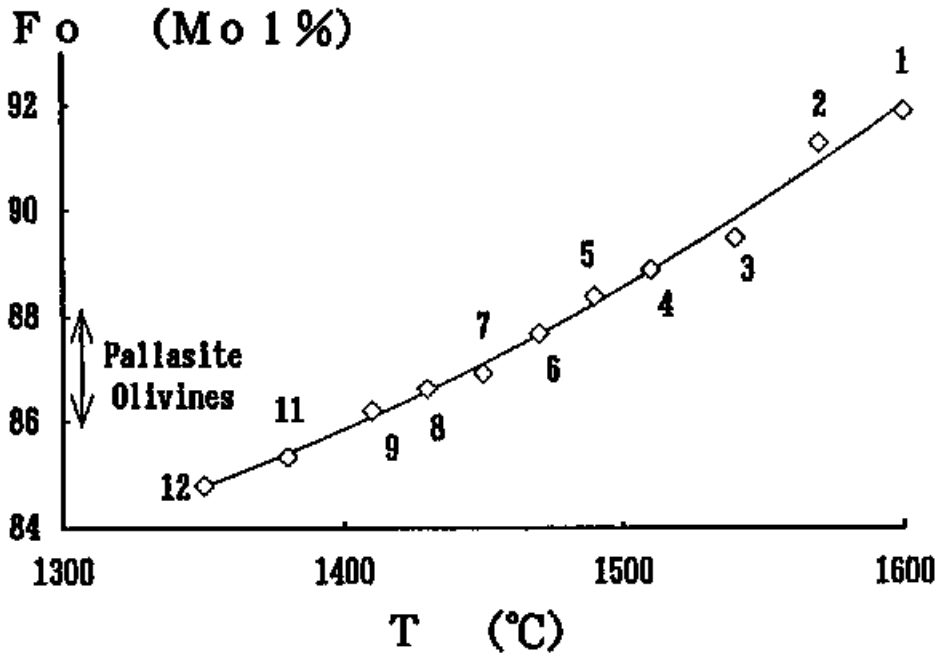

Figure 3-4
Compositions of olivines (forsterite mol %) in the temperature range from 1600°C to 1350°C. Numbers correspond to those in Table 2-4. A solid line is a fitted curve for the Fo content versus temperature. A vertical bar represents the main composition range of pallasitic olivines (Dodd, 1981).

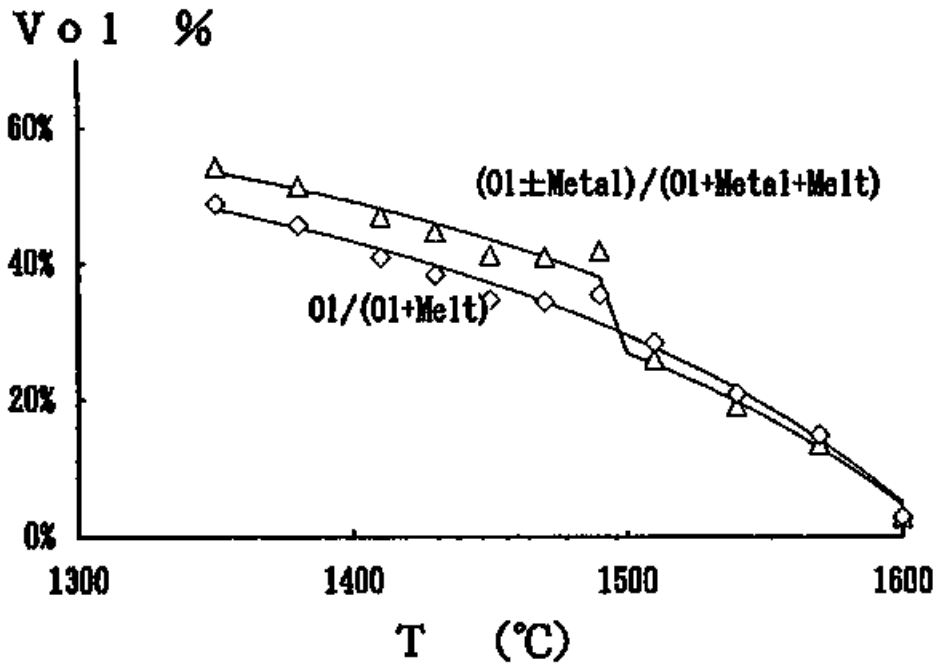

Figure 3-5
Volume fractions of olivine and solid phases including olivine and metallic Fe-Ni below 1500°C are calculated from the compositions of olivine and melt. Curves are calculated using the temperature-composition curves in Figures 3-3 and 4.

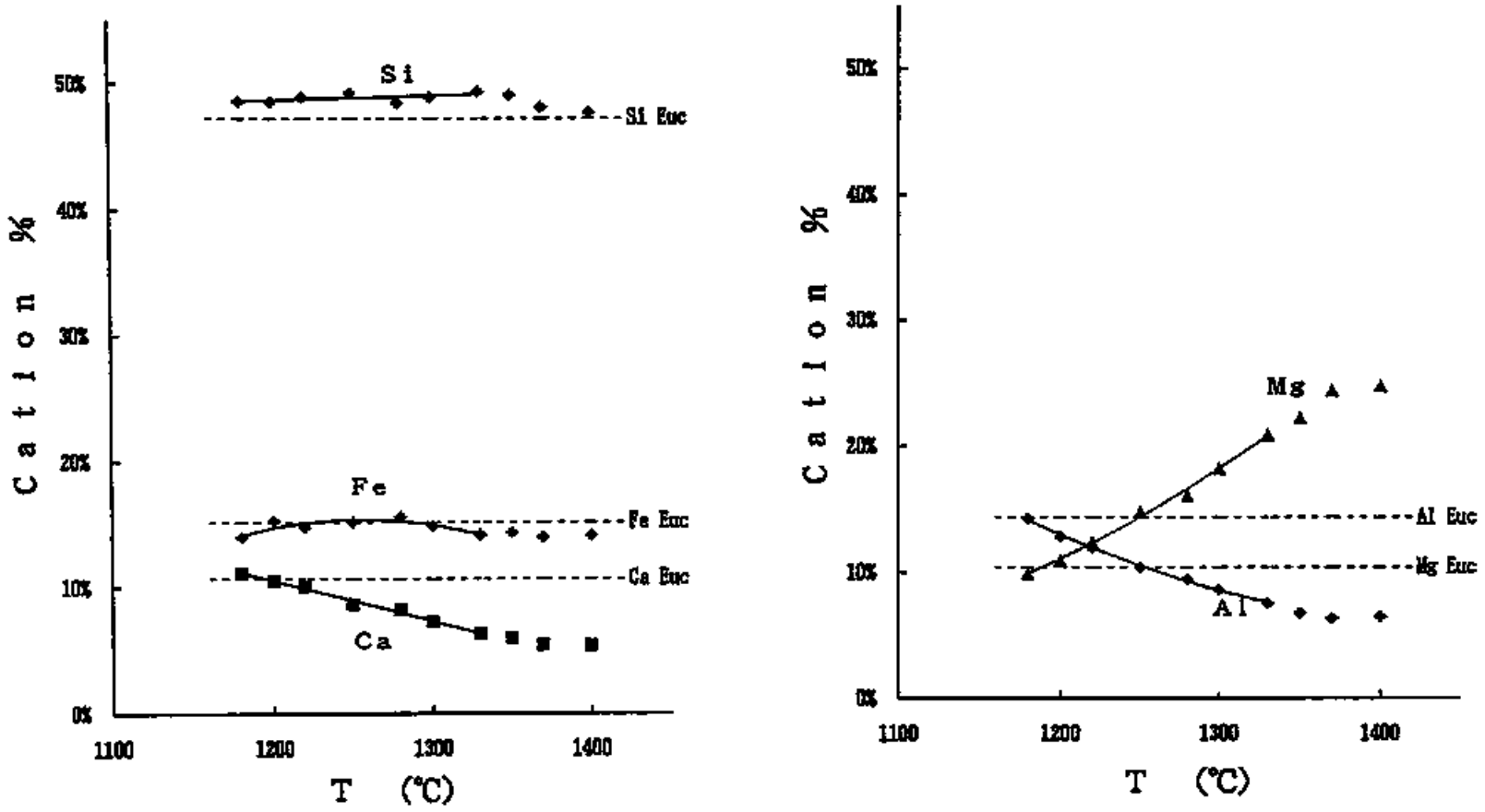

Figure 3-6

Si, Mg, Fe, Al and Ca cation contents of the melt produced in ED experiments (open symbols) and ED-HM experiments (solid symbols) at temperature range from 1140°C to 1420°C. Compared with Figure 3-3, the Al and Ca contents have similar tendency with temperature change, but fitting curves for the Si and Fe are more flat and inclination of the Mg content is steep. Composition of average noncumulate eucrite is also shown.

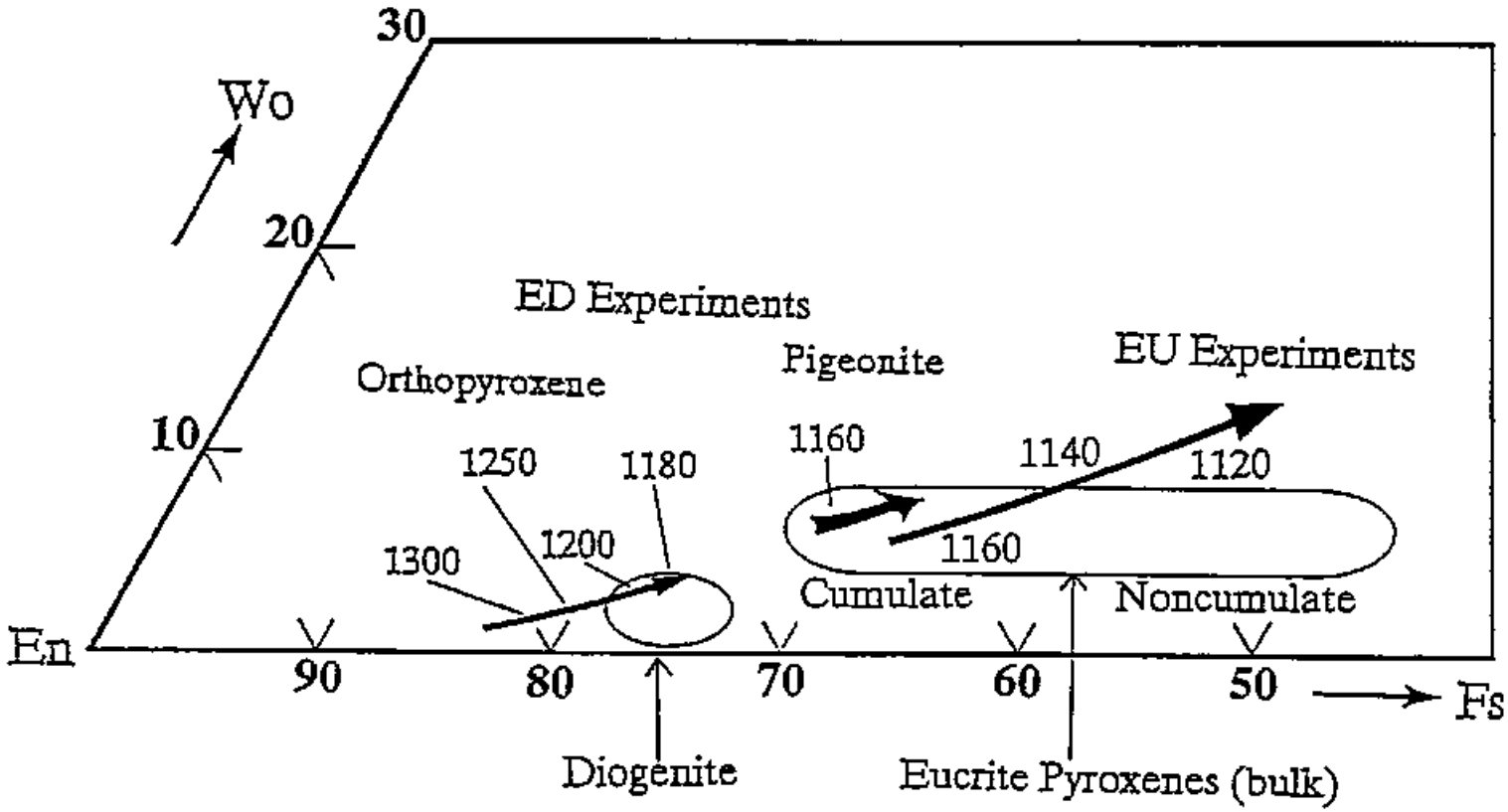

Figure 3-7
Compositional trends of pyroxenes in ED-HM experiments (orthopyroxene) and ED and EU experiments (pigeonite) plotted in a pyroxene quadrilateral (three thick arrows). Numbers indicate the experimental temperatures. Compositional range of diogenitic orthopyroxenes and the bulk composition of eucritic pigeonite are also shown. Pyroxenes of cumulate eucrites have more Mg-rich composition than those of noncumulate eucrites.

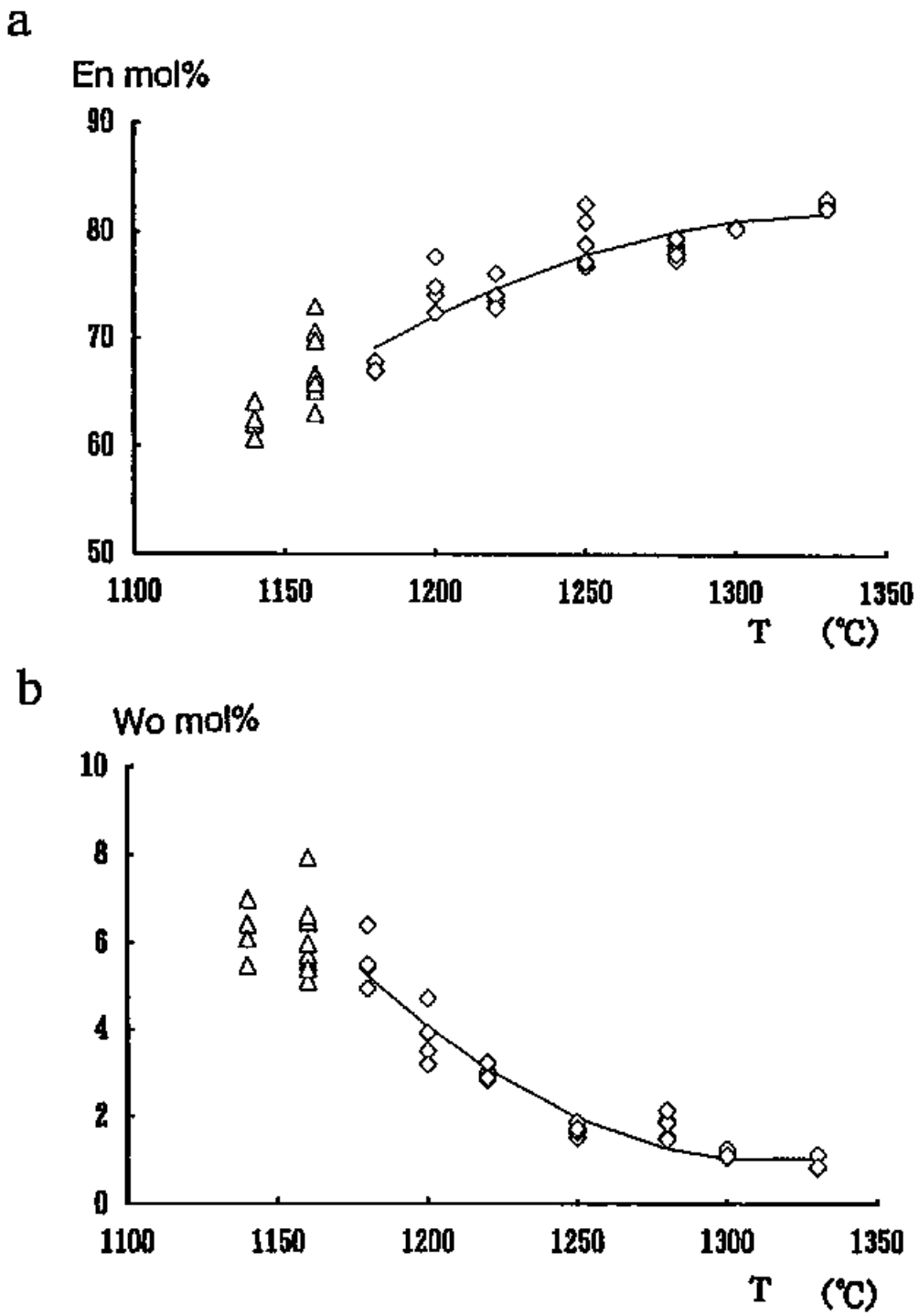

Figure 3-8
(a) Enstatite component and (b) wollastonite component of each analysis of the pyroxenes in ED-HM experiments plotted against temperature. Lines are fitting curves for the orthopyroxene (open diamond) in the temperature range from 1180 to 1330°C. At lower temperature, (1140°C and 1160°C, ED experiments, open triangle), pyroxene is pigeonite, and those are omitted from the calculation.

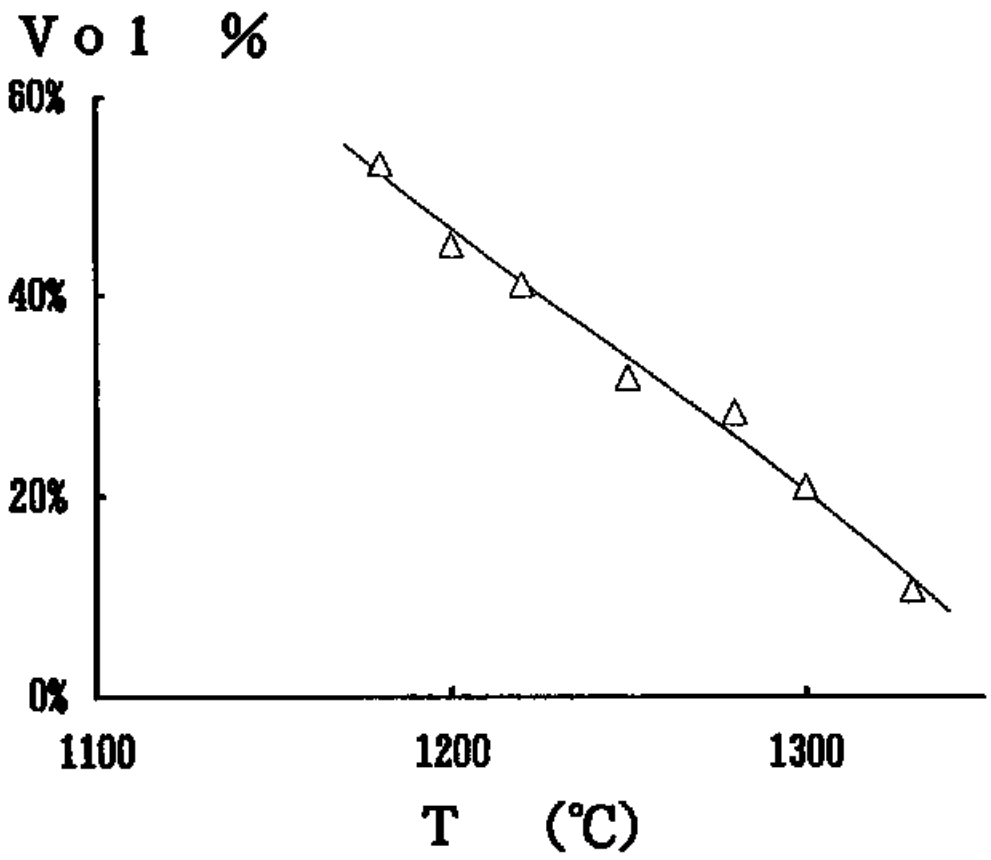

Figure 3-9
Volume fraction of solid phase (olivine and pyroxene) in ED-HM experiments calculated from the compositions of olivine, pyroxene and melt.

4 Discussion

4-1 Melting relations on the 'pseudo-liquidus' diagrams

The 'pseudo-liquidus' diagram of the system SiO_2-Ol-An plotted from Wo component (Stolper, 1977) is convenient to discuss crystallization and melting of the magma in HEDP (or HEDD)-PB. The locations of phase boundaries are important to study the origin of the magma on the parent body. Therefore, the phase relation obtained by the present experiments, especially the locations of the Ol-Px phase boundary and nature of a coexisting point of Ol-Px-Pl are discussed in this section.

[Chondritic material]

The chemical compositions of the starting material and the melts in the CH and CH-HM experiments are plotted in the 'pseudo-liquidus' diagrams (Figures 4-1a and 4-1c). In these diagrams, plots of the individual analyses of the melt composition is scatted typically in an oval of 2%x3%.

In the diagram projected from Wo component to the SiO_2-Ol-An plane, the averaged melt composition of each run moves from the starting material right-upward along the extension of the Ol-starting material tie-line as the temperature decreases until pyroxene appears (olivine control line, CH-1 - CH-12 in Figure 4-1a). Below the crystallization temperature of pyroxene, the melt composition moves rightward nearly horizontally (run CH-13 to CH-17 in Figure 4-1a). In the diagram projected from Wo+An component to the SiO_2-Fo-Fa plane, the olivine control line curves due to the change of the Mg/Fe composition of olivine (Figure 4-1c). After the pyroxene crystallization,

the location of the melt composition does not change largely in this plot. These lines which are formed by the melt composition with decreasing temperature are liquid lines of descent from the CH starting material.

In the 'pseudo-liquidus' diagrams, the average compositions of diogenites and noncumulate eucrites are also shown (Figures 4-1a and 4-1c). As seen in these diagrams and Figure 3-3, any melts in the experiments do not have the composition of diogenite or eucrite. However, it should be noted that the composition of the melt around 1400°C (run CH-9HM and CH-11HM) is similar to that of the mixture of 55 wt.% of average diogenite and 45 wt.% of average noncumulate eucrite.

The compositions of the melt coexisting with olivine (+chromite) and pyroxene in the 'pseudo-liquidus' diagram (Figure 4-1) are plotted again in Figure 4-2. The line on which the plots of the melts with olivine and pyroxene are is the olivine-pyroxene (Ol-Px) phase boundary of the liquid line of descent of the CH material. As seen in the figure, tangents of the boundary cross the Ol-SiO_2 tie line near the point of Px. This shows that the boundary is a middle line between reaction and cotectic lines. Mg# of the melt on the Ol-Px phase boundary changes from 62 to 54 with decreasing temperature.

The position of Ol-Px-Pl peritectic point of CH starting material cannot be determined by the present experiments due to its small melt fraction at around the peritectic point.

[Eucrite-diogenite mixture]

The melt compositions are plotted in the 'pseudo-liquidus' diagrams (Figure 4-4). In both diagrams in the system SiO_2-Ol-An and SiO_2-Fo-Fa, the composition of the melt moves from the starting material to the

composition near noncumulate eucrites as temperature decreases. Especially, the melt at about 1200°C has similar composition to the average of noncumulate eucrites although the SiO_2 content is slightly higher than that of the average eucrite. The bulk compositions of three noncumulate eucrite, Y-74450, Sioux County and Stannern are also shown in Table 3-2.

Like as the case of CH experiments, phase boundaries and the compositions of the melt are plotted in a 'pseudo-liquidus' diagram in Figure 4-2. The Ol-Px phase boundary was determined from the compositions of the melt coexisting with olivine and pyroxene (+chromite). Mg# of the melts on the phase boundary changes from 60 to 41 with decreasing temperature. The boundary is a neutral line between cotectic and reaction lines because extension of the phase boundary crosses the Ol-SiO_2 tie line around the position of Px.

The location of Ol-Px phase boundary by ED experiments with the Mg# of around 60 is almost same position to that by CH experiments (Figure 4-2). Consequently, Ol-Px phase boundaries on the liquid lines of descent from CH and ED experiments must not be essentially different at around 1330°C, the first pyroxenes crystallizing temperature.

Longhi and Pan (1988) determined the phase diagrams of lunar basalt-like materials by partial melting experiments (Figure 4-3). They determined the phase boundary and Ol-Px-Pl peritectic point for each Mg# from the experiments with wide range of Ca composition. Compositions of melts by their experiments have higher TiO_2 and CaO and lower alkali content than those of the present experiments to represent lunar basalt.

The Ol-Px phase boundary in the diagrams of Longhi and Pan (1988) is a reaction line at Mg#=75 and a cotectic line at Mg#=60. As

shown in Figure 4-2, their Ol-Px phase boundary at Mg#=60 is not concordant with the present experiments at around 1330°C. On the other hand, it is concordant with the present experiments at the temperature below 1250°C when variation of Mg# is considered.

The composition of the melt which can first coexist with olivine and pyroxene is very important to discuss the evolution process of diogenites and eucrites. Longhi and Pan (1988) did not determine such composition. Furthermore, their phase boundary can not be extended to the area in which pyroxene begins to crystallize to discuss the HED evolution. Because their phase boundary may shift away from SiO_2 by their lower alkali and higher TiO_2 content than those of the system to be used in discussion of the HED evolution.

[Eucritic material]

Some of the melt compositions are plotted in the 'pseudo-liquidus' diagrams (Figures 4-2 and 4-4). The Fe content in the melts becomes higher, while the Mg and Al contents become lower with decreasing the temperature. Thus, the melt compositions become away from the bulk compositions of eucrites. A line estimated by the row of the data points is the Px(Pig)-Pl phase boundary starting from the Ol-Px-Pl peritectic point. The location of the phase boundary is similar to that of Stolper (1977) reduced from the melting experiments of Juvinas and Sioux County eucrites.

Figure 4-1

Compositional change of melts in CH and CH-HM experiments in the 'pseudo-liquidus' diagrams of Stolper (1977) (SiO_2-Ol-An system projected from Wo component in Figures 4-1a and 1b, SiO_2-Fo-Fa system projected from Wo and An component in Figures 4-1c and 1d). Molar units are used to project and compositions are recalculated as follows.

SiO_2: $SiO_2 - 0.5\cdot(FeO+MgO+MnO) - 5\cdot(Na_2O+K_2O) - Al_2O_3 - CaO$

Forsterite: $0.5\cdot MgO$

Fayalite: $0.5\cdot(FeO+MnO)$

Olivine: Forsterite + Fayalite

Anorthite: $Al_2O_3 - Na_2O - K_2O$

Wollastonite: $CaO + Na_2O + K_2O - Al_2O_3$

Abbreviations; Ol: olivine, An: anorthite, Px: pyroxene, Fo: forsterite, Fa: fayalite, Wo: wollastonite, En: enstatite and Fs: ferrosilite. Numbers of solid circles are the run number listed in Table 2-4. The bulk compositions of three noncumulate eucrite are also plotted, Y: Yamato-74450, ST: Stannern, SC: Sioux County. Figures 4-1b and 1d are reproduced from Stolper's Figures 5 and 6 on the same area of Figures 4-1a and 1c, respectively. Clustering of the bulk compositions of noncumulate eucrites can be seen in Figures 4-1b and 1d.

Figure 4-1a and 1b

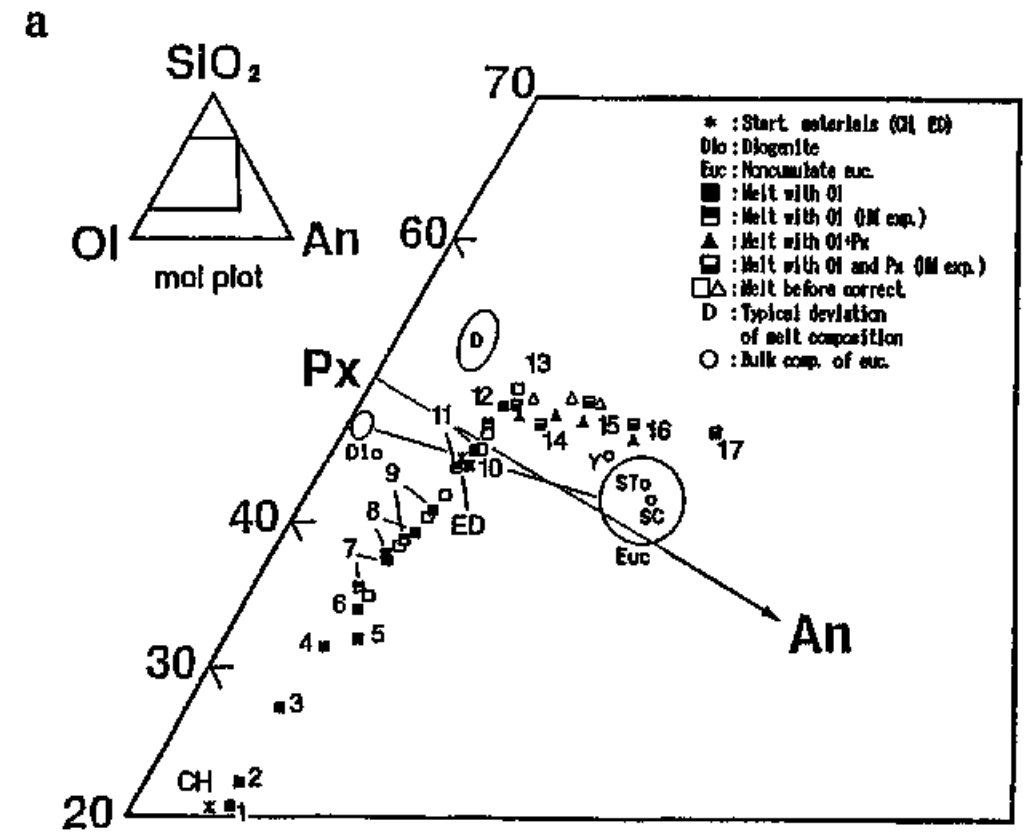

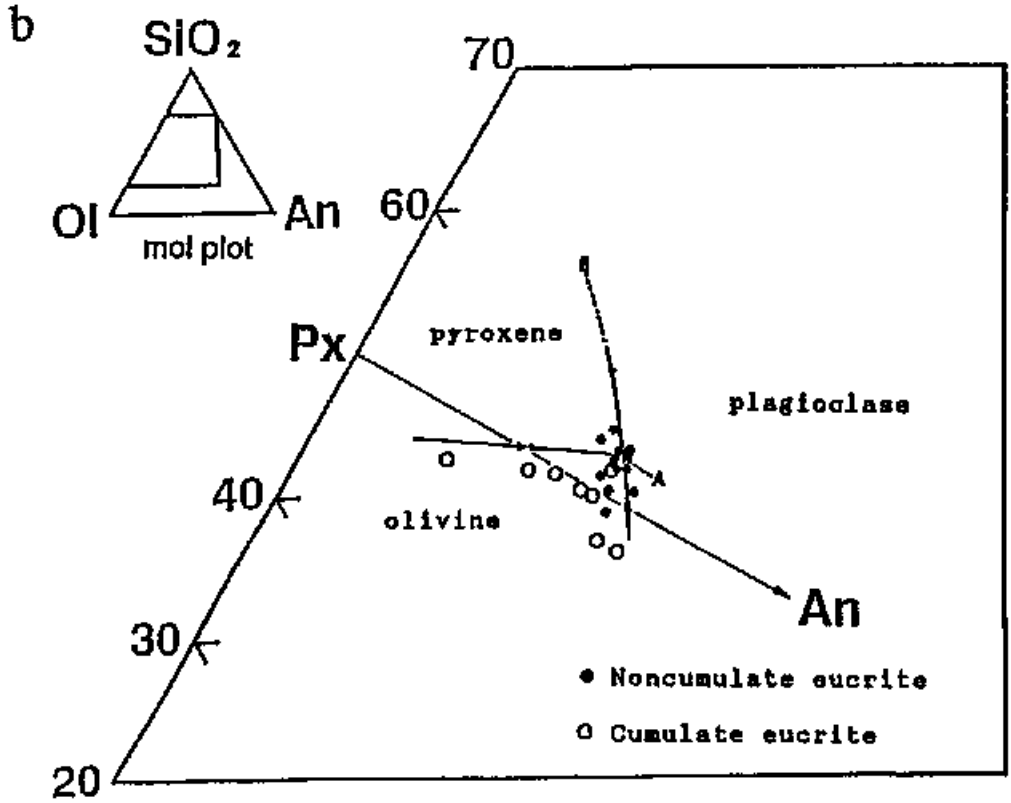

Figure 4-1c and 1d

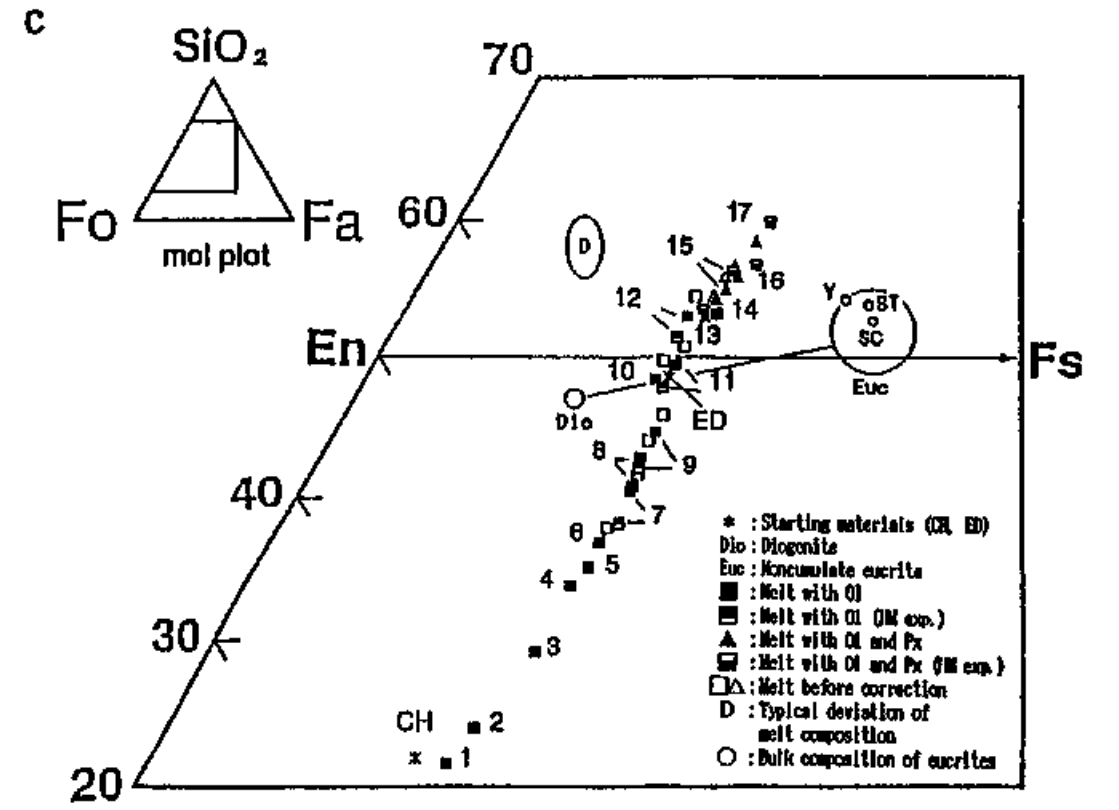

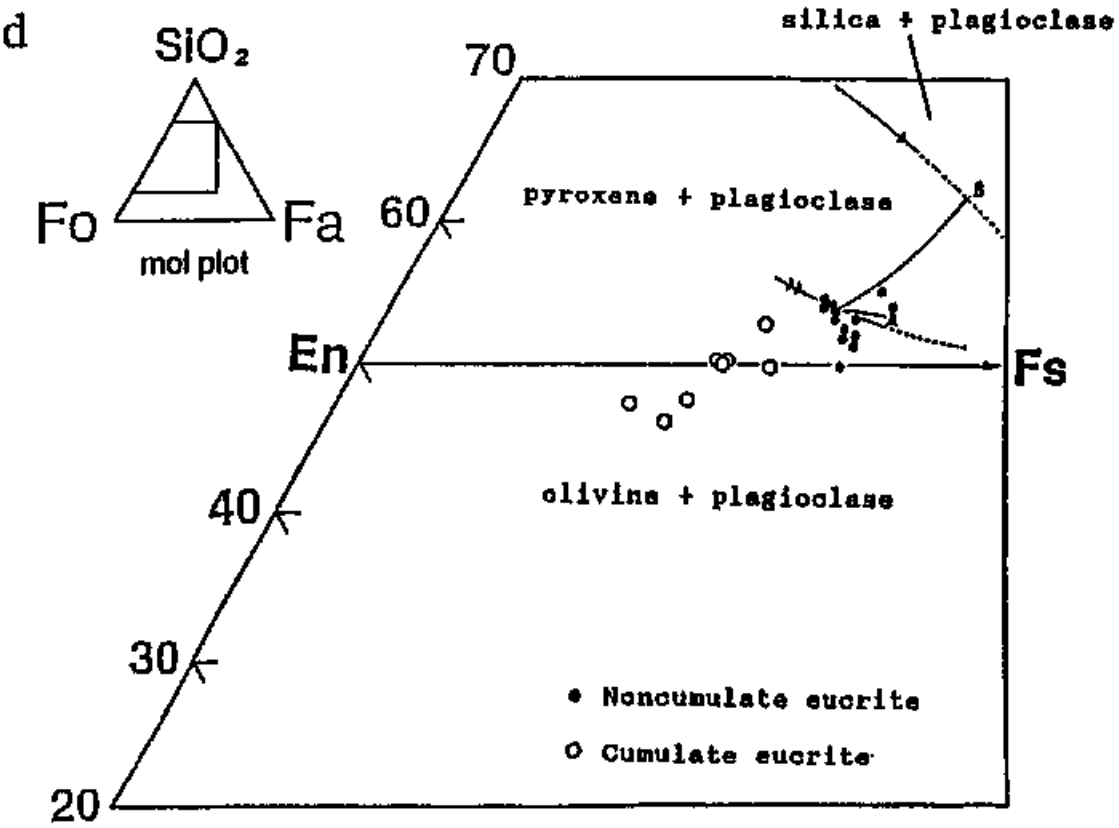

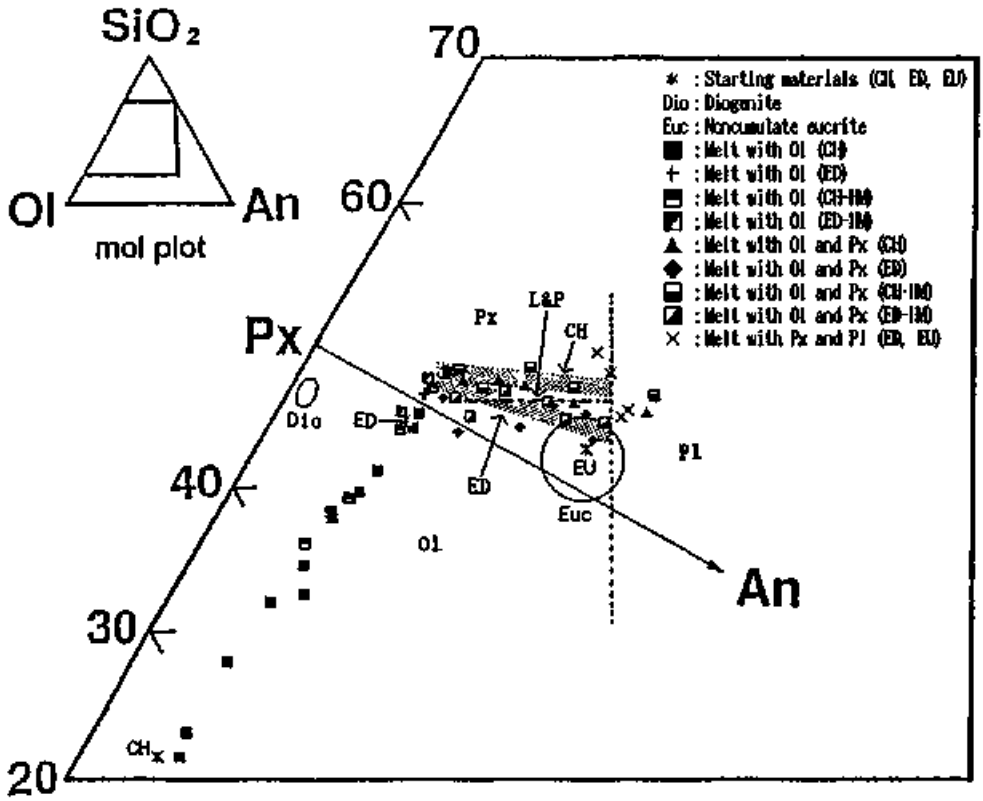

Figure 4-2

Phase diagram of SiO_2-Ol-An system based on the results of CH-HM, ED-HM and EU experiments. Projection is the same as that of Figure 4-1 (mol unit). Hatched bars labeled "CH" and "ED" are the Ol-Px phase boundary on the liquid line of descent from CH and ED starting materials, respectively. Dot-and-dashed line labeled "L&P" is Ol-Px phase boundary from Longhi and Pan (1988) at Mg#=60. Average diogenites (Dio) and noncumulate eucrites (Euc) are also plotted.

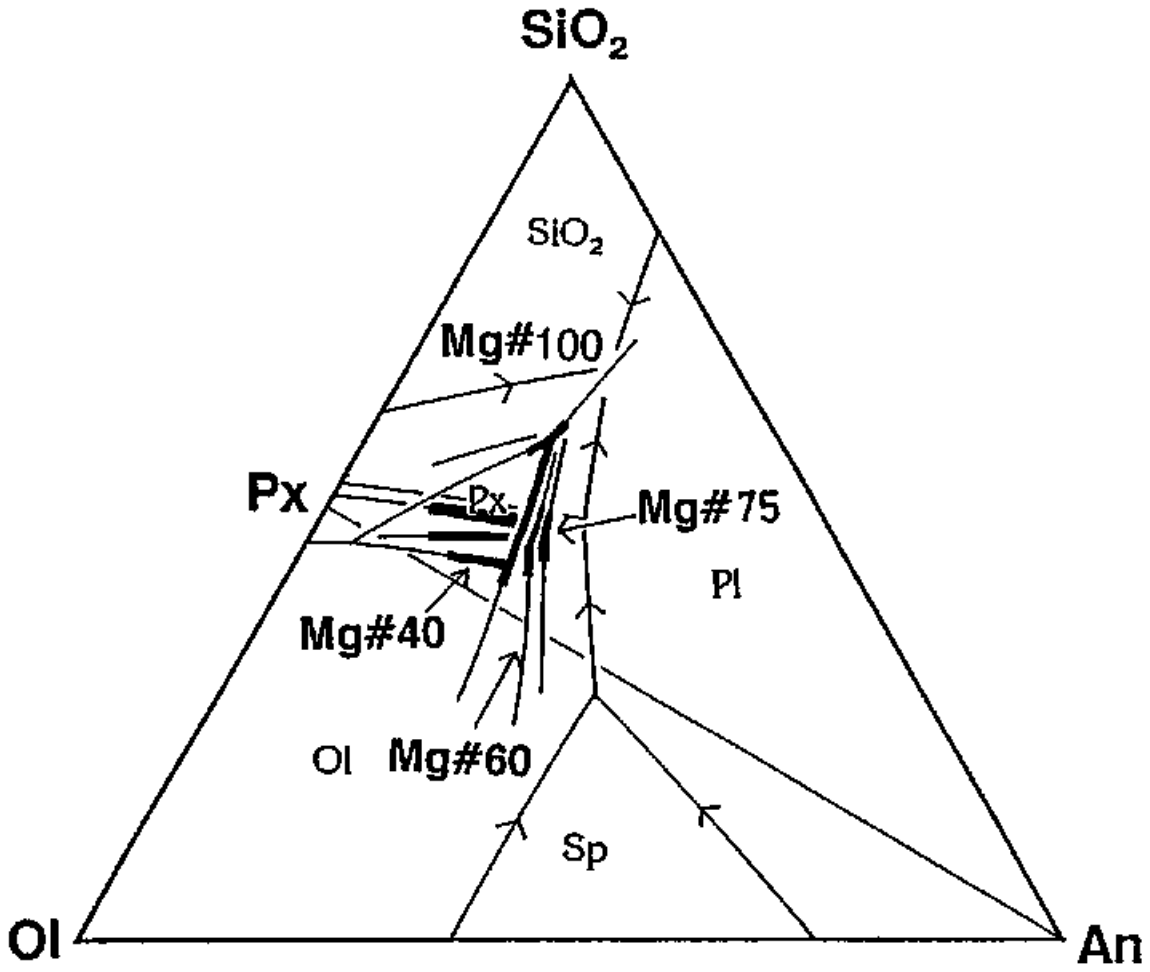

Figure 4-3

Phase diagrams of SiO_2-Ol-An system projected from Wo component obtained by Longhi (1987) for SiO_2-Fo-An system and Longhi and Pan (1988) for lunar basalt-like materials. Ol-Px phase boundary shifts to Ol side with decreasing Mg# of the melt. Those are reaction line at Mg#=75 and Mg#=100, and cotectic lines at Mg#=60 and 40.

Figure 4-4

Compositional change of melts in ED, ED-HM and EU experiments in the 'pseudo-liquidus' diagrams of Stolper (1977) (SiO_2-Olivine-Anorthite system in Figure 4-4a and SiO_2-Forsterite-Fayalite system in Figure 4-4b). Molar units are used. Numbers correspond to those in Table 2-4 and abbreviations are the same as those in Figure 4-1. The composition of melt in run# ED-10HM experiments (1180°C), starting material of EU experiments and Stannern meteorite are plotted almost the same position. Plots of melt compositions of EU experiments are parallel to the pyroxene-plagioclase phase boundary in Figure 4-4b and 4d, and cumulate eucrites are plotted in the area of the counterpart of those of the melt compositions of EU experiments.

Figure 4-4

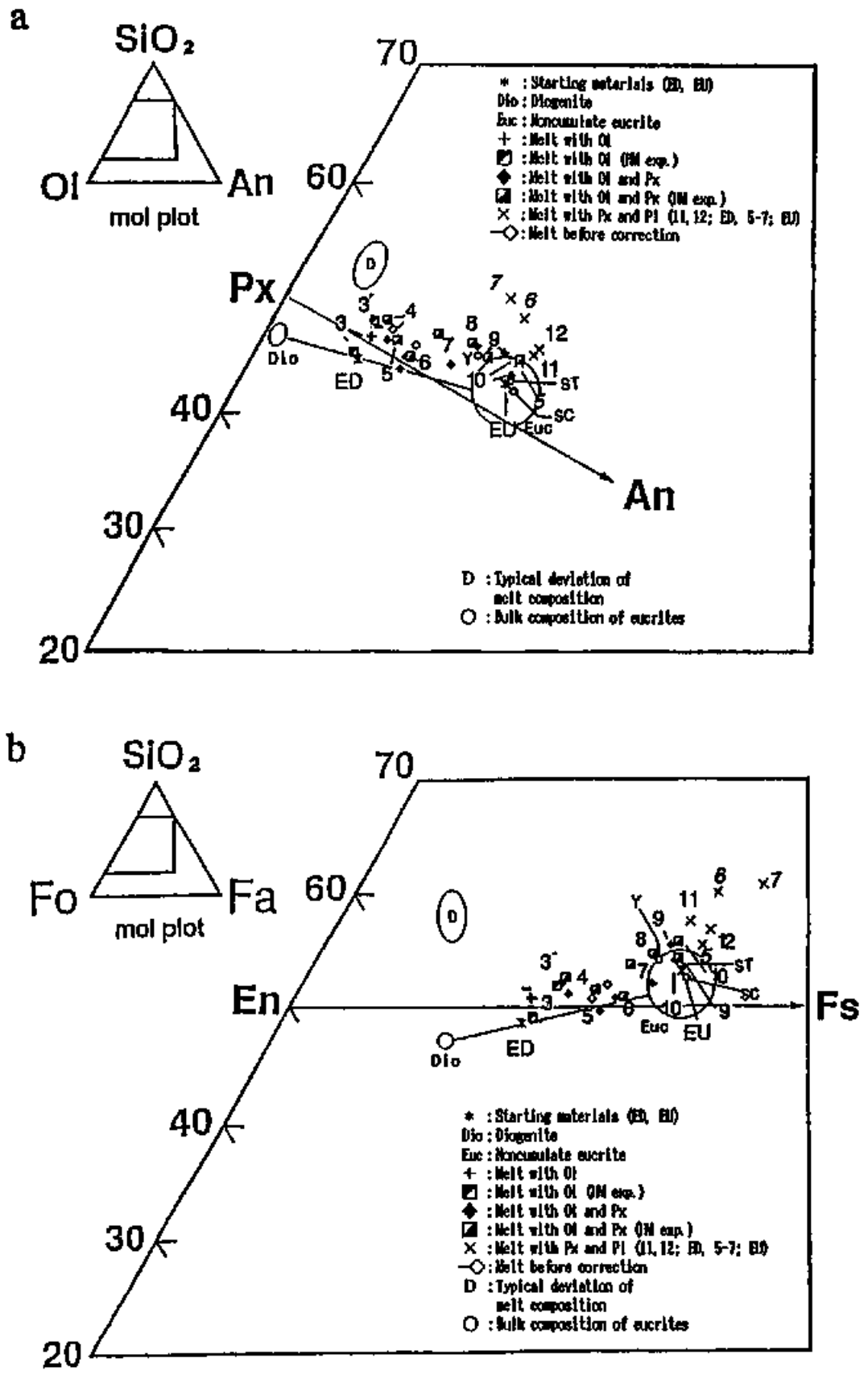
a
SiO2
Ol
An
mol plot
70
60
40
30
20
Px
An
Dio
ED
EU
Euc
ST
SC
* : Starting materials (ED, EU)
Dio : Diogenite
Euc : Noncumulate eucrite
+ : Melt with Ol
: Melt with Ol (FM exp.)
◆ : Melt with Ol and Px
: Melt with Ol and Px (FM exp.)
× : Melt with Px and Pl (11, 12; ED, 5-7; EU)
—◇— : Melt before correction
D : Typical deviation of melt composition
○ : Bulk composition of eucrites
b
SiO2
Fo
Fa
mol plot
70
60
40
30
20
En
Fs
Dio
ED
Euc
EU
ST
SC
* : Starting materials (ED, EU)
Dio : Diogenite
Euc : Noncumulate eucrite
+ : Melt with Ol
: Melt with Ol (FM exp.)
◆ : Melt with Ol and Px
: Melt with Ol and Px (FM exp.)
× : Melt with Px and Pl (11, 12; ED, 5-7; EU)
—◇— : Melt before correction
D : Typical deviation of melt composition
○ : Bulk composition of eucrites

4-2 Fractionation sequence

Three different series of the partial melting experiments with the different starting materials were conducted according to the hypothetical sequence of the solid-liquid separation in the parent body. In this section, the fractionation sequence will be discussed based on the results of the experiments.

[First stage of the solid-liquid separation]

In the HEDP-PB, there are three components to be explained to discuss evolution processes of the parent body. Those components are eucrite, diogenite and pallasite (or dunite and metallic iron). In these three kinds of components, what is generated at first?

First, the case where diogenite is generated at first directly from a chondritic material (case B in Figure 1-2), is simply denied because pyroxene is not a liquidus phase of a chondritic material (Figures 3-2 and 4-2).

Second, the case where eucrite is generated at first from the chondritic material and then diogenite and pallasite (or dunite) are formed (case C in Figure 1-2), will be discussed. Natural eucrites have the compositions around the peritectic point of Ol-Px-Pl (Figure 4-2) and Mg# of around 40 (Stolper, 1977). When the eucrite magma separated from its source material in chemical equilibrium, the source material should consist of olivine, pyroxene and plagioclase (and chromite and metallic Fe). If the bulk composition of the source material is chondritic, its Mg# should be around 65 (e.g., Consolmagno and Drake, 1977; Table 1-1). Solid phases in equilibrium with the eucritic melt is mainly composed of olivine and pyroxene with Mg# of around 75 deduced

from the results of ED experiments (Table 3-2). On the other hand, pyroxene in diogenite and olivine in pallasite have Mg# of around 75 and 87, respectively (See Appendix 1). Pyroxene in diogenite can coexist with the eucritic magma, but olivine in pallasite cannot. Therefore, the solid-liquid separation that generates eucrite from a chondritic material is not suggested as long as a redox reaction did not occur in the formation of pallasite.

The liquidus phase of the chondritic material is olivine (Figure 4-2). Therefore, a maximum fractionation process to produce eucritic magma directly from the chondritic material is also denied in this case because pallasite should be formed first during the cooling of the magma.

Last, the case where pallasite (or dunite) is at first directly formed from a chondritic material and then eucrite and diogenite are formed (case A in Figure 1-2), will be discussed. According to the results of CH experiments, where Mg# of silicate portion in the starting material is around 79, olivine of Fo_{88} can coexist with the melt of eucrite-diogenite mixture with Mg# of 65 at around 1400°C in equilibrium (Figures 3-4, 3-5 and 4-1, Table 3-1). This olivine composition is equal to that of pallasite olivine (see Appendix 1). If Fe-Ni metal in pallasites can also coexist with the olivine and the melt, pallasite can be explained by the separation of the olivine (and metallic Fe) from the coexisting melt in equilibrium. Furthermore, the melt obtained in this condition has the composition of eucrite-diogenite mixture.

Maximum fractionation process can also separate olivine in pallasite from the total melted chondritic material with the composition of the starting material of the CH experiments. The chemical composition of olivine crystallized in the maximum fractionation process can be

calculated based on the Fe-Mg partition coefficients between olivine and melt (Figure 4-5). The olivine crystals separated by the maximum fractionation process have a wide variation in the composition (Fo_{93-80}), and the average composition is $Fo_{88.5}$, which is almost the same as those of pallasitic olivine (Fo_{87}). However, the fractionated melt becomes more rich in Fe (Mg#=57) than the equilibrium melt (Mg#=65) (Figure 4-5) and it is too rich in Fe to generate eucrite and diogenite. Therefore, pallasite and the parent magma of eucrite-diogenite can not be explained by the maximum fractionation process from the present chondritic material.

On the other hand, Ikeda and Takeda (1985) proposed maximum fractionation of olivine to produce a dunite layer added to pallasite in the parent body model, based on the study of olivine fragments in a howardite. Ikeda (1989) further discussed a fractionation trend from a chondritic material with the bulk composition of Dreibus and Wänke (1980). The melt produced in this process has the Mg# of 63, and will produce the eucrite-diogenite association (Figure 4-5). Therefore, the maximum fractionation is possible as long as the hypothetical dunite layer is the member of the parent body of HED meteorites (HEDD-PB model). However, pallasitic olivine can not be formed in his model, because olivine crystallized changes its composition from Fo_{93} to Fo_{94} with the average of $Fo_{89.5}$, which is richer in Mg than the pallasitic olivine (Fo_{87}).

Uncertainty of Mg-Fe partitioning coefficients (±0.02) between olivine and melt brings the errors of ±0.5 mol% in calculated Fo content of olivine and ±1 mol% in Mg# of melt composition. These values of errors are sufficiently small to discuss the difference of the

compositions in the cases of equilibrium and maximum fractionation processes.

In conclusion of this section, pallasite in HEDP-PB can be formed from the present chondritic material by separation of olivine (and metal) in equilibrium with melt. In this case, the ratio of olivine and metal (2:1 in weight ratio) in pallasite deduced from the Fe content in the chondritic material is also consistent with those in natural pallasites. According to the results of the present experiments, temperature of this first stage of the solid-liquid separation is around 1400°C (Figures 3-4, 3-5 and 4-1, Table 3-1).

This temperature of 1400°C cannot be obtained by calculation on the fractionation processes. It can be only obtained by the partial melting experiments of the adequate starting material like the present study.

[Second stage of the solid-liquid separation]

In this section, generation of eucrite and diogenite will be discussed as the second stage of the solid-liquid separation to evolve the HEDP-PB. In ED experiments with the starting material with Mg# of 65, orthopyroxene with the composition similar to that in diogenite, and melt with the composition similar to that of eucrite (Mg#=40) are formed at about 1200°C (Figures 3-6, 3-7 and 4-4, Table 3-2). The composition of the solids mainly composed of orthopyroxene and small amounts of chromite and olivine, is also consistent with those of diogenite. This shows that diogenite and eucrite can be formed by separation of the melt and the solid in equilibrium at about 1200°C from the material with Mg# of 65 which consists of 55 wt.% of diogenite and 45 wt.% of eucrite. This temperature of 1200°C can be also obtained only by the

experiments.

It is not decided whether the Ol-Px phase boundary is reaction or cotectic line from the results of ED experiments as discussed earlier (Figure 4-2). The coexisting point of Ol-Px-Pl is peritectic. As far as the bulk composition of the starting material is in the Ol-Px-An triangle (Figure 4-2), and the system is in equilibrium, the melt change its composition with decreasing temperature and finally fixed at the peritectic point, no matter whether the Ol-Px phase boundary is a reaction or cotectic line.

On the other hand, when a maximum fractionation process takes place, the composition of the fractionated melt moves, depending upon whether the Ol-Px phase boundary is a reaction or cotectic line. The melt leaves from the Ol-Px boundary before reaching to the peritectic point in the case of reaction line, while it reached to the peritectic point in the case of a cotectic line. However, in both cases, the melt composition finally reaches to the eutectic point of Px-An-Silica.

The bulk compositions of noncumulate eucrites are similar to that of the peritectic point (Figure 4-2), and no differentiated meteorites whose chemical compositions are similar to that of the eutectic points of Px-An-Silica. Therefore, an equilibrium process is acceptable for the second stage of the solid-liquid separation, as pointed out by Stolper (1977) in his pioneer work on the formation of eucrite. Ikeda (1989) also prefers an equilibrium process for the formation of diogenite–eucrite.

On the other hand, Ikeda and Takeda (1985) concluded that the HED meteorites are formed by fractional crystallization to explain continuous compositional trend of fragments in a howardite based on the assumption that the Ol-Px phase boundary for the eucrite-diogenite

parent magma is a cotectic line. It might be possible in a local scale in the parent body, but the majority of the eucrite cannot be explained by this process as discussed above. Therefore, an equilibrium process is preferred here for the formation process of diogenite and eucrite.

Stolper (1977) preferred partial melting model to form eucrite magma due to difficulty of equilibrium crystallization in the natural system. However, as described in the above discussion on the fractionation sequence, the source material for eucritic magma should be the melt with the composition of the mixture of diogenite and eucrite. Therefore, if the partial melting process was operated in the formation of eucritic magma, two stages of heating process should be considered because the melt with the composition of the mixture of diogenite and eucrite must once cooled and solidified without the significant fractionation process before the partial melting to form eucrite. Because of the difficulties of the two stage heating, we prefer the equilibrium crystallization process for the diogenite-eucrite separation process.

The processes of the separation will be discussed in details in the next section, after taking the effects of densities and viscosity of the melts into consideration.

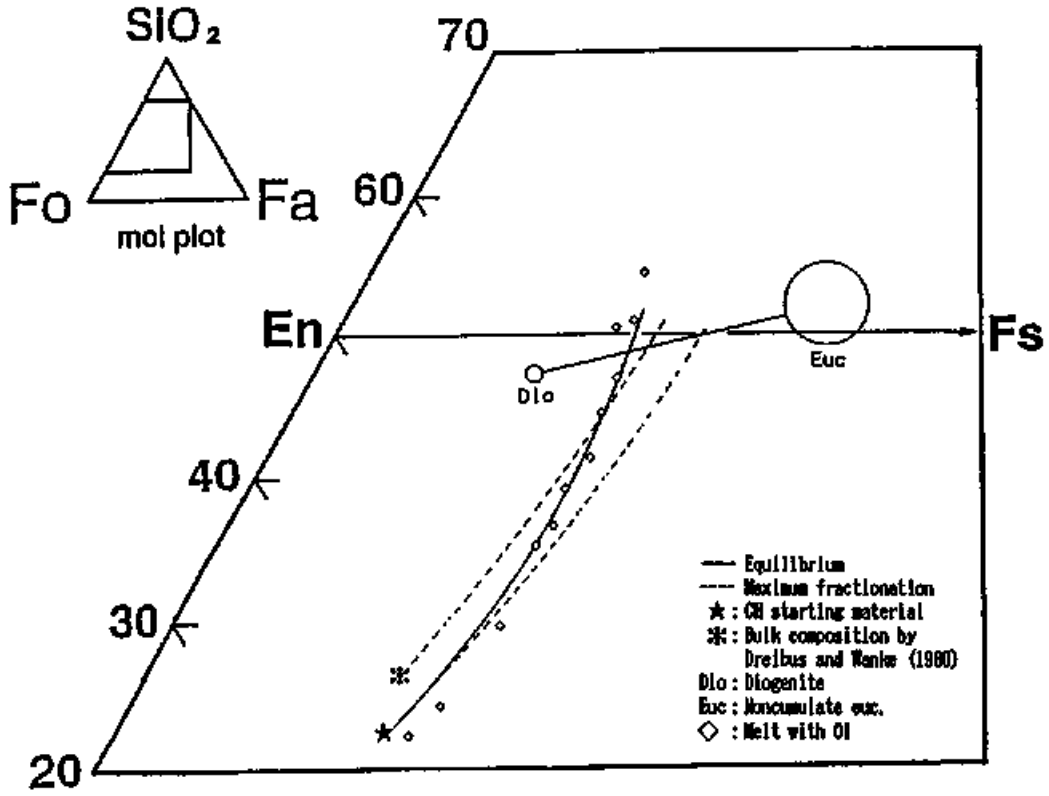

Figure 4-5

Calculations on the equilibrium crystallization process and the maximum fractionation process from the CH starting material. Calculated values and the melts with olivine produced in the CH experiments are plotted on the SiO_2-Fo-Fa system. Fe-Mg partition coefficient between Ol and melt used in the calculations is calculated from the composition of the calculated melt. The composition of the melts in the run products are consistent with the calculation on the equilibrium process. The compositional trend by Ikeda (1989) is also shown.

4-3 Physical conditions of the solid-liquid separations

Solid-liquid separation process in a gravitational field depends on density difference between coexisting two phases, viscosity of liquid, sinking velocity of crystals, condition of natural convection and other variables such as radius of crystals. Conditions for the gravitational separation in a small planet such as HEDP-PB have not been estimated, but must be different from those in the Earth. In this section, conditions for the solid-liquid separation in HEDP-PB will be estimated. And then, possible processes for the two stages of the separation will be discussed.

[Calculations of density of crystal and coexisting melt and viscosity of melt]

Density of crystals and coexisting melt and viscosity of melt were calculated using chemical compositions of melts and crystals fitted by quadratic functions of temperature in the previous chapter (Figures 3-3 and 3-6).

Density

Densities of olivine and pyroxene were calculated as a function of temperature, using thermal expansion coefficients by Hazen (1977) for olivines and those by Sueno *et al.* (1976) and Smyth (1973) for pyroxenes. Calculated densities of olivine and pyroxene change from 3.1 (1600°C) to 3.2 (1350°C) and from 3.3 (1340°C) to 3.35 (1180°C), respectively (Figure 4-6). Each value of densities calculated may comprise a few % of errors.

Density of melt coexisting olivine or pyroxene was calculated using a formula and its coefficients by Bottinga and Weill (1982). The

calculated density of melt changes from 2.75 (1600°C) to 2.72 (1350°C) and from 2.78 (1340°C) to 2.8 (1180°C) for the first and second stages of the separation, respectively (Figure 4-6).

Densities of partial melts including olivine or pyroxene were calculated from weight ratios and densities of the melt and crystal. Calculated densities of partial melts including olivine change from 2.8 (1600°C) to 2.97 (1350°C) and those including pyroxene from 2.85 (1340°C) to 3.1 (1180°C), respectively (Figure 4-6).

Viscosity of melt

Viscosities of melts (η in poise) in the temperature range of the first stage of the separation were calculated as a function of temperature (T°K) using an equation;

$$\mathrm{Log}(\eta) = C_{Mg} \cdot X_{Mg} + C_{Al} \cdot X_{Al} + C_{Si} \cdot X_{Si} + C_{Ca} \cdot X_{Ca} + C_{Fe} \cdot X_{Fe},$$

where X_{Mg}, X_{Al}, X_{Si}, X_{Ca} and X_{Fe} are mol% of each component of melts. And the coefficients are obtained by the least-squares method using data summarized by Ryan and Brevins (1987). Those are as follows;

$C_{Mg} = 4.742 \cdot 10^{-2} - 141.1/T$, $C_{Al} = -1.784 \cdot 10^{-1} + 345.1/T$,

$C_{Si} = -5.110 \cdot 10^{-2} + 179.4/T$, $C_{Ca} = -9.945 \cdot 10^{-2} + 83.97/T$ and

$C_{Fe} = 3.294 \cdot 10^{-1} - 613.6/T$.

Calculated viscosities change from several poise (1600°C) to 30 poise (1350°C) (Figure 4-7). Standard deviation of η is within 0.2 in a log scale.

On the other hand, viscosities of the melts in the temperature range of the second stage were calculated by a method of Bottinga and Weill (1972), because the temperature range is lower than that of data in Ryan and Brevins (1987). Then, the viscosities calculated were fitted by a quadratic function of temperature (T°C) as follows;

$$\mathrm{Log}(\eta) = 52.78 - 7.117\cdot10^{-2}\cdot T + 2.442\cdot10^{-5}\cdot T^2.$$

Calculated viscosities change from 20 poise (1340°C) to 10^3 poise (1180°C) (Figure 4-7). Standard deviation of η is within 0.2 in a log scale.

Viscosity of solid-suspended liquid (η_{sol}) depends on a volume fraction of the solid (V_{sol}), and increases rapidly when the solid fraction exceeds about 50% (Thomas, 1965). The viscosity up to solid volume fraction of 60% is expressed in a following equation with uncertainty in the range over the fraction of about 50% (Thomas, 1965);

$$\eta_{sol} = \eta\cdot(1 + 2.5\cdot V_{sol} + 10.05\cdot V_{sol}^2 + 0.00273\cdot\exp(16.6\cdot V_{sol}).$$

Calculated values of the solid-suspended liquid change from several poise (1600°C) to 10^3 poise (1350°C) and from 30 poise (1340°C) to 10^4 poise (1180°C) for the first and second stages, respectively (Figure 4-7). The viscosity of solid-suspended liquid is much larger than that of liquid including no crystals.

[Sinking velocity of crystals, natural convection and gravitational separation in magma]

As discussed in the previous chapter, the solid-liquid separation in HEDP-PB occurred in two stages. Physical properties of melts and crystals in those stages are calculated in the previous section. And then, in this section, in order to discuss the process at the two stages, several variables related with gravitational separation will be calculated on the assumption that both the stages of the separations occurred in each magma ocean. And an effect of natural convection to sinking of crystals will be discussed.

HEDP-PB is assumed to have a radius of 300 km (Mason, 1967),

average density of 3.4 g/cm^3 and surface gravitic acceleration (g) of 0.3m/sec^2 in the following calculations. Depth of a magma ocean in the first stage is assumed to be 200 km from the surface of HEDP-PB, because gravitic acceleration is negligible in the core region and it is difficult to formulate the motion of convection. As for the second stage, the ocean should have the depth of 60 km from the surface, which is given by the volume fraction of each layer calculated from the bulk composition of HEDP-PB.

Sinking velocity of crystals

Sinking velocity of a crystal in liquid can be calculated by Stokes' law; $v = 2\Delta\rho \cdot g \cdot a^2/9\eta$, where a is radius of a spherical crystal, $\Delta\rho$ is density difference between the crystal and liquid, and η is viscosity of the liquid. Sinking velocities were calculated as a function of temperature, by changing the size of crystals. For an example, spherical grains of pallasitic olivine (2 mm in radius) and diogenitic pyroxene (1 mm in radius) have the velocities of 10^{-4} to 10^{-6} m/sec, respectively (Figure 4-8). The velocities decrease with decreasing temperature. The velocity of a spherical Fe-metal is almost ten times larger than that of olivine grain in the same size proportional to the density differences between metal-silicate melt and olivine-silicate melt.

Natural convection

Behavior of natural convection in a magma ocean is prescribed by Rayleigh number; $Ra = g \cdot \beta \cdot \Delta T \cdot H^3/\alpha \cdot \nu$, where β is a coefficients of cubic expansion (calculated from the average density), ΔT is temperature difference between upper and lower surfaces of the layer, H is depth of the layer, α is a thermal diffusion coefficient (10^{-6} m^2/sec for typical silicate) and ν is kinematic viscosity calculated from solid-suspended

viscosities and average densities. Because ΔT could not estimated in our cases, the calculation was carried out with the different values of ΔT (10, 30 and 100°C). The calculated Rayleigh numbers are more than 10^{20} and 10^{17} at the first and second stages, respectively (Figure 4-9).

Critical Rayleigh number (Rc) is a parameter which describes nature of convection flow in liquid. The numbers for the magma oceans in a spherical shell are around $1.5 \cdot 10^4$ and $7 \cdot 10^5$ for the first and second stages, respectively (Chandrasekhar, 1961). Since Ra >> Rc, convection in both magma oceans must be a fierce turbulent flow.

In a case of the turbulent flow, Nusselt number (Nu), which is a ratio between total heat flow and thermal conductivity heat flow in convecting liquid, is given as $Nu = (Ra/Rc)^{0.27}$ (Booker, 1976). Calculated Nusselt numbers are over 10^4 and over 10^3 for the first and second stages, respectively (Figure 4-10). These values suggest that the heat transportation in both magma oceans is mostly due to natural convection.

Then, total heat flow rate (Q_v) can be calculated by an equation of $Q_v = \kappa \cdot \Delta T \cdot Nu/H$, where κ is thermal conductivity (4 W/m·K for typical silicate). The rates for the first and second stages were calculated to be in the order of 10 - 10^{-2} W/m^2 (Figure 4-11).

By assuming that half of liquid ascends as the other half descends in the natural convection in question (Figure 4-12), effective velocity (V_{eff}) of the half of liquid is given by an equation; $V_{eff} = Qv/0.5 \cdot C \cdot \Delta T$, where C is specific heat. The calculated velocities are 10^{-5} - 10^{-6} and 10^{-7} m/sec for the first and second stages, respectively (Figure 4-13). These values will be compared with sinking velocity of crystals in the next section.

Gravitational separation

It can be roughly estimated whether a crystal in convecting liquid can sink or not, by comparing sinking velocity (v) of the crystal with effective velocity (V_{eff}) in the liquid. For an example, crystals of olivine (2 mm in radius) and pyroxene (1 mm in radius) have sinking velocities much larger than the effective velocity of the magma ocean (Figures 4-8 and 4-13), and then separation of the crystals from the liquid can start.

As an indicator, a critical size is defined as the crystal size which gives $v = V_{eff}$. These critical sizes of olivine, Fe-metal and pyroxene were given in Figure 4-14. If the number of crystals is constant during cooling of magma, the change of radius of a crystal can be calculated by assuming nucleation density of the crystal (e.g., Kouchi *et al*, 1986). These changes in sizes of olivine and pyroxene are given in Figure 4-14.

The critical sizes of olivine and pyroxene in the case of a magma ocean on the surface of the Earth were also calculated using the same values of the depth, heat flow rate and radii of crystals as those in the case of HEDP-PB (Figure 4-14). As can be seen in Figure 4-14, the critical sizes of olivine and pyroxene are much larger than those in the Earth's surface. Since nucleation and growth rates of crystals in a magma are considered to be not so much different in both planets, fractional crystallization differentiation would occur hardly on HEDP-PB, in comparison with the case of the Earth. And then, high degree of equilibration between crystals and melt can be expected in the magma ocean on HEDP-PB more than on the Earth.

[Separation of pallasite at the first stage]

There are two typical cases for pallasite to coexist with the magma; (1) the solid-liquid separation during cooling process of total melt, and (2) that during partial melting by heating of a chondritic material.

In the first case, the magma should be once heated above liquidus temperature of Fe-Ni metal, because liquidus temperature of olivine in the present system is above 1600°C and Fe-Ni metal is solid below 1500°C. If not, the case is almost similar to the second case, a partial melting process. Then, Fe-metal coexisting with silicate melt must be small bubbles of metallic melt due to the immiscibility between metallic and silicate melts. The metallic bubbles can adhere each other and grow rapidly (Takahashi, 1983). Thus, at the temperature of the solid-liquid separation (1400°C), grains of Fe-metal crystal must be larger than those of pallasitic olivine.

The critical size of olivine at 1400°C is about 0.15 mm, which is significantly larger than that of Fe-metal (about 0.05 mm, Figure 4-14). Radius of crystals growing in the magma changes rapidly and moderately in the early and late stages of the cooling (Figure 4-14). Therefore, even when olivine and Fe-metal grains with smaller than the critical size are suspended in the magma at the early stage of the cooling, Fe-metal grains must sink earlier than olivine grains as temperature decreases. This process of the solid-liquid separation results in the formation of not pallasite but layers of dunite and metallic iron. Therefore, it is hardly suggested that pallasite was formed during the cooling of magma.

The second case is that pallasite was formed as a residue from a partial melt during heating process of a chondritic material. At the temperature of the separation of pallasite (1400°C), the volume ratio of crystals (olivine and Fe-metal) and melt is about unity (Figure 3-5).

This ratio can allow to form a network of melt in a chondritic material. The density difference between olivine crystals and the partial melt at 1400°C is about 0.45 g/cm^3 and that between Fe-Ni metal and the partial melt is about 4.6 g/cm^3.

In the partial melting process, the melt composition changes along the olivine control line through the Ol-Px phase boundary from peritectic point (Figure 4-2). While on the phase boundary, the SiO_2 content of the melt is almost constant, the SiO_2 content of the melt on the olivine control line decrease as temperature increases (Figure 3-3). As a result, viscosity of the melt may drastically decrease at above 1350°C.

While the segregation process of the partial melt is not understood, the density difference and the decreasing of the viscosity must allow the segregation of the partial melt after the formation of the network of the melt even in a small planet of HEDP-PB. Therefore, as a conclusion of this stage of the solid-liquid separation, the partial melting process is suggested.

[Separation of diogenite at the second stage]

A partial melting process of the solid-liquid separation in this stage is denied in the previous chapter due to its necessity of a complex thermal history. The other possible process is that diogenite formed as a cumulate in the magma ocean. Since pyroxene crystals must be smaller than the critical size (0.1 mm; Figure 4-14) at the initial stage of crystallization, the crystals can be suspended by the convection in the magma ocean. Size of the pyroxene crystals increases as temperature decreases. However, as seen in Figure 4-14, the

critical size increases more rapidly than the size of the crystals. Therefore, as far as the number of the nucleated crystals is not changed, the pyroxene crystal is suspended in the magma and can not sink in the magma ocean.

On the other hand, at the temperature of the separation of diogenitic pyroxene (1200°C), the volume ratio of melt and crystal is almost unity. While viscosity of the melt in this condition can not be calculated significantly, a rapid increase of viscosity of solid-suspended liquid is expected (Thomas, 1965). This increase of the viscosity of the magma can diminish the effective velocity of the convection much more than the sinking velocity of crystals. Thus, the crystals of pyroxene can be considered to sink and form diogenite at this temperature range. Before the sinking, pyroxene suspended in the magma are easily assumed to be in equilibrium with the melt. This equilibration was required in the previous chapter by chemical compositions of diogenitic pyroxenes and eucritic melt. Therefore, the solid-liquid separation at around 1200°C in the magma can be suggested in the formation of diogenite and eucritic magma.

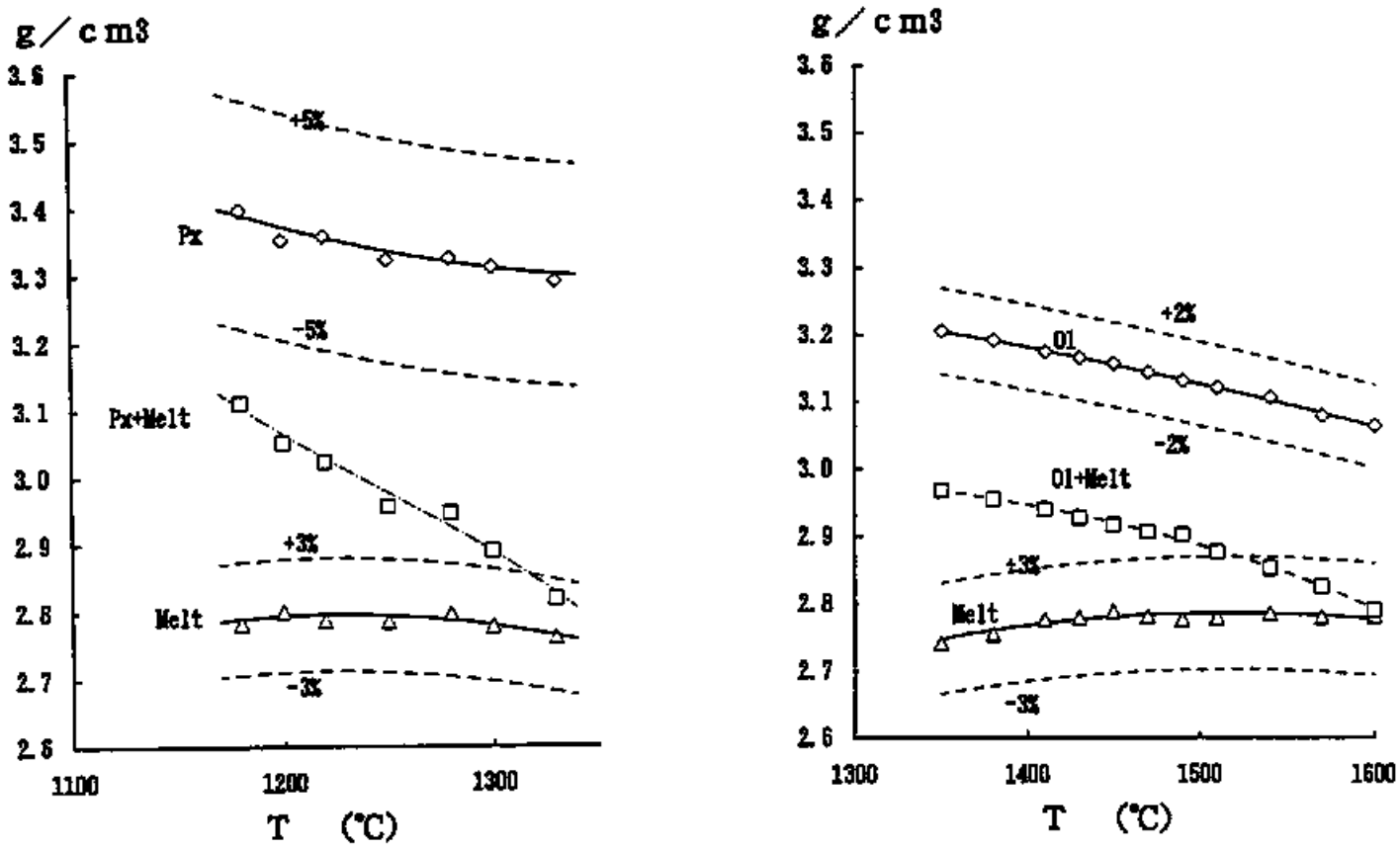

Figure 4-6

Calculated densities of olivine, pyroxene and the melts. Ol: olivine, Px: pyroxene and Ave: overall density of partial melt with olivine or pyroxene. Curves of the average densities are determined by the ratio of crystals and melts. Data points are calculated from compositions of run products. Solid lines represents calculated value using the temperature-composition functions shown in Figures 3-3, 4, 6 and 8. Estimated error of pyroxene density is larger than that of olivine, since thermal expansion coefficients of pyroxenes are extrapolated at the present temperature ranges.

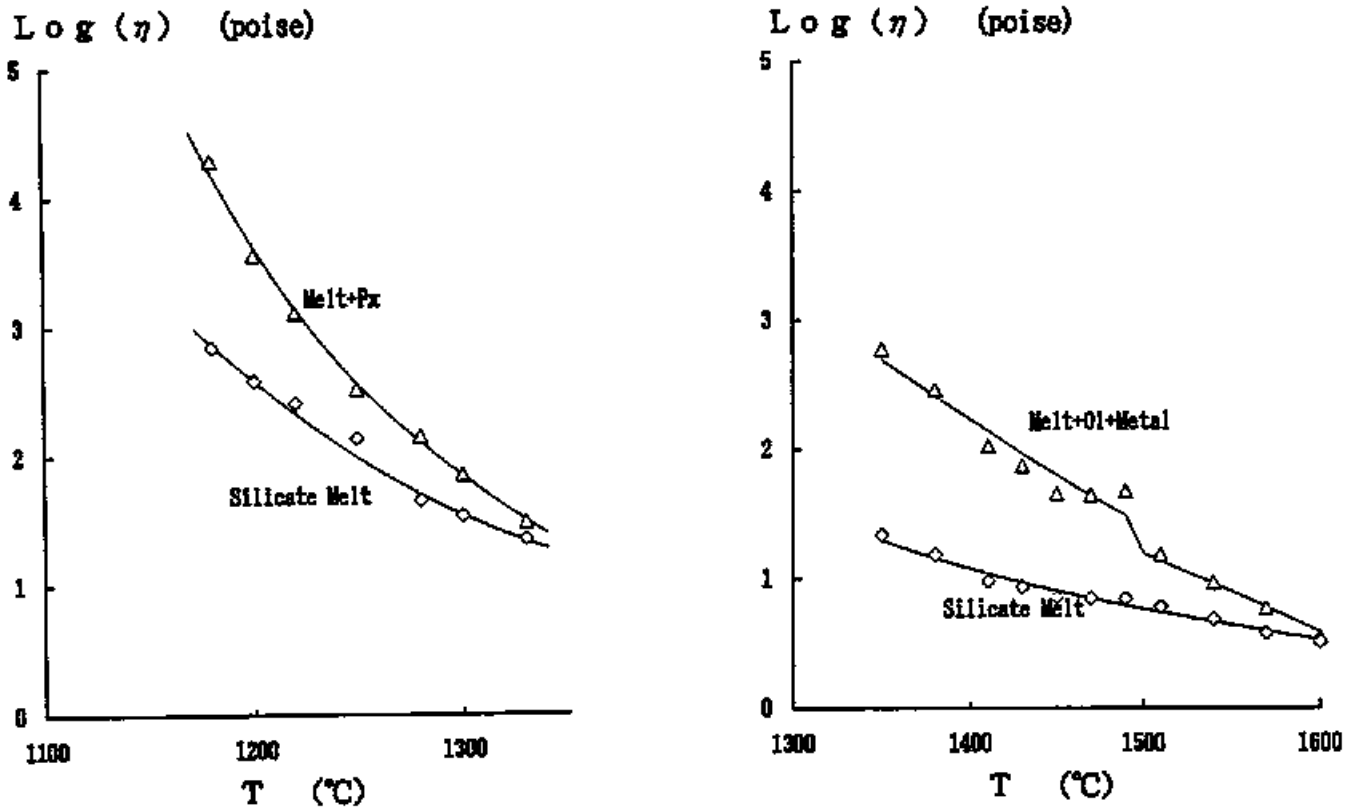

Figure 4-7
Viscosities of the melts and the suspension system of solids and melts. Data points are calculated from compositions of run products, and lines represent calculated value using the temperature-composition functions. Dependence on temperature becomes stronger as temperature decreases. Viscosity of the pyroxene-melt system below 1170°C cannot be calculated because volume fraction of solid is higher than 60%.

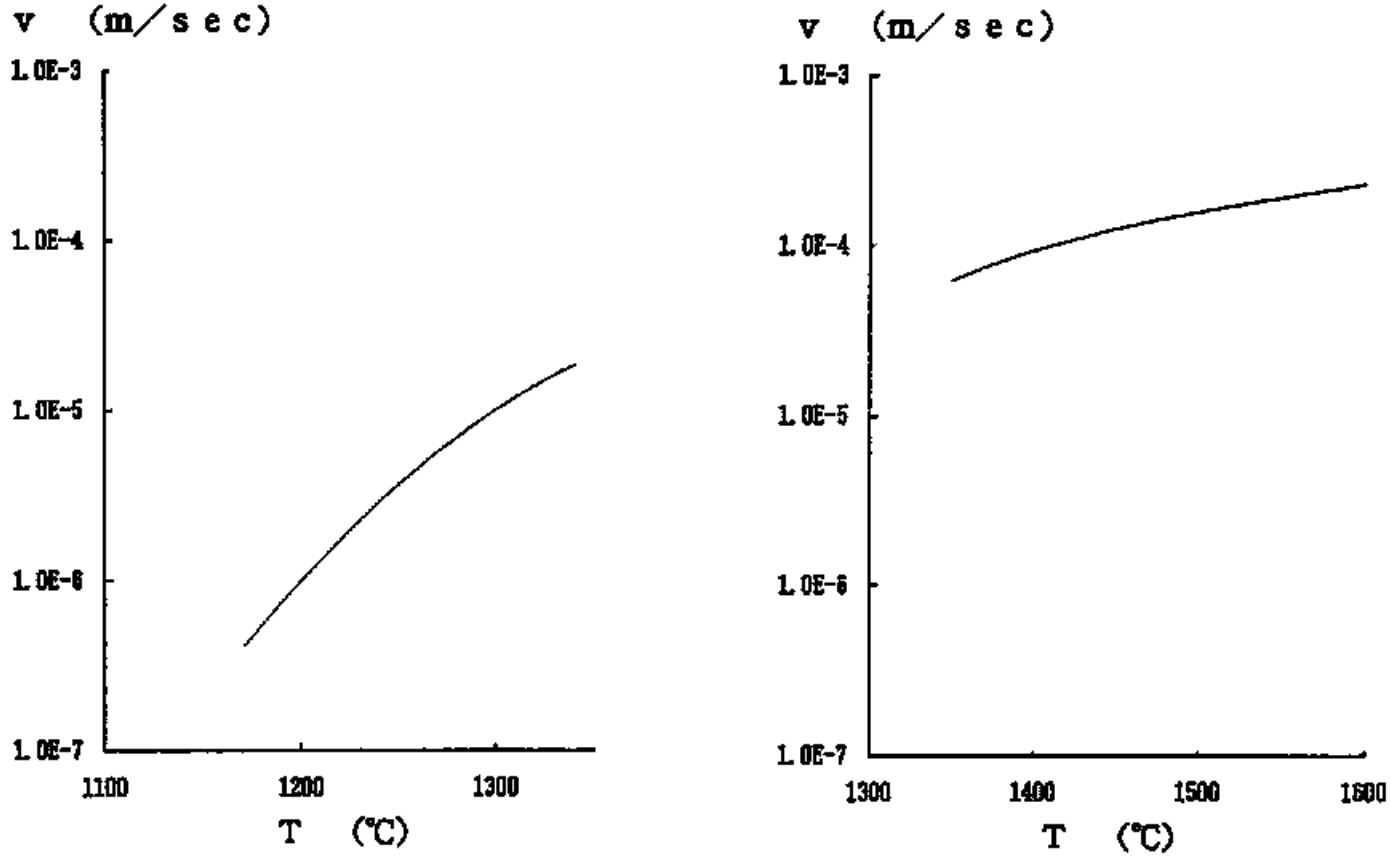

Figure 4-8
Sinking velocities of spherical grains of olivine (right) and pyroxene (left) calculated from the Stokes' law. Sinking velocity in the second stage fractionation is quite smaller than that in the first stage fractionation because of high viscosity of the melt phase (Figure 4-7).

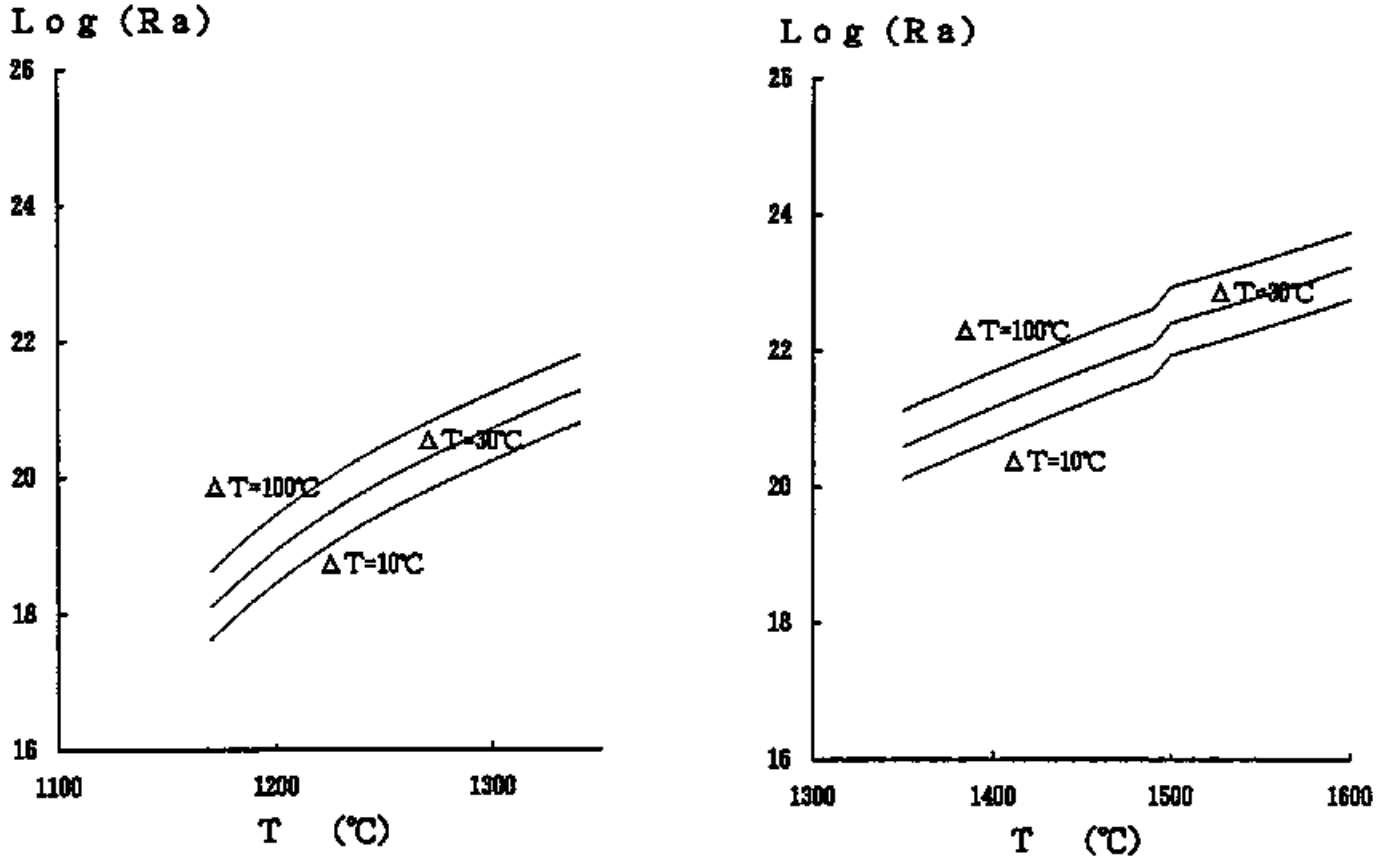

Figure 4-9
Calculated Rayleigh numbers for the magma ocean on the HEDP-PB. These values are more than 10^{20} or 10^{18} and have positive temperature dependence. These gigantic values are mainly due to the depth of the magma ocean.

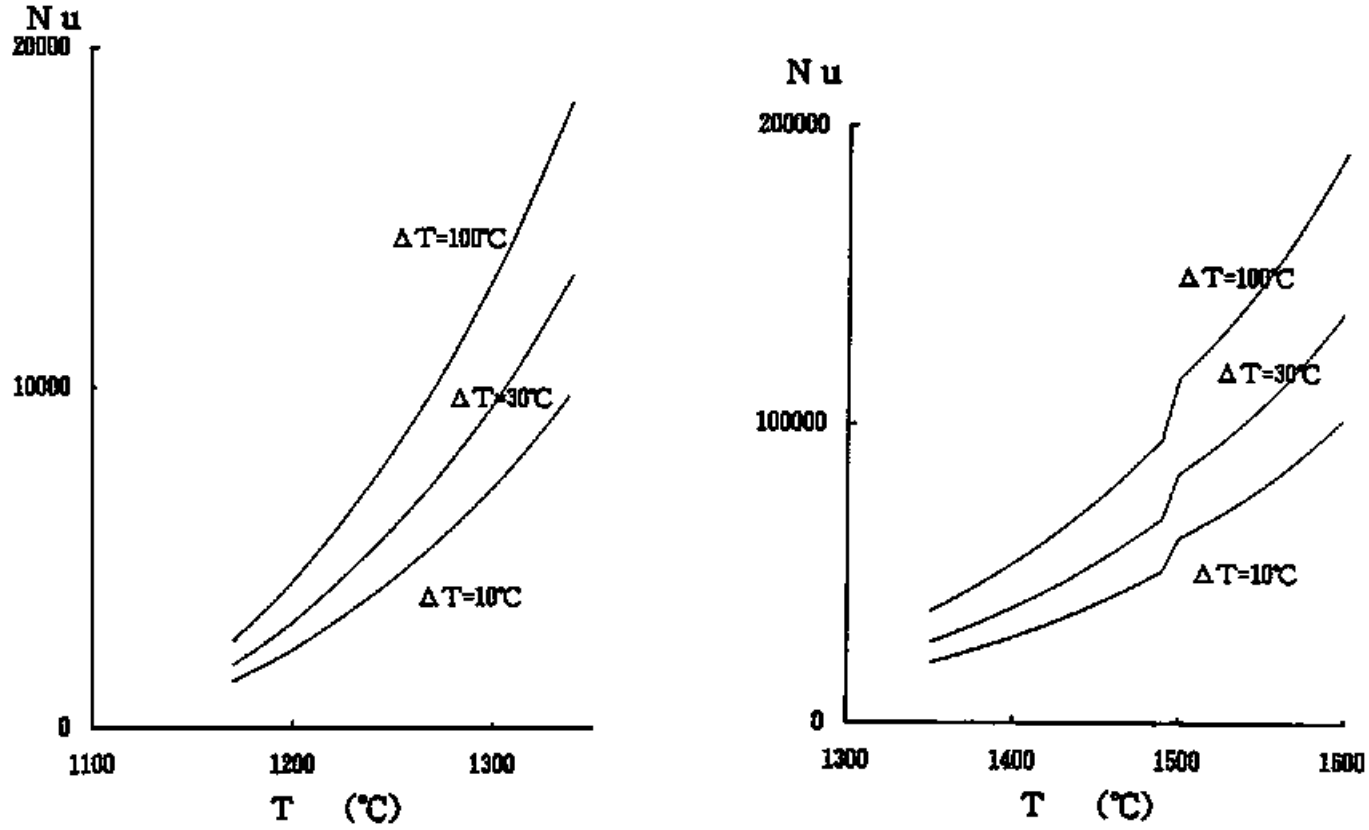

Figure 4-10
Nusselt numbers for the magma ocean. These value show the high efficiency of thermal transportation by convection. The parent body was cooled by the convection.

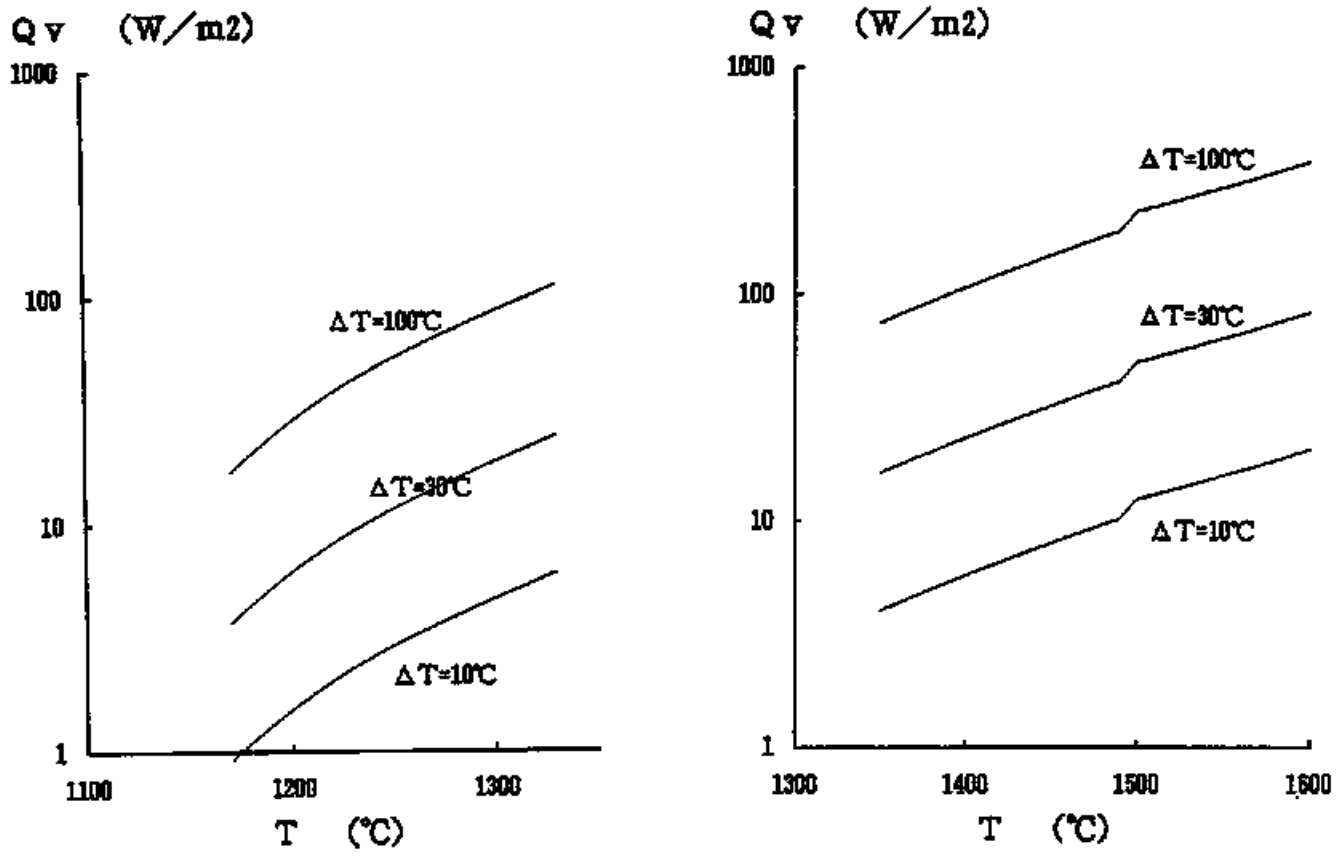

Figure 4-11
Calculated thermal transportation by convection. These values have much stronger ΔT dependence than Ra and Nu numbers. Cooling rate determines thermal gradient in the magma ocean on the parent body.

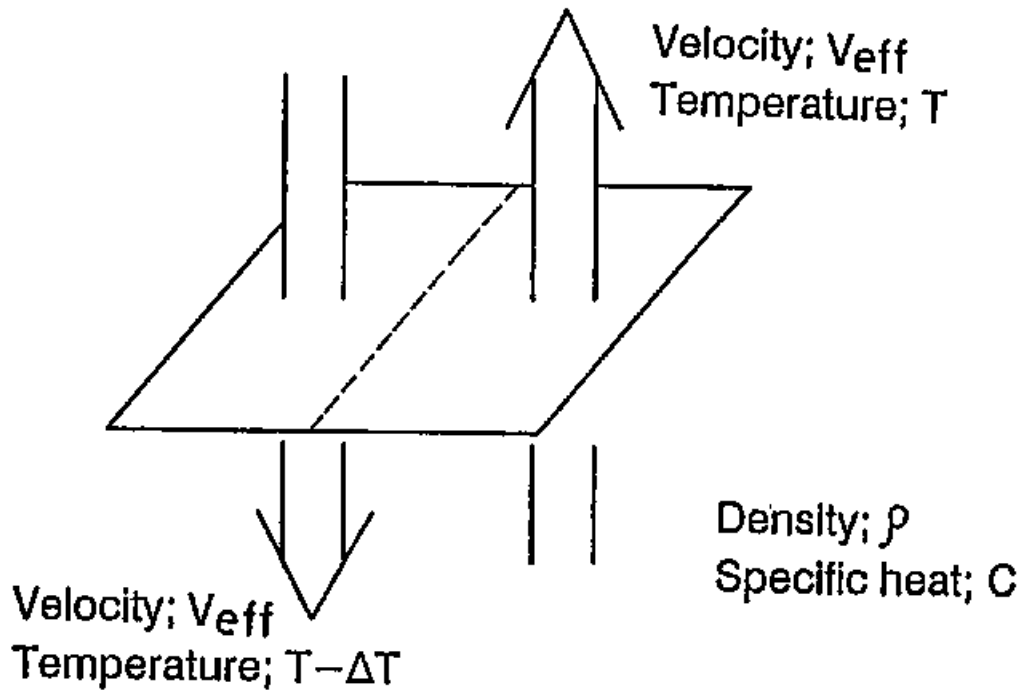

$$Qv = V_{eff} \times 0.5 \times \rho \times C \times T - V_{eff} \times 0.5 \times \rho \times C \times (T-\Delta T)$$

Figure 4-12
Schematic drawing for determination of the equation for Qv. In the convective thermal transport, heat is transported by mass flows which have different temperature.

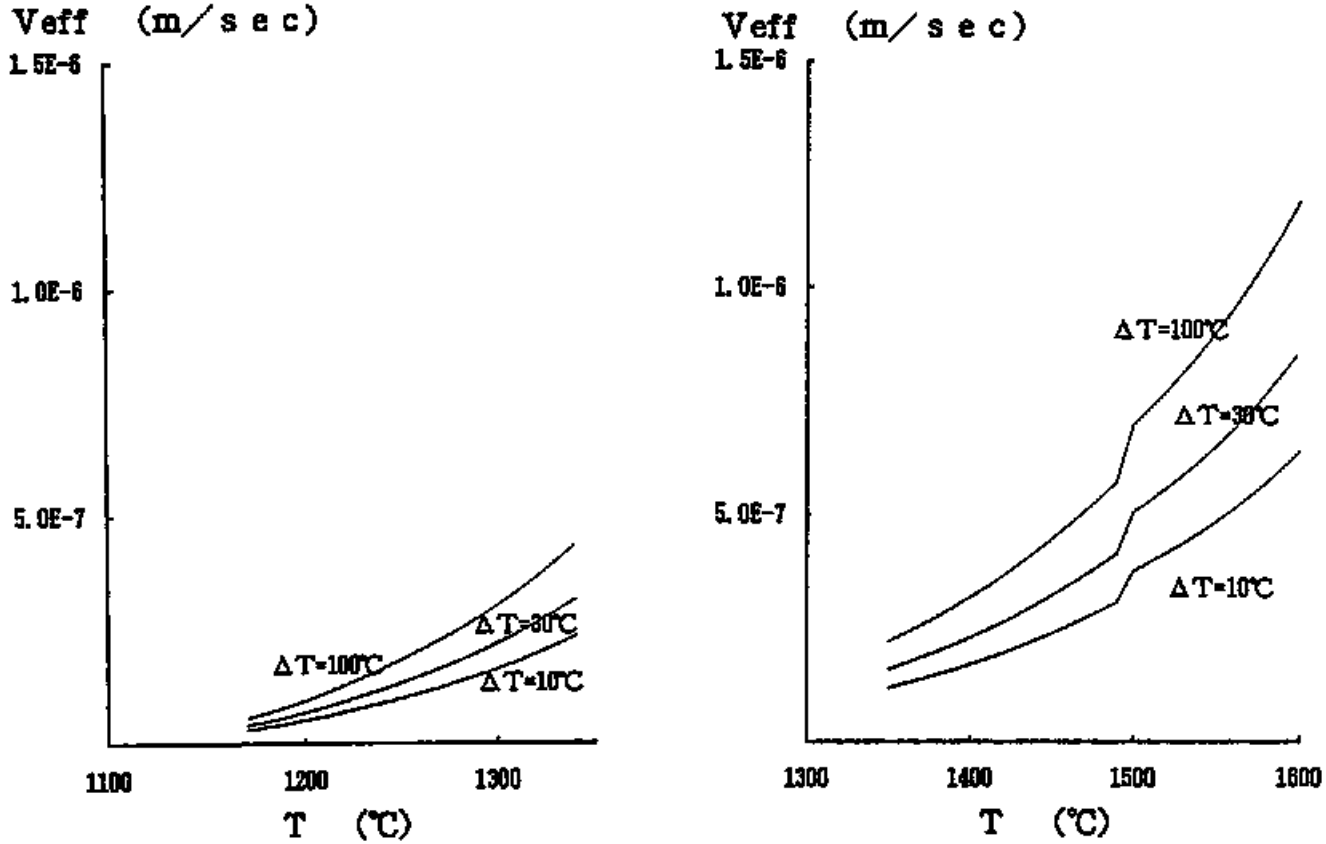

Figure 4-13
Calculated effective velocity in the magma ocean. These values are very slow to take several hundred years to move 1km but enough to thermal transport.

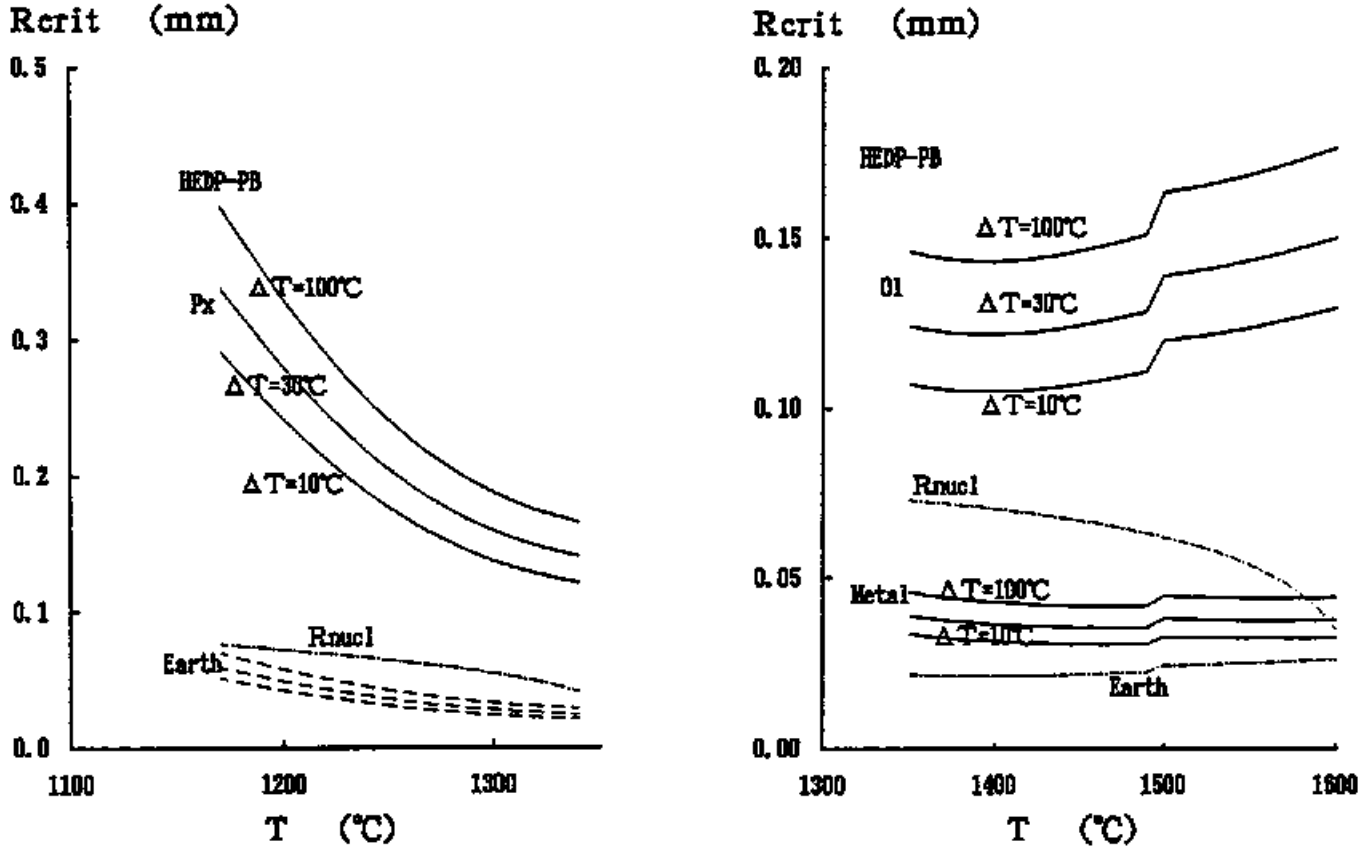

Figure 4-14

Calculated critical radii of olivine, metal and pyroxenes. Grains which is smaller than these values cannot separate from the melt by the motion of convection. From smaller gravity than the Earth, on the HEDP-PB, larger crystals can float in melts than on the Earth. Olivines in the terrestrial magma ocean is more effectively separated from the melt than the metal grains in the magma ocean on the HEDP-PB.

4-4 Summary of the present evolution model of HEDP-PB

As discussed above, a new model on the igneous processes in the evolution of HEDP-PB was constructed based on the chemical compositions of crystals and melt obtained by the experiments and the consideration of the gravitational separation. The sequence and processes of the evolution in the present model are summarized as follows and schematically drown in Figure 4-15.

First, the chondritic materials accreted and formed HEDP-PB with radius of about 300 km. Then, the parent body heated and partially melted. When the temperature raised up to 1400°C, and the volume fractions of olivine and metallic iron to the partial melt became comparable, the melt then segregated towards the surface of the parent body, leaving the coexisting olivine and metallic iron in equilibrium. These residual crystals formed pallasite. The segregated melt formed a magma ocean with a depth of about 60 km on the surface of the parent body, and then, cooled and precipitated pyroxene in equilibrium. When the temperature reached around 1200°C and the volume ratio of the pyroxene and its coexisting melt became around unity, the separation of the pyroxene from the melt occurred, forming diogenite. As the cooling proceeded, the residual melt crystallized and formed eucrites. Howardite and mesosiderites were formed after the solidification of the parent body by collision of other bodies.

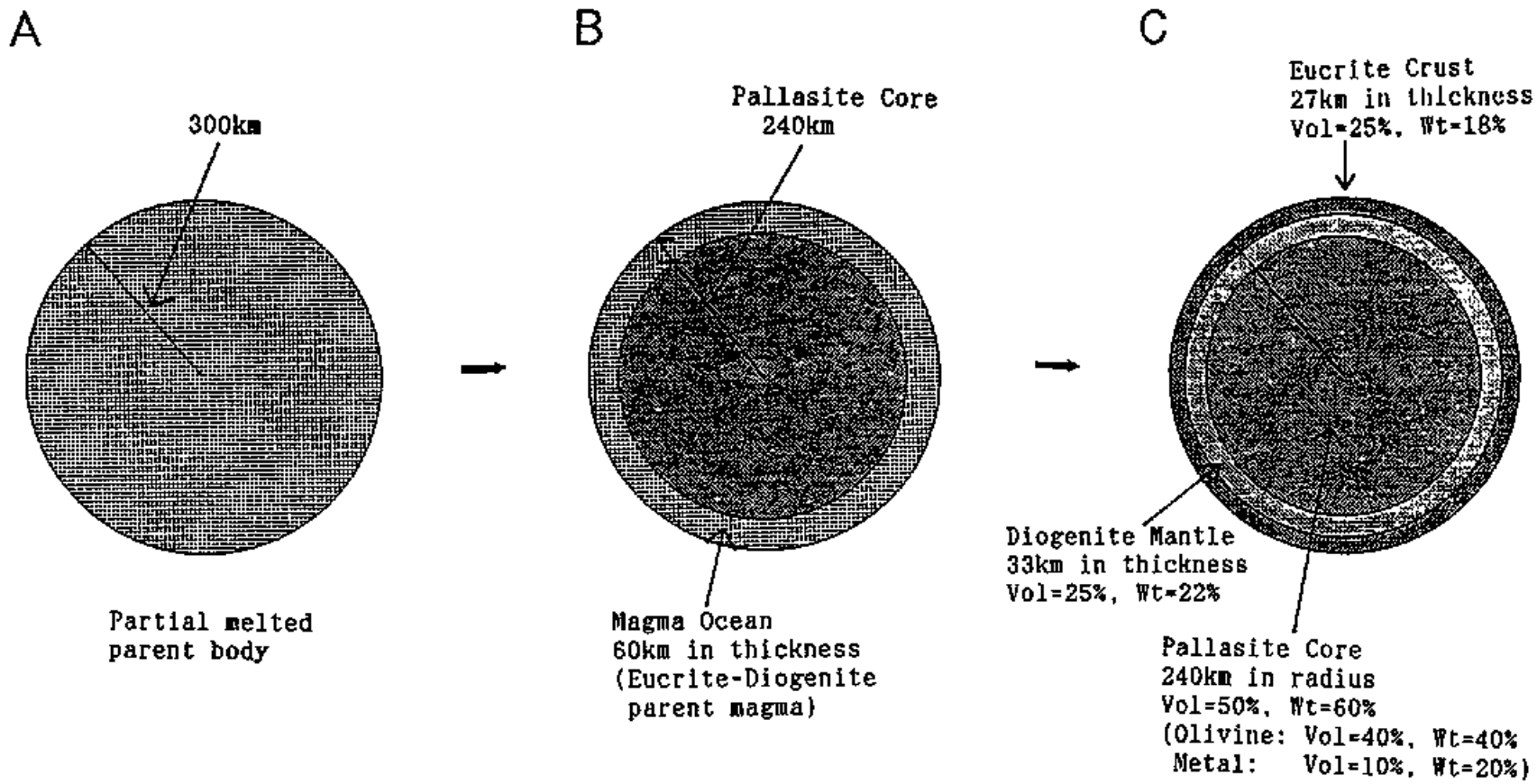

Figure 4-15

Schematic drawing of the evolution process of HED-pallasite parent body. A) The whole parent body heated to at least 1400°C and in partially melted after the accretion. B) After separation of olivine and metal, pallasitic core with radius of 240km and the magma ocean with 60km in depth are formed. C) After the second stage fractionation, diogenitic mantle and eucritic crust are crystallized from the magma ocean. By bombardment of smaller asteroids, final structure of the parent body and various HED meteorites may be formed. Volume fraction of olivine and Fe-Ni metal in pallasite core corresponds to the most olivine-abundant pallasite (see Appendix 1).

Acknowledgements

I am grateful to Prof. N. Morimoto of Osaka Sangyo University, Drs. M. Kitamura and K. Ishizaka of Kyoto University, Prof. Y. Ikeda of Ibaraki University and Dr. A. Tsuchiyama of Osaka University for helpful discussions. I also thank Drs, T. Murakami, H. Mitamura and S. Nakashima of Japan Atomic Energy Research Institute for critical advises and analytical techniques on EPMA. I thank many colleagues in Kyoto University and JAERI. And I am encouraged thoroughly in this work by Kyoko and Tomoko, my dearest family.

References

Booker, J. R. (1976) Thermal convection with strongly temperature-dependent viscosity. *Journal of Fluid Mechanics*, 76, 741-754

Bottinga, Y. and Weill, D. F. (1972) The viscosity of magmatic silicate liquids: A model for calculation. *American Journal of Science*, 272, 438-475

Bottinga, Y., Weill, D. F. and Richet, P. (1982) Density calculations for silicate liquids. I. Revised method for aluminosilicate composition. *Geochimica et Cosmochimica Acta*, 46, 909-919

Burke, J. G. (1986) *Cosmic Debris*. University of California Press, Berkeley, pp445

Buseck, P. R. (1977) Pallasite meteorite - mineralogy, petrology and geochemistry. *Geochimica et Cosmochimica Acta*, 41, 711- 740

Chandrasekhar, S. (1961) *Hydrodynamic and hydromagnetic stability*. Oxford, pp652

Clayton, R. N., Onuma, N. and Mayeda, T. K. (1976) A classification of meteorites based on oxygen isotopes. *Earth and Planetary Science Letters*, 30, 10-18

Clayton, R. N. and Mayeda, T. K. (1978) Multiple parent bodies of polymict brecciated meteorites. *Geochimica et Cosmochimica Acta*, 42, 325-327

Colson, R. O., McKay, G. A. and Taylor, L. A. (1988) Temperature and composition dependencies of trace element partitioning: Olivine/melt and low-Ca pyroxene/melt. *Geochimica et Cosmochimica Acta*, 52, 539-553

Consolmagno, G. J. and Drake, M. J. (1977) Composition and evolution of the eucrite parent body: Evidence from rare earth elements. *Geochimica et Cosmochimica Acta*, 41, 1271-1282

Dodd, R. T. (1981) *Meteorites: A petrologic-chemical synthesis.* Cambridge University Press, New York, pp368.

Donaldson, C. H. (1979) Composition changes in a basalt melt contained in a wire loop of Pt80Rh20: Effects of temperature, time, and oxygen fugacity. *Mineralogical Magazine*, 43, 115-119

Donaldson, C. H., Williams, R. J. and Lofgren, G. (1975) A sample holding technique for study of crystal growth in silicate melts. *American Mineralogist*, 60, 324-326

Dreibus, G. and Wänke, H. (1980) The bulk composition of the eucrite parent asteroid and its bearing on planetary evolution. *Z. Naturforsch.* 35a, 204-216

Duke, M. B. and Silver, L. T. (1967) Petrology of eucrites, howardites and mesosiderites. *Geochimica et Cosmochimica Acta*, 31, 1637-1665

Floran, R. J. (1978) Silicate petrography, classification and origin of the mesosiderites: Review and new observations. Proceedings of 9th Lunar and Planetary Science Conference. *Geochimica et Cosmochimica Acta*, Supplement 9, 1053-1081

Ford, C. E., Russell, D. G., Craven, J. A. and Fisk, M. R. (1983) Olivine-liquid equilibria: Temperature, pressure and composition dependence of the crystal/liquid cation partition coefficients for Mg, Fe^{2+}, Ca and Mn. *Journal of Petrology*, 24, 256-265

Gaffey, M. J. and McCord, T. B. (1977) Asteroid surface materials: Mineralogical characteristics and cosmological implications. *Proceedings of 8th Lunar Science Conference*, 113-143

Grove, T. L. (1981) Use of FePt alloys to eliminate the iron loss problem in 1 atmosphere gas mixing experiments: Theoretical and practical considerations. *Contributions to Mineralogy and Petrology*, 78, 298-304

Hazen, R. M. (1977) Effects of temperature and pressure on the crystal structure of ferromagnesian olivine. *American Mineralogist*, 62, 286-295

Hertogen, J., Vizgirda, J. and Anders, E. (1977) Composition of the parent body of eucritic meteorites (abs). *Bulletin of American Astronomical Society*, 9, 458-459

Hewins, R. H. and Newsom, H. E. (1988) Igneous activity in the early solar system. in *"Meteorites and the early solar system"*, Kerridge, J. F. and Matthews, M. S. ed., The University of Arizona Press, Tucson, 73-101

Ikeda, Y. (1989) Igneous activity in early solar system based on HED and mesosiderite meteorites. *Abstract for 28th International Geological Congress, Washington*, 2, 92-93

Ikeda, Y. and Takeda, H. (1985) A model for the origin of basaltic achondrites based on the YAMATO 7308 howardite. *Proceedings of the 15th Lunar and Planetary Science Conference, Part 2 Journal of Geophysical Research*, 90, C649-C663

Jones, J. H. (1984) The composition of the mantle of the eucrite parent body and the origin of eucrites. *Geochimica et Cosmochimica Acta*, 48, 641-648

Kouchi, A., Tsuchiyama, A. and Sunagawa, I. (1986) Effect of stirring on crystallization kinetics of basalt: Texture and element partitioning. *Contributions to Mineralogy and Petrology*, 93, 429-438

Larimer, J. W. (1968) Experimental studies on the system Fe-MgO-SiO_2-O_2 and their bearing on the petrology of chondritic meteorites. *Geochimica et Cosmochimica Acta*, 32, 1187-1207

Longhi, J. (1987) Liquidus equilibria and solid solution in the system Anorthite-Forsterite-Wollastonite-Silica at low pressure. *American Journal of Science*, 287, 265-331

Longhi, J. and Pan, V. (1988) A reconnaissance study of phase boundaries on low-alkali basaltic liquids. *Journal of Petrology*, 29, 115-147

Mason. B. (1967) Meteorites. *American Scientist*, 55, 429-455

Matsui, Y. (1979) "Genso no sonzaido" in *"Chikyuukagaku"* Vol.4, ed. Matsui, Y. and Banno, S., Iwanami, Tokyo, 265-283, (in Japanese)

McCarthy, T. S., Ahrens, L. H. and Erlank, A. J. (1972) Further evidence in support of the mixing model for howardite origin. *Earth and Planetary Science Letters*, 15, 86-93

McCarthy, T. S., Erlank, A. J. and Willis, J. P. (1973) On the origin of eucrites and diogenites. *Earth and Planetary Science Letters*, 18, 433-442

McCord, T. B. and Gaffey, M. J. (1974) Asteroids: Surface composition from reflection spectroscopy. *Science*, 186, 352-355

Morgan, J. W., Higuchi, H., Takahashi, H. and Hertogen, J (1978) A "chondritic" eucrite parent body: Inference from trace elements. *Geochimica et Cosmochimica Acta*, 42, 27-38

Rhodes, J. M., Lofgran, G. E. and Smith, D. P. (1979) One atmosphere melting experiments on ilmenite basalt 12008. *Proceedings of the 10th Lunar and Planetary Science Conference*, 407-422

Ringwood, A. E. (1989) Significance of the terrestrial Mg/Si ratio. *Earth and Planetary Science Letters*, 95, 1-7

Ryan, M. P. and Blevins, Y. K. (1987) The viscosity of synthetic and natural silicate melts and glasses at high temperature and 1 bar (10^5 Pascals) pressure and high pressures. *U.S.G.S. Bulletin*, 1764, pp563

Seitz, M. G. and Kushiro, I. (1974) Melting relations of the Allende meteorite. *Science*, 183, 954-957

Smyth, J. R. (1973) An orthopyroxene structure up to 850°C. *American Mineralogist*, 56, 636-648

Stolper, E. (1975) Petrogenesis of eucrite, howardite and diogenite meteorites. *Nature*, 258, 220-222

Stolper, E. (1977) Experimental petrology of eucrite meteorites. *Geochimica et Cosmochimica Acta*, 41, 587-611

Sueno, S., Cameron, M. and Prewitt, C. T. (1976) Orthoferrosilicate: High-temperature crystal chemistry. *American Mineralogist*, 61, 38-53

Takahashi, E. (1983) Melting of a Yamato L3 chondrite (Y-74191) up to 30 kbar. *Memoirs of National Institute of Polar Research Special Issue*, No.30, 168-180, National Institute of Polar Research, Tokyo

Takeda, H. (1979) A layered-crust model of a howardite parent body. *Icarus*, 40, 455-470

Takeda, H., Miyamoto, M., Yanai, K. and Haramura, A. (1978) A preliminary mineralogical examination of the Yamato-74 achondrites. *Memoirs of National Institute of Polar Research Special Issue*, No.8, 170-184, National Institute of Polar Research, Tokyo

Takeda, H (1982) *"Wakusei-no bussitsu kagaku"*. University of Tokyo Press, Tokyo, pp150, (in Japanese)

Thomas, D. G. (1965) Transport characteristics of suspension: VIII. A note on the viscosity of newtonian suspensions of uniform spherical particles. *Journal of Colloid Science*, 20, 267-277

Ulmer, P (1989) The dependence of the Fe^{2+}-Mg cation-partitioning between olivine and basaltic liquid on pressure, temperature and composition, An experimental study to 30 kbars. *Contributions to Mineralogy and Petrology*, 101, 261-273

Weill, D. F. and McKay, G. A. (1975) The partitioning of Mg, Fe, Sr, Ce, Sm, Eu and Yb in lunar igneous systems and a possible origin of KREEP by equilibrium partial melting. *Proceedings of the 6th Lunar Science Conference*, 1143-1158

Appendix 1 Chemistry of HED and pallasite meteorites

A large number of differentiated meteorites is HED meteorites (howardite, eucrite and diogenite) (Table A1-1). In this section, petrologic and mineralogical properties of the HED meteorites and pallasite are described briefly (Table A1-2). Petrography and mineralogy of these meteorites are summarized in Duke and Silver (1967), Buseck (1977) and Dodd (1981).

Eucrite is a variety of meteorites which are called to "basaltic achondrites". Some of the eucrites are called *cumulate eucrites* and are interpreted as magmatic cumulates on their unbrecciated equigranular texture and preferred orientation of minerals. The other eucrites are *noncumulate eucrites* and have brecciated textures except a few meteorites which have quenched texture of lava flow. Both of their textures show magmatic origin.

Cumulate eucrites (Number 7 to 9 in Table A1-3) consist of almost equal fraction of pyroxene and calcic plagioclase. Pyroxene is pigeonite with $En_{50-66}Wo_{5-10}$ (Figure 4-9). Pyroxene grains have exsolution texture due to "inversion" from pigeonite to orthopyroxene and augite by annealing during slow cooling. Plagioclase has calcic composition of An_{90-95}.

Noncumulate eucrites have relatively larger modal fraction of pyroxene than cumulate eucrites (Number 1 to 6 in Table A1-3). In noncumulate eucrites, pyroxene is more ferrous (Figure 4-9) and plagioclase is slightly less calcic. Pyroxenes in noncumulate eucrites are chemically zoned pigeonite and subordinate ferroan augite.

Diogenites are distinguished by their chemical homogeneity. These meteorites consist principally of orthopyroxene (Figure 3-9, Table A1-2,

A1-4). Composition of pyroxene is approximately En_{75} and Wo_1. Olivine is rarely found in diogenite. Normative olivine in Table A1-4 is due to metallic iron in diogenite (Table A1-2). Except a few samples, diogenites have monomict brecciated texture with orthopyroxene clasts and crushed matrix. Pyroxene phenocrysts of several cm in diameter are observed. In samples without brecciated textures, intergranular textures represent slow cooling rates in the parent body.

Howardites are polymict breccia of diogenite and eucrite and have a texture similar to that of the lunar surface regolith. Ratios of diogenite to eucrite are not constant in howardite samples (Figure A1-1). Those must form on the surface of the parent body by the cratering to various depths (Figure A1-2). Polymict breccia excluding diogenite component is called to polymict eucrite. Cratering in the layered structure of the parent body must cause complex thermal histories of surface materials. Consequently, howardites contain clasts and minerals showing extremely diverse characteristics. Mesosiderite is polymict breccia meteorite including metallic phase and it is considered to collision products with iron meteorites and the HED parent body.

Pallasites have very exotic textures from terrestrial rocks. Those consist chiefly mm to cm sized olivine crystals and continuous network of Fe-Ni metal. Olivine-metal ratio is various in several cm scale regions in some pallasites and, of course, among individual samples. Modal abundance of major and minor minerals is tabulated in Table A1-5. Composition of olivine crystals has a narrow range (Figure A1-3). Within each sample, zoning in crystals and intergrain variation are not observed with few exception. Widmannstätten structure in metal is indicating extremely slow cooling rates (0.5 to 2.0°C/my at 500°C). This cooling rate corresponds to several tens to hundred km in depth at the

parent body of 200 to 500km of radius.

A number of HED and pallasite samples is smaller than that of chondrites (Table A1-1). Fall frequency of HED meteorites is almost one-fifteenth of that of chondrites. As for pallasites, only three falls were observed up to date. However, HED and pallasite account for almost a half part of non-chondrite meteorites. Fall frequency may not directly correspond to the number of parent bodies formed in the early solar system, but HED and pallasite meteorites must be important portion of differentiated parent bodies.

Numbers of "Finds" in Table A1-2 includes several antarctic meteorites. Total number of antarctic meteorites are more than 5000 even in the Japanese collection. Various HED meteorites are found in these samples and information about HED meteorites are increasing.

Table A1-1 Number of samples and fall frequency of meteorites (percent, from Burke, 1986).

	Fall	Finds	Fall frequency
Chondrites	784	897	86.6
Eucrirtes	25	30	2.8
Diogenites	9	15	1.1
Howardites	18	6	2.0
Other achondrites	17	21	1.9
Pallasites	3	36	0.3
Other stony irons*	7	27	0.8
Irons	42	683	4.6
Total	905	1706	100

*These are mesosiderites except two. Mesosiderites are polymict breccia of metallic Fe-Ni and howardite-like silicates. It is considered that mesosiderites are formed by the collision of metallic asteroids to the HED parent body.

Table A1-2 Major and common minor minerls in HED and pallasite meteorites. (Volume %)

	Eucrites	Diogenites	Howardites	Mesosiderites	Pallasites
Olivine		rare	Polymict	Polymict	37-85
Pyroxene	40-63	-95	breccia of	breccia of	
Plagioclase	55-30(An_{80-95})	-2(An_{85-90})	eucrite and	howarditic	
SiO_2	0-4	minor	diogenite	silicates	
Fe-Ni metal			components	and Fe-Ni metal	14-49
Minor phases	1-4	-2			Troilite (0-7)
	Troilite	Troilite			Schreibersite
	Phosphates	Chromite			($(Fe,Ni)_3P$)
	Ilmenite	Ilmenite			Chromite
	Chromite	Phosphates			Phosphates
	Ni-poor metal	Ni-poor metal			

Table A1-3

Modal and major mineral compositions of nine eucrites, listed in order of decreasing pyroxene (PX) abundance

	Mode (vol.%)				Mineral Composition			
	Px	Pc	SiO_2	Oth	Pyroxene [Fe/(Fe + Mg)]	Plagioclase (mol.% An)	Silica	
1. Ibitira	63	31	4	2	0.56	95–96	C	Noncumulate
2. Pasamonte	63	30	3	4	0.48–0.70	86	T	
3. Nuevo Laredo	62	33	1	4	0.67	85	C, Q	
4. Juvinas	56	40	1	3	0.62	80	T, Q	
5. Sioux County	56	41	2	1	0.59	90	T, Q	
6. Stannern	55	39	3	3	0.62	80	Q	
7. Moama	49	49	1	1	0.40–0.43 (i)	94	T	Cumulate
8. Moore County	44	50	2	4	0.50 (i)	90	T	
9. Serra de Magé	40	56	0	4	0.44 (i)	95	T	

Pyroxene (PX) is pigeonite, which is inverted (i) in some meteorites. The silica polymorphs are quartz (Q), tridymite (T), and cristobalite (C). Pc denotes plagioclase. From Dodd (1981).

Table A1-4 *Analyses (x-ray fluorescence) and mineral norms for five diogenites*

%	1	2	3	4	5	Avg (2–5)	Normative (avg.)	
Si	24.37	25.07	24.08	25.58	24.11	24.69	Chr	1.59
Ti	0.044	0.072	0.034	0.041	0.037	0.046	Ilm	0.11
Al	1.04	0.65	0.49	0.27	0.32	0.3	Plag	2.40 ($An_{87.4}$)
Fe	11.57	12.64	13.48	11.77	12.65	12.62	Hy	92.03 ($Wo_1Fs_{23}En_{74}$)
Mn	0.357	0.387	0.439	0.384	0.428	0.409	Ol	3.87 (Fa_{25})
Mg	16.31	15.62	16.29	17.03	15.55	16.11		
Ca	1.27	1.04	0.57	0.54	0.52	0.67		
Na	n.d.	0.02	0.08	0.02	0.03	0.04		
K	0.008	0.002	0.0027	0.0003	0.0013	0.0015		
P	<0.004	0.006	0.003	0.003	0.001	0.003		
Cr	n.d.	0.59	1.29	0.50	1.65	1.01		

(1) Manegaon, (2) Johnstown, (3) Ellemeet, (4) Tatahouine, and (5) Shalka. In calculating the norm, iron was regarded as FeO, though metal (1<wt.%) is present in Johnstown and Tatahouine and may be present in the others. The average and norm exclude Manegaon. n.d. = not determined. From Dodd (1981).

Table A1-5 *Major and commonly observed minor minerals in pallasites*

		Vol.%	
Mineral	Composition	Range	Mean
Olivine	$(Fe,Mg)_2SiO_4$	37.0–85.3	65.0
Metal	Fe, Ni	14.2–48.6	30.3
Troilite	FeS	0.1–7.3	2.3
Schreibersite	$(Fe,Ni)_3P$	0.2–2.8	1.2
Chromite	$FeCr_2O_4$	0.1–1.7	0.4
Low-Ca pyroxene	$(Fe,Mg)SiO_3$		
Whitlockite	$Ca_9(PO_4)_6$		
Stanfieldite	$Ca_4(Mg,Fe)_5(PO_4)_6$	0–4.2	0.1
Farringtonite	$Mg_3(PO_4)_2$		
Pentlandite	$(Fe,Ni)_9S_8$	—	0.1

From Dodd (1981).

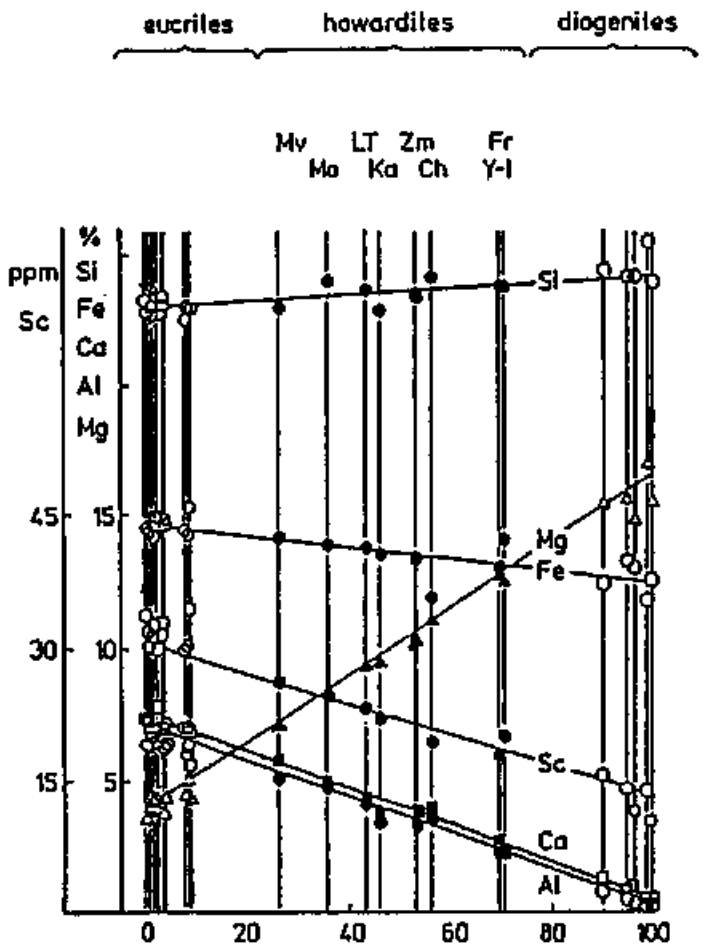

Figure A1-1

Mixing diagram computed from the compositions of howardites, assuming that they are mixtures two components. Mv: Malvern, Mo: Molteno, LT: Le Teilleul, Ka: Kapoeta, Zm: Zmenj, Ch: Chaves, Y-l: Yamato l, Fr: Frankfort. Open symbols are data for eucrites and diogenites plotted on the positions that were calculated by least squares fits. Modified from Dreibus and Wänke (1980).

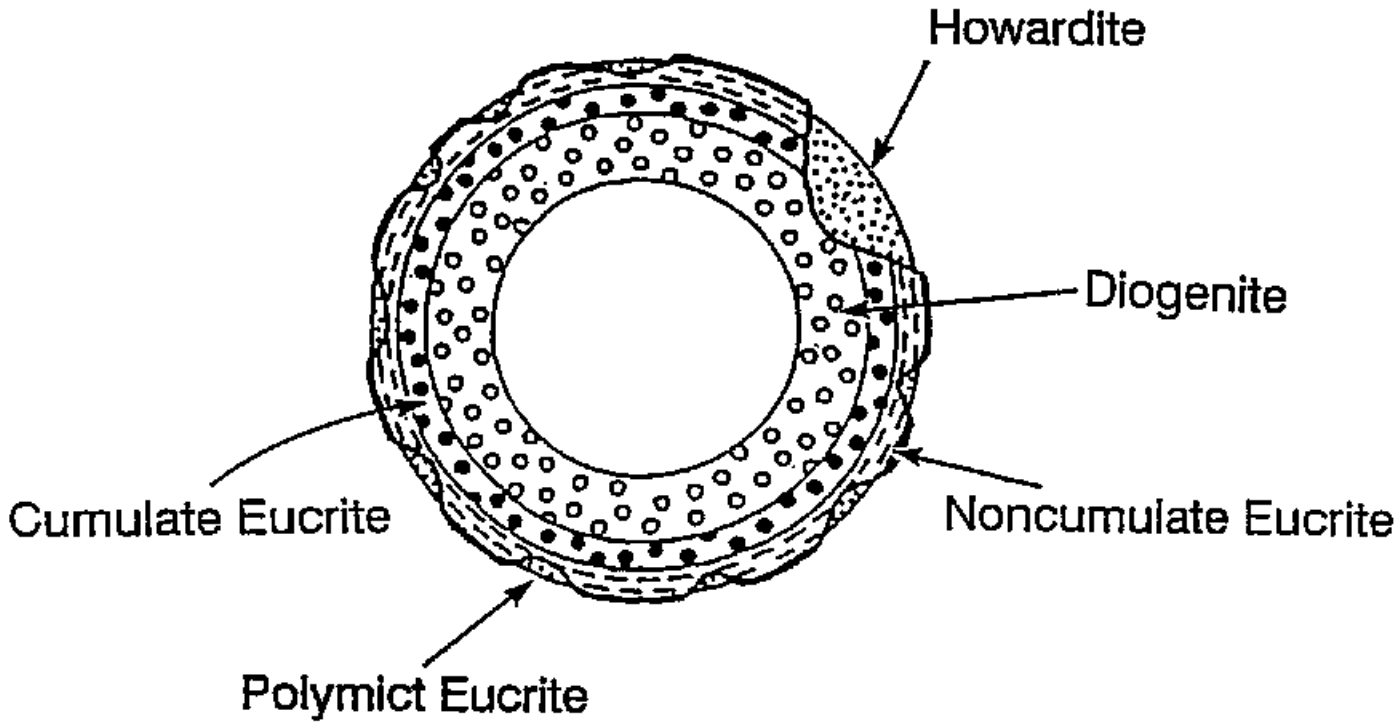

Figure A1-2
Cross section of Howardite, diogenite and eucrites parent body model. Howardite and polymict eucrite are polymict breccia of surface materials formed in craters of various depth. From Takeda (1982).

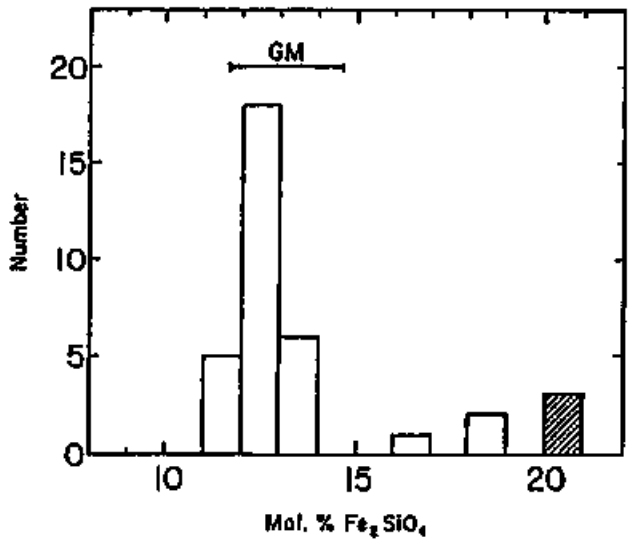

Figure A1-3

Mean composition of olivine in 29 pallasites. The range indicated for GM shows the extent of intergrain variation in Glorieta Mountain meteorite. Paired meteorites are represented by a single entry, and members of the Eagle Station group are marked with a hatched pattern. From Dodd (1981).

Appendix 2 Tables of compositions of run products

All compositions are listed in weight %. K, H and DL denote the data acquired by EDX systems of Kevex 7000Q, HORIBA and Kevex Delta, respectively. Quench and Fe loss effects are not corrected in this table.

Abbreviations; Ol: olivine, Px: pyroxene, Pl: plagioclase,

Ave: average value, Sigma: standard deviation of data,

Kd: Mg-Fe partition coefficient between melt and crystals.

CH-1	Melt						Ol				
H	1	2	3	4	Sigma	Ave	1	2	3	Sigma	Ave
1600											
Na_2O	0.0	0.2	0.0	0.0	0.1						
MgO	30.6	31.8	31.5	30.3	0.6		50.8	51.3	50.4	0.4	
Al_2O_3	3.1	3.4	3.2	3.5	0.1						
SiO_2	43.6	44.5	45.0	45.3	0.6		40.7	41.2	40.6	0.2	
K_2O	0.0	0.0	0.0	0.0	0.0						
CaO	3.1	3.1	3.0	3.2	0.1		0.1	0.1	0.1	0.0	
TiO_2	0.1	0.1	0.1	0.1	0.0						
Cr_2O_3	0.7	0.7	0.7	0.7	0.0		0.3	0.2	0.3	0.0	
MnO	0.5	0.6	0.4	0.6	0.1		0.3	0.2	0.2	0.0	
FeO	16.3	16.2	16.6	16.7	0.2		8.1	7.9	8.1	0.1	
Total	98.2	100.5	100.5	100.3			100.2	100.9	99.7		
Mg#	77.1	77.8	77.2	76.4	0.5	77.1	91.8	92.0	91.7	0.1	91.9

Kdol 0.30

CH-2	Melt							Ol						
H	1	2	3	4	5	Sigma	Ave	1	2	3	4	5	Sigma	Ave
1570														
Na_2O	0.1	0.2	0.2	0.3	0.1	0.1								
MgO	29.5	29.1	28.7	29.1	28.6	0.3		50.3	49.1	49.3	50.0	50.4	0.5	
Al_2O_3	3.7	4.1	3.9	4.0	4.0	0.1								
SiO_2	45.6	46.1	45.7	45.4	46.3	0.3		40.7	40.1	39.9	40.3	40.3	0.3	
K_2O	0.0	0.1	0.0	0.0	0.0	0.0								
CaO	3.5	3.7	3.5	3.5	3.8	0.1		0.1	0.0	0.1	0.1	0.2	0.1	
TiO_2	0.2	0.3	0.1	0.2	0.1	0.1								
Cr_2O_3	0.8	0.8	0.7	0.7	0.8	0.0		0.2	0.3	0.2	0.3	0.3	0.1	
MnO	0.6	0.6	0.6	0.6	0.6	0.0		0.3	0.2	0.2	0.2	0.3	0.0	
FeO	16.7	17.0	17.1	16.9	16.7	0.2		8.0	9.4	8.8	8.5	7.9	0.5	
Total	100.7	101.9	100.6	100.5	100.8			99.5	99.2	98.6	99.5	99.3		
Mg#	75.9	75.3	74.9	75.5	75.3	0.3	75.4	91.8	90.3	90.9	91.3	91.9	0.6	91.3

Kdol 0.29

CH-3	Melt						Ol						
H	1	2	3	4	Sigma	Ave	1	2	3	4	5	Sigma	Ave
1540													
Na_2O	0.2	0.1	0.3	0.2	0.1								
MgO	26.4	27.0	25.1	26.5	0.7		48.5	48.5	48.2	48.9	48.6	0.2	
Al_2O_3	3.7	3.8	4.6	3.7	0.4								
SiO_2	45.7	46.0	46.2	46.2	0.2		40.2	40.1	40.3	40.4	39.8	0.2	
K_2O	0.0	0.0	0.0	0.0	0.0								
CaO	3.8	3.6	4.3	3.7	0.2		0.2	0.2	0.2	0.1	0.1	0.0	
TiO_2	0.2	0.2	0.2	0.1	0.0								
Cr_2O_3	0.8	0.8	0.8	0.7	0.0		0.4	0.4	0.3	0.4	0.3	0.0	
MnO	0.6	0.6	0.6	0.5	0.0		0.2	0.3	0.2	0.3	0.4	0.1	
FeO	17.4	17.3	18.6	17.4	0.5		9.9	10.3	10.4	9.8	10.1	0.2	
Total	98.7	99.3	100.8	98.9			99.4	99.8	99.6	99.9	99.3		
Mg#	73.0	73.5	70.7	73.1	1.1	72.6	89.7	89.3	89.3	89.8	89.6	0.2	89.5

Kdol 0.31

CH-4 H 1510	Melt 1	2	3	4	5	Sigma	Ave	Ol 1	2	3	4	5	Sigma	Ave		
Na_2O	0.1	0.0	0.2	0.1	0.2	0.1										
MgO	25.2	25.0	25.6	21.1	21.5	2.0		47.9	48.2	47.9	48.4	48.3	0.2			
Al_2O_3	4.1	4.2	4.2	5.0	4.9	0.4										
SiO_2	46.7	47.2	47.0	47.6	47.0	0.3		40.0	40.1	39.8	39.9	39.9	0.1			
K_2O	0.0	0.1	0.0	0.0	0.1	0.0										
CaO	4.1	4.2	4.1	4.9	4.8	0.4		0.2	0.2	0.2	0.1	0.2	0.0			
TiO_2	0.2	0.2	0.1	0.1	0.3	0.1										
Cr_2O_3	0.8	0.8	0.8	0.9	0.9	0.0		0.7	0.3	0.4	0.4	0.4	0.1			
MnO	0.6	0.6	0.6	0.5	0.7	0.0		0.4	0.3	0.4	0.3	0.2	0.1			
FeO	17.0	17.4	17.3	18.5	17.7	0.5		10.6	10.6	10.7	10.6	10.8	5.2			
Total	98.7	99.5	99.8	98.7	97.9			99.8	99.8	99.3	99.7	99.8				
Mg#	72.6	71.9	72.5	67.1	68.3	2.3	70.5	88.9	89.0	88.8	89.1	88.9	0.1	88.9	Kdol	0.30

CH-5 H 1490	Melt 1	2	3	4	5	Sigma	Ave	Ol 1	2	3	4	5	Sigma	Ave		
Na_2O	0.3	0.1	0.2	0.2	0.0	0.1										
MgO	23.7	23.8	18.7	22.8	22.9	1.9		47.8	47.7	47.2	47.1	47.2	0.3			
Al_2O_3	5.5	5.5	6.1	5.4	5.7	0.2										
SiO_2	46.7	46.9	49.7	46.8	46.7	1.2		39.9	40.0	39.5	39.6	39.7	0.2			
K_2O	0.0	0.0	0.1	0.0	0.1	0.0										
CaO	4.2	4.3	5.4	4.6	4.5	0.4		0.1	0.1	0.1	0.1	0.1	0.0			
TiO_2	0.2	0.1	0.2	0.2	0.2	0.0										
Cr_2O_3	0.8	0.8	0.9	0.8	0.7	0.1		0.4	0.4	0.3	0.4	0.4	0.0			
MnO	0.6	0.6	0.6	0.5	0.7	0.1		0.2	0.3	0.3	0.3	0.3	0.1			
FeO	17.3	17.5	18.9	17.2	17.4	0.6		11.0	11.0	11.2	11.3	11.1	0.1			
Total	99.1	99.5	100.8	98.6	98.9			99.4	99.6	98.6	98.6	98.8				
Mg#	71.0	70.8	63.8	70.3	70.0	2.7	69.2	88.6	88.5	88.3	88.1	88.4	0.2	88.4	Kdol	0.30

CH-6 H 1470	Melt 1	2	3	Sigma	Ave	Ol 1	2	3	4	5	6	Sigma	Ave		
Na_2O	0.0	0.0	0.0	0.0											
MgO	20.9	21.8	22.4	0.6		47.8	47.3	47.7	47.1	47.1	46.9	0.3			
Al_2O_3	5.2	5.3	5.0	0.1											
SiO_2	48.3	49.0	47.8	0.5		40.3	40.1	40.0	39.9	39.5	39.8	0.3			
K_2O	0.0	0.0	0.0	0.0											
CaO	5.1	5.0	4.7	0.2		0.1	0.1	0.2	0.1	0.1	0.2	0.0			
TiO_2	0.2	0.2	0.2	0.0											
Cr_2O_3	0.8	0.9	0.8	0.0		0.4	0.4	0.4	1.0	1.0	0.4	0.3			
MnO	0.6	0.6	0.7	0.1		0.3	0.3	0.3	0.4	0.3	0.3	0.0			
FeO	16.1	17.6	17.7	0.2		11.9	11.7	11.9	11.9	11.9	11.6	0.1			
Total	99.0	100.2	99.3			100.9	99.8	100.5	100.3	99.8	99.4				
Mg#	87.3	88.6	89.3	0.8	88.4	87.7	87.9	87.8	87.6	87.6	87.6	0.1	87.7	Kdol	0.30

CH-7	Melt							Ol						
H	1	2	3	4	Sigma	Ave		1	2	3	4	5	Sigma	Ave
1450														
Na_2O	0.3	0.0	0.2	0.2	0.1									
MgO	18.5	18.7	18.7	21.3	1.2			46.1	45.2	45.6	46.4	45.9	0.2	
Al_2O_3	5.9	5.2	5.1	5.0	0.4									
SiO_2	49.9	48.6	47.2	47.9	1.0			39.4	39.1	39.6	39.7	39.2	0.2	
K_2O	0.1	0.0	0.1	0.0	0.0									
CaO	5.5	5.4	5.1	5.0	0.2			0.1	0.1	0.1	0.1	0.2	0.0	
TiO_2	0.3	0.2	0.2	0.2	0.0									
Cr_2O_3	1.0	0.9	0.8	0.8	0.1			0.4	0.6	0.4	0.6	0.4	0.1	
MnO	0.6	0.6	0.7	0.6	0.0			0.3	0.4	0.4	0.3	0.4	0.0	
FeO	17.9	18.0	16.6	17.2	0.6			12.2	12.4	12.5	12.1	12.2	0.1	
Total	100.0	97.6	94.5	98.2				98.5	98.7	99.6	99.2	98.3		
Mg#	64.8	64.9	66.8	68.9	1.7	66.4		87.1	86.9	86.9	87.3	87.0	0.1	87.0

Kdol 0.29

CH-8	Melt							Ol						
H	1	2	3	4	5	Sigma	Ave	1	2	3	4	5	Sigma	Ave
1430														
Na_2O	0.0	0.2	0.0	0.3	0.0	0.1								
MgO	17.5	18.7	20.0	18.6	19.0	1.2		45.3	45.1	45.6	45.5	45.3	0.2	
Al_2O_3	5.9	5.9	5.2	5.9	5.7	0.3								
SiO_2	48.9	48.1	47.4	49.4	48.6	0.7		39.0	38.9	38.9	38.9	38.6	0.1	
K_2O	0.1	0.0	0.0	0.0	0.0	0.0								
CaO	5.7	5.6	5.0	5.5	5.5	0.2		0.1	0.1	0.1	0.2	0.1	0.0	
TiO_2	0.3	0.2	0.3	0.1	0.2	0.1								
Cr_2O_3	0.9	0.8	0.9	0.8	0.9	0.1		0.5	0.3	0.4	0.4	0.4	0.1	
MnO	0.6	0.7	0.6	0.6	0.6	0.0		0.4	0.4	0.4	0.4	0.3	0.0	
FeO	17.4	16.8	16.4	16.8	17.1	0.3		12.4	12.4	12.3	12.5	12.5	0.1	
Total	97.2	95.0	95.8	97.7	97.7			97.6	97.1	97.8	97.8	97.2		
Mg#	64.2	63.8	68.5	66.4	66.5	1.7	65.9	86.7	86.7	86.8	86.6	86.6	0.1	86.7

Kdol 0.30

CH-9	Melt								Ol							
H	1	2	3	4	5	6	Sigma	Ave	1	2	3	4	5	Sigma	Ave	
1410																
Na_2O	0.0	0.1	0.0	0.0	0.0	0.1	0.0									
MgO	17.7	19.3	19.0	17.7	16.7	17.5	0.9		45.9	45.9	46.1	45.6	45.3	0.3		
Al_2O_3	6.1	6.0	6.0	6.2	6.3	6.5	0.2									
SiO_2	49.7	50.3	50.0	49.9	50.2	50.5	0.3		39.3	39.6	39.7	39.4	39.3	0.1		
K_2O	0.1	0.0	0.1	0.0	0.0	0.0	0.0									
CaO	5.8	5.5	5.6	5.7	6.1	5.9	0.2		0.2	0.2	0.2	0.2	0.2	0.0		
TiO_2	0.3	0.2	0.2	0.3	0.3	0.3	0.0									
Cr_2O_3	0.9	0.8	0.8	0.8	0.9	0.9	0.0		0.5	0.4	0.5	0.5	0.4	0.0		
MnO	0.6	0.6	0.5	0.6	0.6	0.6	0.0		0.4	0.4	0.4	0.4	0.4	0.0		
FeO	17.2	17.5	16.9	17.3	17.4	17.4	0.2		13.4	13.3	13.1	13.4	13.3	0.1		
Total	98.2	100.3	99.1	98.6	98.4	99.6			99.7	99.8	99.9	99.5	99.0			
Mg#	64.7	66.3	66.7	64.6	63.0	64.1	1.2	64.9	85.9	86.0	86.2	85.9	85.6	0.1	86.0	

Kdol 0.30

CH-10	Melt								Ol								
N	1	2	3	4	5	Sigma	Ave		1	2	3	4	5	6	Sigma	Ave	
1400																	
Na_2O	0.1	0.1	0.0	0.0	0.1	0.0											
MgO	16.4	16.6	16.4	16.3	18.3	0.8			44.6	44.7	45.1	44.9	45.3	45.4	0.3		
Al_2O_3	6.8	6.8	6.5	6.6	6.1	0.3											
SiO_2	50.6	50.3	50.1	50.2	50.0	0.2			38.5	38.6	38.5	38.6	38.6	38.8	0.1		
K_2O	0.0	0.1	0.0	0.1	0.0	0.0											
CaO	6.0	5.9	6.1	6.2	5.5	0.2			0.2	0.1	0.2	0.1	0.1	0.1	0.0		
TiO_2	0.3	0.3	0.2	0.4	0.3	0.0											
Cr_2O_3	0.7	0.8	0.8	0.9	0.7	0.1			0.4	0.4	0.4	0.4	0.4	0.4	0.0		
MnO	0.6	0.6	0.6	0.7	0.6	0.0			0.4	0.4	0.5	0.3	0.4	0.4	0.0		
FeO	15.4	15.8	15.9	15.6	15.2	0.3			11.6	12.3	12.5	12.4	12.6	12.3	0.3		
Total	96.7	97.3	96.5	96.8	96.8				95.7	96.6	97.1	96.7	97.6	97.4			
Mg#	65.5	65.2	64.8	65.1	68.3	1.3	65.8		87.3	86.6	86.6	86.5	86.5	86.6	0.3	86.7	Edol 0.29

CH-11	Melt							Ol							
N	1	2	3	4	Sigma	Ave		1	2	3	4	5	Sigma	Ave	
1380															
Na_2O	0.2	0.1	0.0	0.0	0.1										
MgO	15.8	16.9	16.0	16.3	0.4			45.6	45.8	45.2	45.3	45.4	0.2		
Al_2O_3	6.8	6.9	6.8	6.4	0.2										
SiO_2	51.6	51.4	51.7	51.2	0.2			39.9	39.5	38.9	9.3	39.3	0.3		
K_2O	0.0	0.0	0.1	0.1	0.0										
CaO	6.3	6.2	6.4	6.1	0.1			0.1	0.1	0.1	0.2	0.2	0.0		
TiO_2	0.3	0.3	0.3	0.3	0.0										
Cr_2O_3	0.6	0.7	0.6	0.7	0.0			0.4	0.3	0.3	0.4	0.6	0.1		
MnO	0.5	0.6	0.6	0.6	0.0			0.4	0.4	0.3	0.4	0.4	0.0		
FeO	16.0	16.4	16.5	16.8	0.3			13.5	13.9	13.6	13.8	13.9	0.2		
Total	98.1	98.7	99.0	98.5				99.9	100.0	96.4	99.3	99.8			
Mg#	63.7	64.7	63.3	63.5	0.6	63.8		85.8	85.4	85.5	85.4	85.3	0.2	85.5	Edol 0.30

CH-12	Melt								Ol							
N	1	2	3	4	5	6	Sigma	Ave	1	2	3	4	5	Sigma	Ave	
1350																
Na_2O	0.2	0.0	0.2	0.0	0.2	0.1	0.1									
MgO	15.3	15.6	15.8	15.5	14.4	14.7	0.5		44.9	44.9	45.0	45.3	44.8	0.2		
Al_2O_3	7.0	6.8	6.8	6.7	7.2	7.1	0.2									
SiO_2	52.8	52.7	52.5	52.4	53.2	52.8	0.3		39.0	39.3	38.9	39.4	39.3	0.2		
K_2O	0.0	0.0	0.0	0.0	0.0	0.1	0.0									
CaO	6.6	6.6	6.6	6.7	7.0	6.9	0.2		0.1	0.2	0.2	0.2	0.1	0.0		
TiO_2	0.3	0.2	0.3	0.3	0.3	0.3	0.0									
Cr_2O_3	0.6	0.5	0.7	0.6	0.6	0.6	0.0		0.5	0.4	0.4	0.4	0.4	0.0		
MnO	0.6	0.6	0.6	0.6	0.6	0.6	0.0		0.5	0.4	0.5	0.4	0.4	0.1		
FeO	15.4	15.6	15.6	15.7	16.0	15.9	0.2		14.3	14.1	14.3	14.3	14.2	0.1		
Total	98.7	98.8	99.1	98.5	99.4	98.9			99.2	99.3	99.3	100.0	99.1			
Mg#	64.0	63.7	64.1	63.8	61.6	62.2	1.0	63.2	84.9	85.0	84.9	85.0	84.9	0.1	84.9	Edol 0.31

CH-13	Melt								Ol								Px								
H	1	2	3	4	5	Sigma	Ave		1	2	3	4	5	Sigma	Ave		1	2	3	4	Sigma	Ave			
1330																									
Na_2O	0.2	0.3	0.0	0.2	0.3	0.1																			
MgO	14.3	13.4	14.4	13.8	14.6	0.5			43.8	44.1	44.0	44.3	43.9	0.2			31.9	30.7	32.0	32.5	0.7				
Al_2O_3	7.7	7.8	7.5	7.5	7.6	0.1											0.3	0.4	0.3	0.4	0.0				
SiO_2	52.2	52.3	52.1	52.1	52.4	0.1			39.2	39.1	39.2	39.1	38.8	0.1			56.2	56.3	56.9	55.7	0.4				
K_2O	0.1	0.1	0.1	0.1	0.1	0.0																			
CaO	7.3	7.5	7.1	7.5	7.2	0.2			0.2	0.2	0.1	0.2	0.2	0.0			0.6	0.6	0.5	0.8	0.1				
TiO_2	0.3	0.4	0.3	0.3	0.4	0.0																			
Cr_2O_3	0.5	0.5	0.5	0.5	0.6	0.0			0.4	0.3	0.4	0.4	0.3	0.0			0.7	0.8	0.6	0.7	0.1				
MnO	0.6	0.6	0.8	0.6	0.7	0.0			0.4	0.5	0.4	0.4	0.4	0.0			0.4	0.4	0.4	0.5	0.0				
FeO	16.0	16.3	15.8	16.0	15.8	0.2			15.7	15.4	15.8	15.5	15.3	0.2			9.5	9.7	9.8	9.2	0.2				
Total	99.4	99.0	98.4	98.6	99.7				99.8	99.6	99.8	99.9	98.8				99.5	98.8	100.4	99.8					
Mg#	81.4	59.4	61.9	60.5	62.2	1.0	61.1		83.3	83.7	83.2	83.6	83.6	0.2	83.5		85.6	84.9	85.6	86.3	0.5	85.6		Kdol	0.31
																En	84.7	84.0	84.7	85.0	0.4	84.8		Kdpx	0.26
																Wo	1.1	1.1	1.0	1.5	0.2	1.2			

CH-14	Melt									Ol							Px								
H	1	2	3	4	5	6	7	Sigma	Ave	1	2	3	4	5	Sigma	Ave	1	2	3	4	5	Sigma	Ave		
1300																									
Na_2O	0.3	0.2	0.1	0.5	0.1	0.2	0.3	0.1																	
MgO	13.2	13.2	12.9	12.6	12.7	12.4	12.6	0.3		43.9	43.9	43.7	44.0	43.4	0.2		32.5	32.6	31.3	31.0	31.5	0.7			
Al_2O_3	8.9	9.0	9.0	9.2	9.2	8.9	9.0	0.1									0.7	0.9	0.7	0.7	0.6	0.1			
SiO_2	52.8	52.4	52.8	52.6	52.4	52.5	52.5	0.2		39.3	39.4	39.2	39.6	38.8	0.3		56.2	56.2	56.3	55.9	56.1	0.1			
K_2O	0.3	0.3	0.3	0.2	0.2	0.2	0.3	0.0																	
CaO	8.4	8.3	8.6	8.6	8.5	8.5	8.4	0.1		0.2	0.2	0.2	0.2	0.2	0.0		0.6	0.8	0.9	0.9	0.8	0.1			
TiO_2	0.5	0.4	0.4	0.4	0.4	0.3	0.3	0.0																	
Cr_2O_3	0.4	0.4	0.4	0.4	0.5	0.5	0.5	0.0		0.3	0.4	0.3	0.3	1.5	0.5		0.3	0.3	0.7	0.6	0.6	0.2			
MnO	0.6	0.6	0.6	0.6	0.6	0.5	0.6	0.0		0.5	0.5	0.5	0.5	0.4	0.0		0.4	0.5	0.5	0.4	0.4	0.0			
FeO	15.0	15.0	15.3	15.3	14.7	15.5	15.4	0.3		15.6	16.1	16.5	16.4	16.5	0.3		8.9	9.0	10.5	10.2	10.1	0.7			
Total	100.2	99.7	100.3	100.4	99.2	99.5	99.6			99.8	100.5	100.5	101.0	100.8			99.7	100.2	100.8	99.7	100.1				
Mg#	61.1	60.9	60.0	59.6	60.7	58.9	59.3	0.8	60.1	63.4	62.9	62.5	62.7	62.4	0.3	62.8	86.7	86.6	84.1	84.5	84.7	1.1	85.3	Kdol	0.31
																	En	85.6	85.3	82.6	83.0	83.5	1.2	84.0	Kdpx	0.28
																	Wo	1.2	1.5	1.8	1.6	1.4	0.2	1.5		

CH-15	Melt						Ol							Px								
H	1	2	3	4	Sigma	Ave	1	2	3	4	5	Sigma	Ave	1	2	3	4	5	Sigma	Ave		
1280																						
Na_2O	0.5	0.3	0.3	0.3	0.1																	
MgO	11.6	11.6	11.3	12.0	0.3		43.5	43.5	43.3	43.5	43.6	0.1		31.1	30.2	30.9	30.8	31.1	0.3			
Al_2O_3	9.9	9.9	10.2	9.9	0.1									0.5	0.4	0.6	0.7	0.7	0.1			
SiO_2	52.1	52.3	52.6	51.7	0.3		39.8	39.5	39.2	39.6	38.9	0.3		56.0	55.9	56.2	56.1	56.3	0.1			
K_2O	0.1	0.2	0.2	0.1	0.0																	
CaO	8.9	9.3	9.4	8.8	0.3		0.2	0.2	0.3	0.2	0.2	0.0		0.9	1.3	1.1	1.0	1.0	0.1			
TiO_2	0.4	0.4	0.4	0.4	0.0																	
Cr_2O_3	0.4	0.3	0.3	0.2	0.1		0.1	0.3	0.2	0.3	0.5	0.1		0.6	0.4	0.6	0.6	0.6	0.1			
MnO	0.5	0.6	0.6	0.5	0.0		0.4	0.6	0.5	0.5	0.5	0.0		0.4	0.4	0.5	0.5	0.4	0.0			
FeO	14.4	14.7	14.9	15.1	0.3		16.7	17.0	17.2	17.3	17.2	0.2		10.5	10.7	10.9	10.6	10.3	0.2			
Total	99.1	99.3	100.2	99.1			100.8	101.0	100.7	101.3	100.9			100.0	99.2	100.7	100.3	100.4				
Mg#	69.4	68.4	67.5	68.7	0.7	68.5	82.3	82.0	81.7	81.7	81.9	0.2	81.9	84.1	83.4	83.5	83.8	84.3	0.3	83.8	Kdol	0.31
														En	82.6	81.4	81.8	82.3	82.7	0.5	82.1	Kdpx	0.27
														Wo	1.8	2.4	2.0	1.9	1.9	0.2	2.0		

CH-16	Melt								Ol								Px							
K	1	2	3	4	5	6	Sigma	Ave	1	2	3	4	5	6	Sigma	Ave	1	2	3	4	Sigma	Ave		
1250																								
Na_2O	0.5	0.4	0.3	0.3	0.3	0.3	0.1																	
MgO	11.1	10.3	9.6	11.0	9.8	10.5	0.6		41.3	41.3	41.8	41.2	41.8	41.8	0.3		29.2	28.9	29.5	28.8	0.3			
Al_2O_3	10.7	11.0	11.5	11.0	11.5	10.8	0.3										0.8	1.2	0.7	1.0	0.2			
SiO_2	48.7	48.6	49.6	49.3	49.8	48.2	0.6		38.2	38.5	39.1	38.3	38.3	38.4	0.3		55.3	55.1	54.9	55.1	0.1			
K_2O																								
CaO	8.4	9.5	9.9	9.0	9.6	9.6	0.5		0.3	0.3	0.3	0.2	0.3	0.3	0.0		1.8	1.8	1.6	1.6	0.1			
TiO_2	0.2	0.4	0.3	0.3	0.5	0.4	0.1																	
Cr_2O_3	0.2	0.2	0.3	0.4	0.3	0.2	0.1		0.4			0.3	0.3	0.8	0.2		0.5	0.6	0.5	0.4	0.1			
MnO	0.5	0.5	0.4	1.0	0.4	0.5	0.2		0.7	0.5	0.5	0.5		0.7	0.1		0.5	0.9	0.6	0.5	0.1			
FeO	13.0	13.3	13.3	13.5	13.3	13.5	0.1		17.1	17.0	16.8	16.9	17.0	16.7	0.1		11.0	10.8	11.2	11.0	0.1			
Total	93.5	94.2	95.3	95.8	95.4	93.9			98.0	97.5	98.5	97.4	97.6	96.8			99.1	99.2	98.8	98.4				
Mg#	60.4	57.9	56.3	59.2	56.8	58.1	1.4	58.2	81.1	81.2	81.6	81.3	81.4	81.7	0.2	81.4	82.5	82.7	82.5	82.3	0.1	82.5	Kdol	0.32
																	En	79.6	79.8	80.0	79.6	0.2	79.8	Kdpx	0.29
																	Wo	3.5	3.5	3.0	3.2	0.2	3.3		

CH-17	Melt							Ol								Px							
K	1	2	3	4	5	Sigma	Ave	1	2	3	4	5	Sigma	Ave		1	2	3	4	5	Sigma	Ave	
1200																							
Na_2O	0.5	0.8	0.3	0.4	0.6	0.2																	
MgO	9.0	9.1	7.5	7.7	8.0	0.7		39.7	40.1	40.0	39.7	40.3	0.2			28.0	27.9	28.0	26.8	27.2	0.5		
Al_2O_3	12.9	12.5	13.0	13.2	12.7	0.2										1.4	1.2	1.3	1.3	1.4	0.1		
SiO_2	47.5	47.6	47.7	47.5	46.2	0.5		36.6	36.0	36.3	37.0	36.1	0.4			50.9	51.2	50.6	51.0	51.6	0.3		
K_2O																							
CaO	9.9	9.9	10.7	10.8	10.3	0.4		0.3	0.2	0.3	0.3	0.3	0.0			1.9	1.9	1.5	2.6	2.8	0.5		
TiO_2	0.5	0.4	0.3	0.4	0.5	0.1																	
Cr_2O_3																0.5	0.5	0.4	0.5	0.3	0.1		
MnO	0.5	0.4	0.4	0.5	0.3	0.1		0.5	0.5	0.5	0.5	0.7	0.1			0.4	0.5				0.0		
FeO	11.5	11.3	11.8	11.4	11.1	0.2		16.5	17.0	16.8	16.6	16.6	0.2			10.1	9.7	10.3	10.3	10.1	0.2		
Total	92.2	92.1	91.6	91.9	89.8			93.5	93.8	93.9	94.1	93.9	0.2			93.3	92.8	92.0	92.4	93.3			
Mg#	58.0	59.0	53.1	54.6	56.2	2.1	56.3	81.1	80.8	81.0	81.0	81.3	0.1	81.0		83.1	83.7	83.0	82.3	82.7	0.5	83.0	Kdol 0.30
																En	80.0	80.5	80.5	77.8	78.0	1.2	79.3	Kdpx 0.26
																Wo	3.9	3.9	3.0	5.5	5.6	1.1	4.4	

ED-1	Melt						
K	1	2	3	4	Sigma	Ave	
1420							
Na_2O	0.2	0.3	0.3	0.1	0.1		
MgO	18.0	18.7	18.3	18.0	0.3		
Al_2O_3	6.9	6.3	6.6	6.1	0.3		
SiO_2	51.8	50.2	50.5	51.7	0.7		
K_2O							
CaO	5.0	5.3	5.1	4.9	0.2		
TiO_2	0.4	0.3	0.4	0.3	0.1		
Cr_2O_3	0.9	0.8	0.7	0.7	0.1		
MnO	0.6	0.4	0.6	0.5	0.1		
FeO	16.7	16.2	17.3	16.5	0.4		
Total	100.5	98.6	99.7	98.8			
Mg#	65.7	67.3	65.3	66.1	0.8	66.1	

ED-2	Melt						
K	1	2	3	4	5	Sigma	Ave
1400							
Na_2O	0.1	0.3	0.4	0.1	0.2	0.1	
MgO	18.4	18.5	18.4	18.5	18.5	0.1	
Al_2O_3	7.4	6.4	6.5	6.1	6.3	0.4	
SiO_2	51.6	52.1	51.9	51.3	51.0	0.4	
K_2O							
CaO	5.2	5.2	5.1	5.3	5.3	0.1	
TiO_2	0.3	0.4	0.3	0.3	0.2	0.0	
Cr_2O_3	0.6	0.7	0.7	0.7	0.6	0.1	
MnO	0.6	0.5	0.6	0.6	0.6	0.0	
FeO	15.2	16.6	16.0	15.3	15.2	0.6	
Total	99.7	100.7	99.7	98.3	97.9		
Mg#	68.4	66.5	67.2	68.2	68.5	0.8	67.8

KD-3	Melt							Ol						
K	1	2	3	4	5	Sigma	Ave	1	2	3	4	5	Sigma	Ave
1370														
Na_2O	0.3	0.1	0.4	0.2	0.0	0.2								
MgO	17.3	17.4	17.1	17.2	17.3	0.1		44.4	44.4	45.1	44.4	45.5	0.5	
Al_2O_3	6.4	6.1	6.7	6.2	6.2	0.2								
SiO_2	51.7	52.2	51.9	52.1	52.6	0.3		40.2	40.2	40.3	39.7	40.2	0.2	
K_2O														
CaO	5.3	5.2	5.3	5.2	5.2	0.1		0.0	0.2	0.4	0.2	0.2	0.1	
TiO_2	0.3	0.4	0.3	0.3	0.2	0.1								
Cr_2O_3	0.7	0.5	0.6	0.6	0.4	0.1		0.2	0.5	0.4	0.4	0.4	0.1	
MnO	0.8	0.8	0.6	0.6	0.4	0.2		0.5	0.5	0.5	0.4	0.5	0.1	
FeO	16.2	15.8	17.3	16.9	16.1	0.6		14.3	14.8	14.6	14.4	14.4	0.2	
Total	98.9	98.5	100.2	99.2	99.3			99.6	100.5	101.3	99.4	101.1		
Mg#	65.5	66.2	63.6	64.4	65.6	0.9	65.1	84.7	84.2	84.6	84.6	84.9	0.2	84.6

Kdol 0.34

KD-4	Melt							Ol						Px								
K	1	2	3	4	5	Sigma	Ave	1	2	3	4	Sigma	Ave	1	2	3	4	5	Sigma	Ave		
1330																						
Na_2O	0.3	0.1	0.3	0.2	0.4	0.1																
MgO	15.2	14.9	15.0	15.1	15.1	0.1		43.0	43.1	43.1	42.7	0.2		31.0	31.0	31.0	31.4	31.2	0.2			
Al_2O_3	7.2	7.2	7.2	7.1	7.2	0.1								0.4	0.7	0.6	0.4	0.2	0.2			
SiO_2	52.2	51.6	51.9	52.1	52.0	0.2		39.1	39.4	39.1	39.1	0.1		55.8	55.4	56.0	56.3	56.2	0.3			
K_2O	0.0	0.1	0.1	0.1	0.0	0.0																
CaO	6.2	6.2	6.2	6.2	6.2	0.0		0.2	0.2	0.2	0.2	0.0		0.5	0.6	0.5	0.5	0.5	0.0			
TiO_2	0.3	0.3	0.5	0.4	0.3	0.1																
Cr_2O_3	0.4	0.4	0.5	0.5	0.5	0.0		0.3	0.3	0.3	0.3	0.0		0.8	1.9	0.6	0.5	0.6	0.5			
MnO	0.6	0.6	0.6	0.6	0.5	0.0		0.5	0.4	0.5	0.5	0.0		0.4	0.4	0.3	0.6	0.5	0.1			
FeO	17.9	17.7	17.9	17.8	17.9	0.1		17.2	17.5	17.3	17.5	0.1		10.8	11.0	10.9	10.8	10.9	0.1			
Total	100.2	99.0	100.1	100.0	100.1			100.2	100.9	100.4	100.2			99.7	101.0	99.9	100.5	100.0				
Mg#	60.2	59.9	59.9	60.2	60.0	0.1	60.0	81.7	81.4	81.6	81.3	0.1	81.5	83.7	83.3	83.5	83.8	83.6	0.2	83.6	Kdol	0.34
														En	82.8	82.5	82.7	83.0	82.8	0.2	82.8	Kdpx 0.30
														Wo	1.0	1.1	0.9	0.9	1.0	0.0	1.0	

KD-5	Melt							Ol						Px								
K	1	2	3	4	5	Sigma	Ave	1	2	3	4	Sigma	Ave	1	2	3	4	Sigma	Ave			
1300																						
Na_2O	0.7	0.7	0.5	0.2	0.3	0.2																
MgO	12.5	12.6	12.8	12.9	12.6	0.2		40.8	40.0	40.8	39.6	0.5		29.9	29.3	29.8	29.3	0.3				
Al_2O_3	8.2	8.3	8.1	8.0	8.4	0.1								0.2	0.4	0.8	0.3	0.2				
SiO_2	49.7	49.8	50.3	49.9	50.4	0.3		38.7	38.5	39.6	38.7	0.4		56.4	56.1	55.8	56.7	0.3				
K_2O																						
CaO	7.0	7.0	6.9	6.9	6.9	0.0				0.2	0.2	0.0		0.8	0.8	0.7	0.7	0.0				
TiO_2	0.3	0.4	0.4	0.4	0.3	0.1																
Cr_2O_3	0.2	0.4	0.3	0.4	0.4	0.0		0.3	0.2	0.3	0.3	0.0		0.5	0.5	0.6	0.5	0.0				
MnO	0.6	0.6	0.6	0.7	0.6	0.0		0.5	0.3	0.6	0.6	0.1		0.5	0.6	0.6	0.4	0.1				
FeO	18.5	18.2	17.8	18.5	18.6	0.3		19.7	19.7	19.2	19.4	0.2		12.8	11.8	11.8	12.4	0.4				
Total	97.8	97.9	97.7	98.0	98.4			100.0	98.7	100.6	98.7			101.0	99.4	100.0	100.2					
Mg#	54.6	55.3	56.2	55.5	54.7	0.6	55.3	78.7	78.3	79.1	78.4	0.3	78.6	80.6	81.5	81.6	80.9	0.5	81.2	Kdol	0.34	
														En	79.4	80.3	80.7	79.6	0.5	80.1	Kdpx	0.29
														Wo	1.5	1.5	1.4	1.3	0.1	1.4		

ED-6	Melt							Ol						Px								
H	1	2	3	4	5	Sigma	Ave	1	2	3	4	Sigma	Ave	1	2	3	4	5	Sigma	Ave		
1280																						
Na_2O	0.3	0.5	0.7	0.4	0.3	0.1																
MgO	12.6	11.7	11.7	11.7	11.8	0.3		39.9	39.5	39.8	39.5	0.2		29.8	32.2	29.7	29.1	30.7	1.1			
Al_2O_3	8.3	8.4	8.5	8.8	8.6	0.2								0.6	0.7	0.7	0.5	0.6	0.1			
SiO_2	51.8	51.1	51.1	51.3	51.1	0.3		38.3	38.2	38.6	38.0	0.2		55.5	55.7	55.6	55.1	55.6	0.3			
K_2O	0.1	0.0	0.1	0.1	0.2	0.0																
CaO	7.5	7.6	7.9	7.7	7.7	0.1		0.2	0.2	0.2	0.2	0.0		0.8	0.7	0.8	0.9	0.7	0.1			
TiO_2	0.4	0.5	0.5	0.5	0.5	0.0																
Cr_2O_3	0.4	0.5	0.3	0.6	0.3	0.1		0.3	0.2	0.2	0.3	0.0		0.4	0.5	0.5	0.5	0.3	0.1			
MnO	0.5	0.7	0.6	0.6	0.6	0.0		0.5	0.6	0.6	0.6	0.0		0.5	0.5	0.5	0.4	0.5	0.0			
FeO	18.5	18.7	18.8	19.0	18.7	0.1		21.2	21.3	21.5	21.5	0.2		12.4	10.1	12.7	12.9	11.1	1.1			
Total	100.4	99.5	100.2	100.8	99.8			100.4	100.0	101.0	100.0			100.0	100.4	100.5	99.4	99.8				
Mg#	54.7	52.8	52.7	52.4	52.8	0.8	53.1	77.1	76.7	76.8	76.6	0.2	76.8		81.0	85.1	80.7	80.1	83.2	1.9	82.0	
														En	79.7	83.9	79.4	78.7	82.0	1.9	80.8	
														Wo	1.6	1.3	1.6	1.7	1.4	0.1	1.5	

																					Kdol	0.34
																					Kdpx	0.25

ED-7	Melt							Ol						Px								
K	1	2	3	4	5	Sigma	Ave	1	2	3	4	Sigma	Ave	1	2	3	4	5	Sigma	Ave		
1250																						
Na_2O	0.4	0.3	0.5	0.4	0.6	0.2																
MgO	9.4	9.4	9.2	9.2	9.0	0.2		36.7	36.7	36.5	36.6	0.1		32.1	27.2	27.4	30.4	29.9	1.9			
Al_2O_3	10.0	9.8	9.7	9.7	9.8	0.1								1.1	0.3	0.7	1.0	1.2	0.3			
SiO_2	48.7	49.1	48.6	48.8	48.8	0.2		37.8	37.9	38.3	37.8	0.2		56.0	55.4	55.7	55.6	56.0	0.2			
K_2O	0.0	0.0	0.0	0.0	0.0																	
CaO	8.6	8.4	8.4	8.6	8.7	0.1		0.2	0.2	0.2	0.3	0.1		1.1	1.1	1.0	1.0	1.1	0.0			
TiO_2	0.4	0.5	0.5	0.5	0.5	0.0																
Cr_2O_3	0.0	0.0	0.0	0.0	0.0					0.2	0.3	0.0		0.3	0.5	0.4	0.3	0.3	0.1			
MnO	0.6	0.6	0.6	0.6	0.6	0.0		0.7	0.6	0.7	0.7	0.0		0.7	0.7	0.6	0.6	0.5	0.1			
FeO	20.2	19.2	19.9	18.9	20.4	0.6		24.0	23.9	23.7	23.8	0.1		9.1	14.7	13.9	11.3	12.1	2.0			
Total	98.2	97.4	97.5	96.8	98.5			99.4	99.3	99.6	99.5			100.3	99.9	99.8	100.3	100.9				
Mg#	45.2	46.6	45.3	46.6	43.9	1.0	45.5	73.2	73.2	73.3	73.2	0.0	73.2		86.3	76.7	77.8	82.8	81.6	3.5	79.7	
														En	84.6	75.1	76.2	81.2	79.9	3.4	78.1	
														Wo	2.0	2.1	2.0	1.9	2.1	0.1	2.0	

																					Kdol	0.31
																					Kdpx	0.22

ED-8	Melt							Ol							Px								
H	1	2	3	4	5	Sigma	Ave	1	2	3	4	5	Sigma	Ave	1	2	3	4	5	6	7	Sigma	Ave
1220																							
Na_2O	0.4	0.5	0.7	0.4	0.4	0.1																	
MgO	8.7	8.5	8.9	8.7	8.8	0.1		36.0	36.4	36.1	36.1	36.6	0.2		29.1	27.0	30.1	26.8	28.3	29.0	26.6	1.3	
Al_2O_3	10.9	10.8	10.8	10.8	10.9	0.1									0.9	0.7	0.7	0.6	1.4	1.5	0.8	0.3	
SiO_2	50.6	51.3	50.6	50.8	50.6	0.3		37.1	37.3	36.6	37.3	36.0	0.4		54.7	54.1	55.3	54.1	54.2	54.4	54.7	0.4	
K_2O	0.2	0.1	0.1	0.1	0.1	0.0																	
CaO	9.6	9.4	9.5	9.5	9.5	0.1		0.3	0.3	0.3	0.3	0.4	0.0		1.2	1.4	1.4	1.3	1.2	1.3	1.7	0.2	
TiO_2	0.6	0.6	0.6	0.6	0.6	0.0																	
Cr_2O_3	0.3	0.2	0.2	0.2	0.2	0.0		0.2	0.2	1.5	0.2	0.2	0.5		0.3	0.6	0.3	0.5	0.6	0.3	0.6	0.1	
MnO	0.6	0.5	0.6	0.5	0.5	0.0		0.6	0.7	0.7	0.7	0.7	0.0		0.6	0.6	0.6	0.6	0.5	0.6	0.5	0.0	
FeO	18.6	17.9	18.5	18.2	18.3	0.2		25.6	26.0	26.2	26.0	25.7	0.2		12.9	16.0	11.9	15.9	13.1	13.2	16.0	1.6	
Total	100.3	99.9	100.4	99.8	99.8			99.8	100.7	101.4	100.5	101.6			99.6	100.4	100.4	99.7	99.2	100.2	100.8		
Mg#	45.3	46.2	46.2	46.0	46.0	0.3	45.9	71.5	71.4	71.0	71.2	71.8	0.3	71.4	80.1	75.0	81.9	75.0	79.3	79.7	74.8	2.7	77.6
															En	78.3	72.9	79.7	73.1	77.5	77.7	72.3	2.8	75.5
															Wo	2.2	2.7	2.7	2.6	2.4	2.5	3.2	0.3	2.7

																					Kdol	0.34
																					Kdpx	0.25

ED-9	Melt									Px							
K	1	2	3	4	5	6	7	Sigma	Ave	1	2	3	4	5	6	Sigma	Ave**
1200																	
Na_2O	0.4	0.6	0.4	0.5	0.1	0.9	0.2	0.3									
MgO	7.3	6.8	7.3	7.5	7.5	7.5	7.3	0.2		26.1	25.2	27.8	30.0	26.0	29.4	1.8	
Al_2O_3	11.3	11.1	11.6	11.4	11.6	11.1	11.4	0.2		0.2	1.5	1.7	1.7	1.5	1.8	0.5	
SiO_2	48.9	47.6	47.8	46.2	47.9	47.3	47.7	0.5		53.9	52.5	53.1	54.1	53.4	53.9	0.6	
K_2O																	
CaO	9.3	9.4	9.4	9.2	9.3	9.3	9.3	0.0		1.5	2.3	1.5	1.4	1.4	1.4	0.3	
TiO_2	0.6	0.5	0.6	0.5	0.5	0.6	0.6	0.0									
Cr_2O_3	0.1	0.2	0.1	0.0	0.3	0.0	0.1	0.1		0.3	0.5	0.3		0.4		0.1	
MnO	0.5	0.5	0.4	0.5	0.5	0.4	0.5	0.1		0.6	0.5	0.6	0.6	0.5	0.6	0.0	
FeO	17.2	17.1	17.3	18.8	17.7	17.3	17.7	0.3		14.3	15.0	12.9	9.3	15.0	10.7	2.2	
Total	95.7	93.8	94.8	95.0	95.5	94.4	94.9			97.0	97.5	98.0	97.1	98.1	97.7		
Mg#	43.2	41.6	43.0	44.3	43.0	43.6	42.2	0.8	43.1	76.5	75.0	79.4	85.2	75.5	83.1	3.9	77.9
										En 74.1	71.6	77.0	82.8	73.3	80.6	4.1	75.4
										Wo 3.1	4.6	3.0	2.8	2.9	2.8	0.6	3.3

Kdpx 0.21

ED-10	Melt								Ol					Px					
H	1	2	3	4	5	6	Sigma	Ave	1	2	3	Sigma	Ave	1	2	3	Sigma	Ave	
1180																			
Na_2O	0.7	0.9	0.8	0.6	0.7	0.4	0.2												
MgO	7.3	7.2	7.3	7.4	7.1	7.0	0.1		34.5	33.0	36.1	1.3		25.4	29.4	27.1	1.7		
Al_2O_3	12.6	12.4	12.5	12.5	12.4	12.1	0.1							1.4	1.8	1.6	0.1		
SiO_2	50.2	50.8	50.8	50.0	49.4	49.1	0.6		37.4	37.3	37.5	0.1		54.0	54.2	54.3	0.1		
K_2O	0.1	0.1	0.2	0.1	0.2	0.1	0.0												
CaO	10.2	10.5	10.6	10.4	10.4	10.2	0.2		0.3	0.2	0.4	0.1		1.8	2.3	1.9	0.2		
TiO_2	0.7	0.6	0.7	0.6	0.8	0.6	0.1												
Cr_2O_3	0.2	0.0	0.2	0.2	0.2	0.2	0.1		0.1	0.2	0.1	0.0		0.5	0.3	0.3	0.1		
MnO	0.5	0.4	0.5	0.5	0.5	0.4	0.0		0.6	0.5	0.4	0.1		0.6	0.7	0.7	0.0		
FeO	17.6	17.6	17.5	17.5	17.4	17.7	0.1		28.7	28.2	27.3	0.8		17.2	11.4	14.8	2.4		
Total	100.0	100.5	101.0	99.8	99.2	97.8			101.7	100.4	101.9			100.9	100.1	100.5			
Mg#	42.4	42.0	42.6	43.1	42.2	41.4	0.5	42.3	68.2	66.9	70.2	1.4	68.4		72.4	82.2	76.5	4.0	77.0
														En	69.8	78.6	73.7	3.6	74.0
														Wo	3.6	4.4	3.7	0.4	3.9

Kdol 0.34
Kdpx 0.22

ED-11	Melt							Px										Pl					
K	1	2	3	4	Sigma	Ave		1	2	3	4	5	6	7	8	9	Sigma	Ave	1	2	3	Sigma	Ave
1160																							
Na_2O	0.5	0.5	0.5	0.4	0.0														1.1	1.3	0.6	0.3	
MgO	6.0	6.2	6.2	6.2	0.1			28.8	25.8	24.8	23.5	22.9	21.9	23.3	23.0	23.2	1.5		1.4	1.1	2.0	0.4	
Al_2O_3	12.8	13.0	13.0	13.1	0.1			2.0	1.9	0.9	0.7	1.1	0.7	1.5	1.1	1.2	0.4		31.1	32.3	31.2	0.5	
SiO_2	49.5	49.6	49.0	49.6	0.3			54.8	54.3	54.4	54.2	53.4	53.6	53.3	53.9	54.5	0.5		47.4	47.1	46.9	0.2	
K_2O	0.2	0.2	0.2	0.2	0.0																		
CaO	10.0	10.1	10.2	10.2	0.1			2.6	3.3	2.7	2.8	3.2	3.8	2.7	3.2	2.9	0.4		16.8	17.3	17.0	0.2	
TiO_2	1.0	0.9	1.1	1.0	0.1																		
Cr_2O_3										0.3	0.5	0.3	0.5	0.5	0.4	0.5	0.1						
MnO	0.5	0.5	0.4	0.5	0.0			0.6	0.8	0.5	0.6	0.6		0.5	0.5	0.6	0.1						
FeO	17.3	17.2	16.7	17.5	0.3			14.3	14.8	15.7	17.3	17.8	18.0	17.7	17.2	17.2	1.3		2.8	1.6	1.8	0.5	
Total	97.9	98.2	97.3	98.7				101.1	100.9	99.3	99.5	99.2	98.5	99.5	99.4	100.2			100.6	100.7	99.5		
Mg#	38.2	39.2	39.7	38.6	0.6	39.0		77.0	75.6	73.8	70.8	69.6	68.5	70.1	70.5	70.7	2.8	71.8	An	89.4	88.4	93.9	2.4	90.6
							En	73.1	70.7	69.8	66.7	65.1	63.1	66.2	65.8	66.4	3.0	67.4						
							Wo	5.1	6.5	5.4	5.7	6.5	7.9	5.6	6.8	6.0	0.8	6.1						

Kdpx 0.25

ED-12	Melt						Px						Pl							
K	1	2	3	Sigma	Ave		1	2	3	4	Sigma	Ave	1	2	3	Sigma	Ave			
1140																				
Na_2O	0.4	0.2	0.7	0.2									2.0	2.7	1.6	0.4				
MgO	6.0	5.4	5.7	0.2			23.1	22.8	21.0	20.9	1.0		1.4	1.0	1.8	0.3				
Al_2O_3	12.4	12.6	13.2	0.3			0.7	0.9	1.0	1.2	0.2		31.1	32.5	31.3	0.6				
SiO_2	49.0	49.9	49.2	0.4			55.0	54.6	53.7	53.5	0.6		48.3	47.6	46.9	0.6				
K_2O	0.2	0.3	0.1	0.1																
CaO	10.3	10.3	10.0	0.1			2.7	3.1	3.4	3.0	0.2		16.0	15.3	16.1	0.4				
TiO_2	2.2	1.7	2.0	0.2				0.3												
Cr_2O_3							0.4	0.4	0.4	0.3	0.0									
MnO	0.4	0.4	0.4	0.0			0.7	0.7	0.6	0.6	0.1									
FeO	17.9	17.1	16.7	0.6			19.5	20.4	20.0	19.0	0.5		2.8	1.4	2.3	0.6				
Total	98.9	98.0	100.0				102.1	103.1	100.1	98.6			101.6	100.5	100.2					
Mg#	37.3	35.6	35.0	0.9	36.0		67.8	66.6	65.3	66.3	0.9	66.5			An	81.5	75.8	84.5	3.6	80.6
						En	64.1	62.5	60.7	62.0	1.2	62.3								
						Wo	5.5	6.1	7.0	6.4	0.5	6.2								

ED-13	Px								Pl					
K	1	2	3	4	5	Sigma	Ave		1	2	3	Sigma	Ave	
1120														
Na_2O									1.5	1.6	1.8	0.1		
MgO	19.3	20.2	20.3	20.7	20.3	0.4			1.5	1.8	2.3	0.3		
Al_2O_3	1.5	1.8	2.3	1.1	1.2	0.4			29.8	27.6	29.0	0.9		
SiO_2	51.6	52.9	52.5	52.6	53.3	0.6			47.9	46.9	47.0	0.8		
K_2O														
CaO	5.4	4.5	5.1	3.5	4.5	0.7			16.0	14.6	16.1	0.6		
TiO_2	0.3				0.3	0.0								
Cr_2O_3	0.9	0.3	0.4	0.5	0.5	0.2								
MnO	0.6	0.7	0.7	0.7	0.6	0.1								
FeO	20.0	20.1	18.2	19.4	19.2	0.7			1.8	2.5	3.5	0.7		
Total	99.9	100.4	99.4	98.6	99.9	0.6			98.7	96.9	98.9			
Mg#	63.3	64.1	66.6	65.5	65.3	1.1	65.0				An	85.5	83.9	82.0	1.5	83.8
En	56.1	58.2	59.4	60.7	59.2	1.5	58.7									
Wo	11.3	9.3	10.7	7.4	9.4	1.4	9.6									

ED-14	Px						Pl	
K	1	2	3	4	Sigma	Ave	1	2
1100								
Na_2O							2.0	1.5
MgO	21.0	21.8	20.4	19.4	0.9		2.5	2.8
Al_2O_3	2.1	2.1	2.4	3.1	0.4		25.7	25.4
SiO_2	52.3	53.3	52.7	51.9	0.5		51.0	48.5
K_2O							0.3	0.2
CaO	4.6	4.3	4.8	6.0	0.7		14.1	13.6
TiO2								
Cr_2O_3	0.2	0.4	0.3	0.2	0.1			
MnO	0.7	0.7	0.7	0.7	0.0			
FeO	18.0	18.3	18.3	17.3	0.4		2.6	4.8
Total	98.8	100.8	99.4	98.6			98.3	96.8
Mg#	67.6	68.0	66.6	66.6	0.6	67.2	An	79.4	83.1
En	61.1	62.0	59.9	58.0	1.5	60.2			
Wo	9.5	8.8	10.1	13.0	1.6	10.3			

Kdpx 0.28

EU-1	Melt					
K	1	2	3	4	Sigma	Ave
1250						
Na_2O	0.1	0.1	0.2	0.0	0.1	
MgO	7.2	7.5	7.6	7.2	0.2	
Al_2O_3	12.6	12.2	12.3	12.2	0.2	
SiO_2	50.4	50.9	50.2	50.7	0.3	
K_2O	0.2	0.2	0.2	0.3	0.0	
CaO	10.2	10.3	10.4	10.4	0.1	
TiO_2	0.8	0.7	0.7	0.7	0.0	
Cr_2O_3						
MnO	0.7	0.5	0.4	0.7	0.1	
FeO	18.0	17.4	18.3	18.4	0.4	
Total	100.3	99.8	100.3	100.5		
Mg#	41.5	43.6	42.6	40.9	1.0	42.2

EU-2	Melt					
K	1	2	3	4	Sigma	Ave
1220						
Na_2O	0.5	0.2	0.5	0.3	0.1	
MgO	7.7	7.4	7.9	7.5	0.2	
Al_2O_3	12.4	12.2	12.5	12.2	0.1	
SiO_2	51.0	50.5	50.5	50.0	0.4	
K_2O	0.2	0.2	0.3	0.2	0.0	
CaO	10.4	10.4	10.3	10.0	0.2	
TiO_2	0.8	0.7	0.7	0.6	0.1	
Cr_2O_3						
MnO	0.6	0.6	0.6	0.6	0.0	
FeO	17.0	17.3	16.8	17.8	0.4	
Total	100.6	99.6	100.1	99.3		
Mg#	44.7	43.2	45.7	42.9	1.1	44.1

EU-3	Melt					
K	1	2	3	4	Sigma	Ave
1200						
Na_2O	0.2	0.0	0.0	0.0	0.1	
MgO	7.7	7.7	7.6	7.3	0.1	
Al_2O_3	12.4	12.3	12.4	12.4	0.1	
SiO_2	51.2	50.9	50.1	49.7	0.6	
K_2O	0.2	0.2	0.2	0.2	0.0	
CaO	10.6	10.3	10.5	10.4	0.1	
TiO_2	0.7	0.7	0.7	0.6	0.0	
Cr_2O_3						
MnO	0.6	0.6	0.6	0.6	0.0	
FeO	17.5	17.6	17.3	18.6	0.5	
Total	100.9	100.2	99.3	99.7		
Mg#	43.9	43.8	43.8	41.2	1.1	43.2

EU-4	Melt						
K	1	2	3	4	5	Sigma	Ave
1160							
Na_2O	0.3	0.4	0.3	0.3	0.2	0.1	
MgO	7.5	7.0	7.2	7.1	7.3	0.2	
Al_2O_3	13.1	13.1	12.7	12.3	12.4	0.3	
SiO_2	50.1	49.1	49.6	49.9	49.8	0.3	
K_2O	0.2	0.1	0.2	0.1	0.2	0.0	
CaO	10.3	10.5	10.2	10.3	10.5	0.1	
TiO_2	0.7	0.6	0.7	0.7	0.6	0.1	
Cr_2O_3							
MnO	0.6	0.7	0.5	0.6	0.5	0.0	
FeO	17.0	16.3	16.8	16.9	17.8	0.5	
Total	99.8	97.9	98.3	98.3	99.2		
Mg#	43.9	43.4	43.3	42.8	42.2	0.6	43.2

EU-6	Melt					
K	1	2	3	4	Sigma	Ave
1160						
Na_2O	0.1	0.4	0.0	0.1	0.2	
MgO	6.0	6.0	6.4	6.3	0.2	
Al_2O_3	11.9	12.2	12.2	12.2	0.1	
SiO_2	49.1	49.5	49.0	49.3	0.2	
K_2O	0.2	0.2	0.2	0.0	0.0	
CaO	10.9	10.7	10.9	10.8	0.1	
TiO_2	0.8	0.8	0.7	0.6	0.1	
Cr_2O_3						
MnO	0.6	0.5	0.6	0.0	0.0	
FeO	18.2	18.6	18.3	17.8	0.3	
Total	97.9	99.0	98.3	97.1		
Mg#	37.1	36.6	38.3	38.6	0.8	37.7

Ol					
1	2	3	Sigma	Ave	
30.4	29.3	29.6	0.5		
38.1	36.8	35.8	0.9		
0.5	0.4	0.8	0.2		
1.0	1.0	0.9	0.0		
33.3	31.9	31.6	0.7		
103.3	99.4	98.7			
61.9	62.0	62.5	0.3	62.1	

Px							
1	2	3	4	Sigma	Ave		
21.7	22.5	22.3	24.0	0.9			
1.1	1.0	1.2	1.7	0.3			
53.2	52.8	53.0	54.5	0.7			
3.2	2.9	3.5	4.8	0.7			
0.3	0.3	0.3	0.3	0.0			
0.8	0.8	0.9	0.9	0.0			
18.0	18.0	17.6	14.8	1.3			
98.3	98.2	98.8	101.1				
68.3	69.0	69.4	74.4	2.4	70.3		
En 63.8	64.9	64.3	67.2	1.3	65.0		
Wo 6.6	5.9	7.3	9.7	1.4	7.4		

Pl							
1	2	3	Sigma	Ave			
1.2	1.6	0.7	0.3				
1.3	1.8	1.4	0.2				
32.1	30.7	31.7	0.6				
45.2	46.3	45.1	0.5				
0.4	0.1	0.2	0.1				
16.5	16.2	17.3	0.4				
2.2	3.1	2.2	0.4				
98.9	99.7	98.7	0.4				
An 48.3	45.2	93.0	38.6	88.8	Kdol 0.37		
					Kdpx 0.26		

EU-6	Melt						Px						Pl							
K	1	2	3	4	Sigma	Ave	1	2	3	4	Sigma	Ave	1	2	3	Sigma	Ave			
1140																				
Na_2O	0.4	0.0	0.1	0.4	0.2								1.6	1.5	1.2	0.2				
MgO	5.4	5.7	5.2	5.6	0.2		20.1	21.7	21.4	20.8	0.6		1.4	1.0	1.3	0.2				
Al_2O_3	11.7	11.7	11.6	11.7	0.0		1.6	0.8	0.6	1.5	0.4		33.0	31.8	31.5	0.7				
SiO_2	50.5	50.0	50.5	50.4	0.2		52.8	54.4	53.4	52.9	0.6		46.1	46.4	45.9	0.2				
K_2O				0.2									0.4	0.2	0.3	0.1				
CaO	10.8	10.7	10.6	10.7	0.1		5.5	3.8	3.8	4.9	0.7		16.3	16.2	17.6	0.8				
TiO_2	0.7	0.9	0.9	1.0	0.1															
Cr_2O_3							0.5	0.3	0.3	0.3	0.1									
MnO	0.5	0.7	0.6	0.6	0.1		0.7	0.7	0.8	0.9	0.1									
FeO	20.0	19.4	19.7	18.8	0.4		18.3	18.9	18.5	18.6	0.2		1.7	1.9	2.3	0.3				
Total	100.0	99.1	99.2	99.4			99.5	100.5	98.6	99.8			100.6	100.9	100.1	0.3				
Mg#	32.6	34.2	32.1	34.6	1.0	33.4	65.1	67.2	67.4	66.5	0.5	66.8	An	84.6	86.8	88.8	1.7	86.7	Kdpx	0.25
							En	58.6	61.9	62.1	59.8	1.5	60.6							
							Wo	11.4	7.8	7.9	10.1	1.5	9.3							

EU-7	Melt						Px						Pl								
K	1	2	3	4	Sigma	Ave	1	2	3	4	Sigma	Ave	1	2	3	4	5	Sigma	Ave		
1120																					
Na_2O	0.3	0.0	0.1	0.2	0.1								1.3	0.8	1.5	1.0	1.4	0.3			
MgO	4.1	4.0	4.1	3.7	0.2		15.4	17.2	16.2	16.6			1.6	1.4	1.1	1.1		0.2			
Al_2O_3	10.6	10.6	11.0	10.8	0.2		1.4	0.9	1.0	1.0			30.3	31.6	31.8	32.3	32.2	0.7			
SiO_2	48.9	50.0	50.4	49.7	0.6		52.0	52.4	51.1	52.9			46.3	45.3	46.3	46.5	46.4	0.4			
K_2O	0.2	0.3	0.2	0.2	0.0								0.1	0.2	0.2	0.2		0.0			
CaO	10.3	10.6	10.5	10.7	0.2		6.0	5.8	6.1	6.1			16.6	17.2	17.1	17.0	17.6	0.3			
TiO_2	1.2	1.3	1.4	1.4	0.1																
Cr_2O_3							0.6	0.8	0.5	0.5											
MnO	0.6	0.7	0.7	0.6	0.0		0.7	0.9	0.9	1.0											
FeO	20.4	20.7	22.3	20.8	0.7		22.5	22.4	21.9	23.2			3.1	2.2	2.0	1.4	1.4	0.6			
Total	96.4	98.3	100.7	98.1			99.5	100.6	97.6	101.3			99.3	98.7	100.0	99.6	99.0	0.5			
Mg#	26.4	25.7	24.7	24.1	0.9	25.2	56.5	57.8	56.8	56.1	0.6	56.8	An	87.5	92.5	86.6	90.2	87.1	2.2	88.8	Kdpx	0.26
							En	49.1	50.6	49.3	48.9	0.7	49.5								
							Wo	13.0	12.3	13.3	12.9	0.3	12.9								

EU-8	Ol					Px		Pl					
K	1	2	3	Sigma	Ave	1	2	1	2	3	4	Sigma	Ave
1100													
Na_2O								1.5	2.5	2.3	2.1	0.4	
MgO	17.8	17.6	17.7	0.0		13.3	13.1		0.8	1.9	0.8	0.5	
Al_2O_3						2.5	1.1	31.5	28.0	25.1	29.6	2.0	
SiO_2	34.1	35.1	34.6	0.4		51.1	51.0	45.7	49.9	51.5	46.9	2.1	
K_2O													
CaO	0.9	0.7	0.9	0.1		14.4	9.4	17.3	15.0	14.4	15.4	1.1	
TiO_2						0.4	0.3						
Cr_2O_3							0.5						
MnO	1.3	1.2	1.2	0.1		0.8	0.8						
FeO	46.3	47.1	46.9	0.3		17.7	22.2	2.9	2.4	5.0	2.2	1.1	
Total	100.4	101.8	101.4	0.6		100.1	98.5	98.9	98.7	101.2	99.0	1.0	
Mg#	40.7	40.3	40.2	0.2	40.4	57.4	51.2	An	86.4	76.5	77.4	80.0	3.9	80.1
						En	39.7	40.5					
						Wo	30.7	20.9					

EU-9 K 1000	Ol		Px 1	2	3	Sigma	Ave		Pl 1	2
Na_2O									1.2	1.3
MgO	15.7		14.7	13.2	13.3	0.7			0.8	1.1
Al_2O_3			1.1	5.5	1.4	2.0			30.9	30.4
SiO_2	33.3		52.3	47.0	51.6	2.4			46.0	46.3
K_2O									0.3	0.3
CaO	0.4		7.2	15.0	10.0	3.2			16.6	16.4
TiO2									0.2	
Cr_2O_3										
MnO	1.2		1.0		1.0	0.0				
FeO	48.2		25.1	15.5	23.1	4.1			2.5	3.0
Total	98.8		101.4	96.1	100.5	2.3			96.7	96.9
Mg#	36.7		51.1	60.3	50.7	4.4	54.0	An	88.9	87.2
		En	43.3	40.4	39.6	1.5	41.2			
		Wo	15.3	32.9	21.5	7.3	23.3			

CH-7HM	Melt							Ol						
K	1	2	3	4	5	Sigma	Ave	1	2	3	4	Sigma	Ave	
1450														
Na_2O	0.1	0.0	0.1	0.1	0.0	0.0								
MgO	21.2	20.8	21.3	21.1	20.4	0.3		45.9	45.8	46.1	46.5	0.6		
Al_2O_3	4.7	4.6	4.3	4.4	4.6	0.1								
SiO_2	48.5	47.7	47.4	47.4	48.1	0.3		39.9	40.4	39.9	40.5	0.2		
CaO	5.0	5.0	5.0	5.0	5.1	0.1		0.1	0.1	0.1	0.1	0.0		
TiO_2	0.0	0.0	0.0	0.0	0.0	0.0								
Cr_2O_3	0.7	0.7	0.7	0.8	0.8	0.0		0.5	0.3	0.5	0.4	0.1		
MnO	0.6	0.4	0.6	0.3	0.3	0.1		0.3	0.4	0.2	0.3	0.1		
FeO	18.1	18.6	18.2	18.3	18.2	0.2		12.1	12.3	12.4	12.6	0.3		
Total	99.0	97.8	97.7	97.5	97.6			98.9	99.4	99.2	100.5			
Mg#	67.8	66.6	67.5	67.2	66.6	0.4	67.1	87.1	86.9	86.9	86.8	0.1	86.9	Kdol 0.31

CH-8HM	Melt							Ol						
K	1	2	3	4	5	Sigma	Ave	1	2	3	4	Sigma	Ave	
1430														
Na_2O	0.2	0.1	0.1	0.2	0.1	0.0								
MgO	20.0	19.5	20.4	20.5	19.4	0.3		45.6	46.0	45.9	46.1	0.1		
Al_2O_3	5.0	4.8	4.9	4.9	5.0	0.1								
SiO_2	48.9	48.3	48.7	48.9	48.4	0.2		40.2	40.2	40.7	40.3	0.2		
CaO	5.5	5.4	5.3	5.4	5.4	0.1		0.1	0.0	0.0	0.0	0.1		
TiO_2	0.0	0.0	0.0	0.0	0.0	0.0								
Cr_2O_3	0.7	0.8	0.8	0.8	0.8	0.0		0.3	0.4	0.3	0.4	0.1		
MnO	0.5	0.6	0.5	0.6	0.6	0.1		0.2	0.2	0.3	0.3	0.0		
FeO	17.9	17.6	17.5	18.0	17.6	0.2		12.4	12.7	12.7	12.7	0.1		
Total	98.6	97.3	98.2	99.3	97.4			98.9	99.5	99.9	99.8			
Mg#	66.6	66.1	67.5	66.9	66.2	0.5	66.7	86.7	86.6	86.6	86.6	0.1	86.6	Kdol 0.31

CH-9HM	Melt							Ol						
K	1	2	3	4	5	Sigma	Ave	1	2	3	4	Sigma	Ave	
1410														
Na_2O	0.2	0.2	0.1	0.2	0.2	0.0								
MgO	19.5	19.3	19.5	18.8	19.5	0.3		46.1	45.7	45.9	45.8	0.4		
Al_2O_3	5.1	5.4	5.3	5.5	5.3	0.1								
SiO_2	49.0	49.2	48.9	48.9	48.5	0.1		39.8	41.0	40.8	39.5	0.4		
CaO	5.5	5.6	5.4	5.7	5.4	0.1		0.1	0.1	0.2	0.2	0.0		
TiO_2	0.4	0.3	0.3	0.3	0.3	0.0								
Cr_2O_3	0.7	0.8	0.7	0.6	0.7	0.1		0.4	0.4	0.3	0.3	0.0		
MnO	0.4	0.6	0.4	0.5	0.3	0.1		0.3	0.3	0.3	0.3	0.0		
FeO	17.4	17.9	17.3	17.8	17.3	0.2		13.2	13.2	13.0	12.9	0.1		
Total	98.2	99.2	98.2	98.3	97.6			100.0	100.8	100.4	98.0			
Mg#	66.5	65.7	66.8	65.3	66.8	0.6	66.2	86.1	86.1	86.3	86.3	0.1	86.2	Kdol 0.31

CH-11HM Melt								Ol						
DL	1	2	3	4	5	Sigma	Ave	1	2	3	4	Sigma	Ave	
1380														
Na_2O	0.1	0.1	0.2	0.2	0.1	0.0								
MgO	18.0	17.7	17.9	17.4	16.7	0.6		45.5	45.1	45.1	44.7	0.2		
Al_2O_3	5.8	5.8	5.9	6.2	6.2	0.1								
SiO_2	50.1	49.4	50.7	50.7	52.0	0.4		40.1	40.4	39.7	39.5	0.1		
CaO	5.8	6.0	5.9	6.1	6.2	0.1		0.1	0.1	0.2	0.2	0.0		
TiO_2	0.2	0.3	0.2	0.3	0.3	0.0		0.1	0.1	0.1	0.1	0.0		
Cr_2O_3	0.5	0.6	0.5	0.6	0.5	0.0		0.3	0.4	0.4	0.3	0.0		
MnO	0.4	0.5	0.5	0.5	0.4	0.0		0.4	0.4	0.4	0.3	0.0		
FeO	16.7	16.4	16.2	16.7	17.1	0.2		14.1	14.1	13.7	13.5	0.1		
Total	97.7	96.7	97.9	98.6	99.6			100.5	100.5	99.6	98.4			
Mg#	65.7	65.9	66.2	65.0	63.5	1.0	65.3	85.2	85.1	85.5	85.5	0.2	85.3	Kdol 0.32

CH-12HM Melt								Ol						
DL	1	2	3	4	5	Sigma	Ave	1	2	3	4	Sigma	Ave	
1350														
Na_2O	0.1	0.2	0.2	0.2	0.2	0.0								
MgO	15.7	15.7	16.6	16.8	15.7	0.4		45.0	44.8	44.9	44.8	0.2		
Al_2O_3	6.6	6.1	6.6	6.5	6.6	0.2								
SiO_2	51.8	51.5	52.0	52.9	52.5	0.3		40.5	40.2	40.1	39.9	0.1		
CaO	6.4	6.5	6.6	6.6	6.7	0.1		0.2	0.2	0.1	0.2	0.0		
TiO_2	0.3	0.2	0.3	0.3	0.3	0.0		0.1	0.1	0.1	0.1	0.0		
Cr_2O_3	0.4	0.4	0.5	0.4	0.4	0.0		0.3	0.3	0.3	0.3	0.0		
MnO	0.5	0.5	0.5	0.4	0.5	0.0		0.4	0.4	0.4	0.4	0.0		
FeO	16.0	16.0	16.2	15.9	16.1	0.1		14.6	14.3	14.1	14.3	0.1		
Total	98.8	98.1	99.3	100.1	99.0			101.2	100.3	100.0	100.0			
Mg#	64.9	65.0	64.5	65.2	63.6	0.6	64.6	84.6	84.8	85.0	84.8	0.1	84.8	Edol 0.33

CH-13HM Melt								Ol						Px							
DL	1	2	3	4	5	Sigma	Ave	1	2	3	4	Sigma	Ave	1	2	3	4	5	Sigma	Ave	
1330																					
Na_2O	0.2	0.2	0.2	0.1	0.1	0.0															
MgO	15.2	15.0	13.7	14.9	14.2	0.6		43.9	43.8	43.5	43.4	0.1		31.6	31.0	31.4	31.5	31.4	0.1		
Al_2O_3	7.0	7.0	7.3	6.9	7.0	0.1								0.0	0.1	0.0	0.1	0.0	0.0		
SiO_2	51.3	51.8	52.5	51.5	51.3	0.2		39.7	40.3	39.9	40.1	0.2		57.2	56.9	57.1	56.9	56.8	0.1		
CaO	7.0	7.1	7.6	7.1	7.3	0.2		0.2	0.2	0.2	0.2	0.0		0.6	0.6	0.6	0.5	0.7	0.1		
TiO_2	0.5	0.5	0.4	0.5	0.4	0.0		0.1	0.1	0.1	0.1	0.0		0.1	0.1	0.1	0.1	0.1	0.0		
Cr_2O_3	0.4	0.4	0.4	0.3	0.4	0.0		0.3	0.3	0.3	0.3	0.0		0.5	0.5	0.5	0.6	0.5	0.0		
MnO	0.5	0.4	0.4	0.5	0.5	0.0		0.4	0.4	0.4	0.4	0.0		0.4	0.4	0.4	0.4	0.4	0.0		
FeO	15.6	16.1	16.1	15.9	16.1	0.2		15.6	15.4	15.4	15.4	0.1		9.9	9.6	9.7	9.6	9.6	0.1		
Total	97.6	98.4	98.5	97.7	97.3			100.1	100.4	99.8	99.8			100.3	99.4	99.8	99.9	99.6			
Mg#	63.5	62.4	60.2	62.4	61.1	1.1	61.9	83.4	83.6	83.4	83.4	0.1	83.4	85.0	84.9	85.2	85.1	85.4	0.2	85.1	Kdol 0.32
														En 84.1	83.9	84.2	84.2	84.2	0.1	84.1	Kdpx 0.29
														Wo 1.1	1.2	1.1	1.0	1.4	0.1	1.2	

CH-14HM	Melt							Ol							Px							
DL	1	2	3	4	5	Sigma	Ave	1	2	3	4	5	Sigma	Ave	1	2	3	4	5	Sigma	Ave	
1300																						
Na_2O	0.1	0.2	0.2	0.2	0.3	0.0																
MgO	13.3	13.1	13.3	13.5	13.3	0.1		42.6	42.9	42.9	42.6	42.7	0.2		30.5	30.6	30.7	30.5	31.0	0.1		
Al_2O_3	8.2	7.9	8.5	8.0	8.2	0.2									0.1	0.1	0.0	0.0	0.0	0.0		
SiO_2	50.9	51.2	51.6	51.9	51.4	0.2		38.8	39.7	39.4	38.5	39.6	0.2		56.6	56.7	56.5	56.9	57.7	0.1		
CaO	8.5	8.5	8.5	8.6	8.7	0.1		0.2	0.2	0.2	0.2	0.3	0.0		0.8	0.8	0.7	0.8	0.8	0.0		
TiO_2	0.5	0.4	0.5	0.4	0.4	0.0		0.1	0.1	0.1	0.1	0.1	0.0		0.1	0.1	0.1	0.1	0.1	0.0		
Cr_2O_3	0.3	0.3	0.3	0.3	0.3	0.0		0.3	0.5	0.3	0.3	0.3	0.1		0.5	0.5	0.5	0.5	0.6	0.0		
MnO	0.5	0.5	0.5	0.5	0.5	0.0		0.5	0.4	0.4	0.4	0.5	0.0		0.4	0.4	0.4	0.4	0.3	0.0		
FeO	15.5	15.4	15.6	15.9	15.7	0.1		16.8	16.7	16.6	16.2	16.7	0.1		10.5	10.3	10.3	10.5	10.8	0.1		
Total	97.6	97.4	98.9	99.1	98.9			99.2	100.4	99.8	98.3	100.0	0.0		99.4	99.4	99.2	98.6	101.2	0.0		
Mg#	60.5	60.3	60.3	60.2	60.1	0.1	60.3	81.9	82.1	82.1	82.4	82.0	0.2	82.1	83.8	84.1	84.2	83.8	83.7	0.2	83.9	Kdol 0.33
															En 82.4	82.9	83.0	82.6	82.4	0.3	82.6	Kdpx 0.29
															Wo 1.6	1.6	1.4	1.5	1.5	0.1	1.5	

CH-15HM	Melt							Ol						Px							
DL	1	2	3	4	5	Sigma	Ave	1	2	3	4	Sigma	Ave	1	2	3	4	5	Sigma	Ave	
1280																					
Na_2O	0.2	0.1	0.3	0.2	0.2	0.1															
MgO	12.0	12.4	11.1	12.3	11.8	0.4		43.1	42.7	42.7	42.2	0.1		30.4	30.6	29.1	30.6	30.6	0.4		
Al_2O_3	9.5	9.3	9.7	9.5	9.6	0.1								0.2	0.0	0.1	0.2	0.2	0.1		
SiO_2	52.1	52.2	52.1	52.0	52.4	0.2		40.6	39.9	39.7	39.0	0.2		55.8	56.0	56.0	57.2	56.9	0.4		
CaO	9.1	9.1	9.3	9.2	9.1	0.1		0.3	0.3	0.3	0.3	0.0		1.1	0.9	1.1	0.9	1.3	0.1		
TiO_2	0.5	0.5	0.5	0.5	0.4	0.0		0.1	0.1	0.1	0.1	0.0		0.1	0.1	0.1	0.1	0.1	0.0		
Cr_2O_3	0.2	0.2	0.2	0.2	0.2	0.0		0.1	0.1	0.2	0.2	0.0		0.4	0.3	0.4	0.5	0.4	0.1		
MnO	0.5	0.4	0.3	0.4	0.4	0.1		0.4	0.5	0.4	0.4	0.0		0.4	0.4	0.3	0.3	0.5	0.0		
FeO	15.0	14.7	15.2	14.7	14.9	0.2		17.0	16.9	16.7	16.8	0.1		11.1	10.5	10.9	10.8	11.1	0.2		
Total	99.1	99.0	98.7	99.0	99.1			101.6	100.4	100.1	98.9			99.4	98.7	98.0	100.5	100.9			
Mg#	58.8	60.0	56.5	59.9	58.5	1.3	58.7	81.9	81.8	82.0	81.7	0.1	81.9	83.1	83.9	82.7	83.5	83.1	0.4	83.2	Kdol 0.32
														En 81.3	82.4	80.6	82.1	81.0	0.6	81.5	Kdpx 0.29
														Wo 2.2	1.8	2.3	1.7	2.4	0.3	2.1	

CH-16HM	Melt							Ol							Px							
DL	1	2	3	4	5	Sigma	Ave	1	2	3	4	5	Sigma	Ave	1	2	3	4	5	Sigma	Ave	
1250																						
Na_2O	0.3	0.2	0.2	0.2	0.2	0.1																
MgO	10.0	10.1	10.3	10.0	10.2	0.1		42.0	42.1	41.1	41.8	41.8	0.2		29.9	29.6	30.0	28.7	28.7	0.1		
Al_2O_3	11.0	11.0	11.4	11.0	11.0	0.1									0.0	0.4	0.5	0.0	0.0	0.0		
SiO_2	50.1	50.7	51.3	50.8	51.2	0.1		39.5	38.8	37.9	39.3	39.5	0.4		56.8	55.8	56.4	56.1	55.6	0.1		
CaO	10.2	10.0	10.1	10.3	10.2	0.1		0.2	0.3	0.2	0.3	0.3	0.0		1.6	1.4	1.2	2.3	2.4	0.0		
TiO_2	0.3	0.4	0.4	0.4	0.4	0.0		0.1	0.1	0.1	0.1	0.1	0.0		0.1	0.1	0.1	0.1	0.1	0.0		
Cr_2O_3	0.2	0.1	0.2	0.2	0.2	0.0		0.2	0.2	0.9	0.1	0.1	0.3		0.4	0.5	0.5	0.3	0.3	0.0		
MnO	0.5	0.4	0.4	0.4	0.4	0.0		0.4	0.5	0.4	0.4	0.4	0.0		0.4	0.4	0.4	0.4	0.4	0.0		
FeO	14.2	14.2	14.2	14.3	14.5	0.1		18.4	18.3	18.4	18.2	18.4	0.1		11.2	11.5	11.5	11.5	11.3	0.1		
Total	96.7	97.1	98.5	97.5	98.4			100.9	100.2	99.0	100.1	100.4	0.0		100.4	99.7	100.3	99.4	98.9			
Mg#	55.5	56.0	56.3	55.4	55.6	0.3	55.8	80.3	80.4	79.9	80.4	80.1	0.2	80.2	82.7	82.0	82.3	81.6	82.0	0.4	82.1	Kdol 0.31
															En 80.1	79.8	80.5	78.0	78.1	1.1	79.3	Kdpx 0.27
															Wo 3.1	2.7	2.2	4.5	4.7	1.0	3.4	

CH-17EM Melt								Ol							Px							
DL	1	2	3	4	5	Sigma	Ave	1	2	3	4	5	Sigma	Ave	1	2	3	4	5	Sigma	Ave	
1200																						
Na_2O	0.3	0.2	0.2	0.3	0.2	0.0																
MgO	8.3	8.4	8.2	8.2	8.2	0.1		40.9	41.0	40.5	41.0	40.3	0.3		27.3	26.9	28.9	27.8	28.2	0.8		
Al_2O_3	13.8	13.7	13.9	13.9	13.6	0.1									0.1	0.3	0.3	0.1	0.4	0.1		
SiO_2	50.8	51.5	51.4	50.7	50.9	0.3		39.0	39.0	39.0	38.7	38.4	0.1		53.5	55.5	56.8	56.4	56.3	0.1		
CaO	11.6	11.8	11.8	11.4	11.3	0.1		0.3	0.4	0.3	0.3	0.3	0.0		2.7	4.5	2.7	2.8	2.6	0.7		
TiO_2	0.5	0.5	0.5	0.5	0.4	0.0		0.1	0.1	0.1	0.1	0.1	0.0		0.1	0.1	0.2	0.1	0.1	0.0		
Cr_2O_3	0.0	0.0	0.1	0.1	0.1	0.0		0.1	0.2	0.1	0.2	0.1	0.0		0.1	0.0	0.1	0.0	0.1	0.0		
MnO	0.4	0.4	0.4	0.4	0.4	0.0		0.5	0.5	0.5	0.4	0.4	0.0		0.5	0.5	0.5	0.5	0.4	0.0		
FeO	12.7	12.9	12.6	12.2	11.8	0.3		19.6	19.1	19.5	18.6	18.3	0.4		11.3	11.7	11.8	13.0	12.2	0.5		
Total	96.5	99.4	99.0	97.7	96.9			100.3	100.1	99.9	99.2	97.9			95.5	99.5	101.1	100.7	100.1			
Mg#	53.8	53.7	53.6	54.4	55.4	0.7	54.2	78.8	79.3	78.7	79.7	79.7	0.4	79.3	81.2	80.4	81.4	79.2	80.5	0.8	80.5	Kdol 0.31
															En 76.7	73.2	77.2	74.8	76.5	1.4	75.7	Kdpx 0.29
															Wo 5.5	8.9	5.2	5.4	5.0	1.5	6.0	

ED-2EM1 Melt										
DL	1	2	3	4	5	6	7	8	Sigma	Ave
1400										
Na_2O	0.1	0.2	0.1	0.2	0.2	0.1	0.1	0.2	0.1	
MgO	16.3	18.1	17.7	17.7	17.4	17.5	17.3	17.3	0.1	
Al_2O_3	5.6	6.0	5.6	5.6	5.5	5.9	5.8	5.8	0.2	
SiO_2	47.1	51.4	50.3	50.6	50.6	50.9	49.9	49.7	0.2	
CaO	5.0	5.4	5.3	5.3	5.4	5.4	5.4	5.3	0.0	
TiO_2	0.3	0.4	0.3	0.3	0.3	0.3	0.3	0.4	0.0	
Cr_2O_3	0.7	0.7	0.8	0.7	0.8	0.8	0.8	0.8	0.0	
MnO	0.6	0.6	0.7	0.6	0.6	0.7	0.7	0.6	0.0	
FeO	16.4	17.7	18.0	17.9	17.9	18.1	18.1	17.7	0.2	
Total	92.0	100.6	98.8	99.2	98.6	99.8	98.3	97.7		
Mg#	63.9	64.6	63.7	63.8	63.4	63.3	63.0	63.5	0.5	63.7

ED-2EM2 Melt									
DL	1	2	3	4	5	6	7	Sigma	Ave
1400									
Na_2O	0.2	0.1	0.2	0.1	0.2	0.2	0.2	0.1	
MgO	17.0	16.9	17.4	17.6	17.6	17.8	17.3	0.2	
Al_2O_3	5.6	5.4	5.5	5.7	5.7	5.4	5.5	0.1	
SiO_2	49.5	49.4	50.9	50.4	51.1	50.7	50.5	0.1	
CaO	5.3	5.2	5.4	5.3	5.4	5.4	5.3	0.0	
TiO_2	0.3	0.3	0.4	0.3	0.3	0.4	0.3	0.0	
Cr_2O_3	0.9	0.8	0.8	0.8	0.8	0.8	0.9	0.0	
MnO	0.6	0.7	0.6	0.6	0.5	0.6	0.6	0.1	
FeO	17.6	17.3	17.5	17.3	17.6	17.5	17.5	0.2	
Total	96.9	96.1	98.6	98.0	99.3	98.7	98.1		
Mg#	63.3	63.4	63.9	64.5	64.1	64.4	63.9	0.4	63.9

ED-2EM3 Melt								
DL	1	2	3	4	5	6	Sigma	Ave
1400								
Na_2O	0.2	0.1	0.1	0.2	0.1	0.2	0.0	
MgO	17.8	17.9	17.4	17.8	17.9	17.5	0.1	
Al_2O_3	5.4	5.8	5.7	5.7	5.8	5.4	0.1	
SiO_2	50.5	51.0	50.5	51.0	51.2	51.0	0.2	
CaO	5.3	5.3	5.2	5.1	5.3	5.1	0.1	
TiO_2	0.4	0.4	0.3	0.4	0.3	0.2	0.1	
Cr_2O_3	0.8	0.8	0.8	0.8	0.8	0.7	0.0	
MnO	0.6	0.7	0.6	0.6	0.6	0.6	0.0	
FeO	17.5	17.6	17.5	17.4	17.3	17.3	0.1	
Total	96.5	99.2	98.0	99.0	99.3	98.1		
Mg#	64.4	64.4	63.9	64.6	64.9	64.2	0.3	64.4

ED-3HM	Melt							OL														
K	1	2	3	4	5	Sigma	Ave	1	2	3	4	5	Sigma	Ave								
1370																						
Na_2O	0.2	0.1	0.2	0.3	0.2	0.0																
MgO	17.0	17.4	17.4	16.8	17.2	0.1		45.1	43.7	43.9	43.9	43.1	0.4									
Al_2O_3	5.4	5.7	5.6	5.7	5.6	0.1																
SiO_2	50.5	50.5	50.6	49.6	50.9	0.3		40.0	38.8	39.6	39.4	39.7	0.2									
CaO	5.4	5.3	5.3	5.4	5.3	0.1		0.1	0.1	0.1	0.2	0.1	0.0									
TiO_2	0.3	0.3	0.3	0.3	0.4	0.0																
Cr_2O_3	0.7	0.7	0.6	0.7	0.7	0.0		0.5	0.5	0.5	0.5	0.5	0.0									
MnO	0.7	0.5	0.7	0.7	0.7	0.1		0.3	0.4	0.3	0.4	0.3	0.0									
FeO	17.0	17.9	17.8	17.6	17.5	0.3		14.4	14.1	14.5	14.3	14.6	0.2									
Total	97.2	98.5	98.6	97.1	98.4			100.4	97.5	98.9	98.6	98.4										
Mg#	64.0	63.4	63.5	63.0	63.7	0.3	63.5	84.8	84.7	84.4	84.6	84.0	0.3	84.5	Kdol	0.32						

ED-3HM'	Melt							OL														
K	1	2	3	4	5	Sigma	Ave	1	2	3	4	5	Sigma	Ave								
1350																						
Na_2O	0.2	0.2	0.3	0.2	0.1	0.0																
MgO	15.6	15.3	15.4	15.4	15.5	0.1		42.9	43.7	43.8	43.0	43.2	0.1									
Al_2O_3	5.9	6.1	5.8	5.9	5.9	0.1																
SiO_2	51.0	51.0	51.0	50.6	50.6	0.3		39.5	40.3	40.6	39.9	40.0	0.1									
CaO	5.9	5.7	5.7	5.8	5.6	0.1		0.2	0.2	0.2	0.1	0.2	0.0									
TiO_2	0.3	0.3	0.4	0.3	0.3	0.0																
Cr_2O_3	0.7	0.6	0.6	0.5	0.6	0.1		0.3	0.4	0.4	0.4	0.4	0.0									
MnO	0.8	0.3	0.6	0.7	0.7	0.2		0.4	0.3	0.3	0.5	0.4	0.1									
FeO	17.9	18.0	17.4	17.7	17.8	0.2		16.2	16.0	16.4	15.9	15.9	0.2									
Total	98.5	97.5	97.2	97.3	97.0			99.5	100.9	101.6	99.9	100.0										
Mg#	60.8	60.3	61.1	60.8	60.8	60.7	0.3	82.5	82.9	82.6	82.8	82.9	0.2	82.7	Kdol	0.32						

ED-4HM	Melt							OL							Px									
DL	1	2	3	4	5	Sigma	Ave	1	2	3	4	5	Sigma	Ave	1	2	3	4	5	Sigma	Ave			
1330																								
Na_2O	0.2	0.2	0.3	0.2	0.3	0.0																		
MgO	14.4	14.4	15.0	14.8	14.5	0.2		44.2	40.9	43.5	42.9	43.3	0.2		30.7	30.6	30.8	31.0	30.6	0.3				
Al_2O_3	6.7	6.6	6.7	6.4	6.7	0.1									0.4	0.1	0.0	0.0	0.0	0.1				
SiO_2	51.0	51.3	51.6	51.0	52.1	0.1		40.6	37.4	40.3	39.2	39.8	0.3		56.7	57.0	56.3	56.7	57.4	0.3				
CaO	6.1	6.2	6.2	6.1	6.1	0.0		0.2	0.2	0.2	0.2	0.2	0.0		0.6	0.4	0.4	0.4	0.5	0.1				
TiO_2	0.4	0.4	0.4	0.4	0.4	0.0		0.1	0.1	0.1	0.1	0.1	0.0		0.1	0.1	0.1	0.1	0.1	0.0				
Cr_2O_3	0.5	0.5	0.5	0.5	0.5	0.0		0.4	0.5	0.4	1.1	0.3	0.3		0.9	0.8	0.6	0.7	0.6	0.1				
MnO	0.7	0.7	0.7	0.7	0.6	0.0		0.5	0.5	0.5	0.6	0.5	0.0		0.5	0.5	0.5	0.5	0.5	0.0				
FeO	17.7	17.4	17.4	17.6	18.2	0.2		17.0	16.5	16.8	17.1	16.9	0.3		11.1	10.9	10.5	10.6	11.2	0.2				
Total	97.6	97.7	98.8	97.8	99.3			103.0	96.0	101.8	101.2	101.2	0.0		100.9	100.7	99.1	100.0	100.9					
Mg#	59.3	59.7	60.4	59.9	58.6	0.6	59.6	82.3	81.5	82.1	81.7	82.0	0.3	81.9	83.2	83.4	83.9	83.9	83.0	0.4	83.5	Kdol	0.33	
															En	82.3	82.7	83.2	83.2	82.3	0.4	82.7	Kdpx	0.29	
															Wo	1.1	0.8	0.8	0.8	0.9	0.1	0.9			

ED-5HM	Melt							OL							Px								
DL	1	2	3	4	5	Sigma	Ave	1	2	3	4	5	Sigma	Ave	1	2	3	4	5	Sigma	Ave		
1300																							
Na_2O	0.2	0.3	0.2	0.2	0.1	0.1																	
MgO	12.7	12.7	12.3	12.4	13.0	0.2		41.2	40.9	40.5	40.7	40.5	0.3		29.4	29.2	29.2	29.5	29.6	0.1			
Al_2O_3	7.4	7.5	7.5	7.6	7.7	0.1									0.2	0.1	0.2	0.1	0.1	0.0			
SiO_2	50.6	50.4	50.9	50.5	51.0	0.1		38.6	39.9	38.7	38.9	38.8	0.3		55.0	54.8	55.9	56.0	56.4	0.2			
CaO	7.0	6.8	7.1	7.1	7.1	0.1		0.2	0.1	0.2	0.2	0.2	0.0		0.6	0.6	0.6	0.6	0.6	0.0			
TiO_2	0.4	0.5	0.5	0.5	0.4	0.1		0.1	0.1	0.1	0.1	0.1	0.0		0.1	0.1	0.1	0.1	0.1	0.0			
Cr_2O_3	0.4	0.4	0.4	0.4	0.4	0.0		0.3	0.3	0.3	0.3	0.4	0.0		0.7	0.7	0.7	0.6	0.5	0.1			
MnO	0.7	0.7	0.6	0.7	0.7	0.0		0.6	0.7	0.6	0.6	0.6	0.0		0.5	0.5	0.5	0.5	0.6	0.0			
FeO	18.5	18.3	18.7	18.6	18.1	0.2		19.6	20.0	19.3	19.0	18.9	0.2		11.8	11.8	12.0	12.0	12.1	0.1			
Total	97.8	97.7	98.2	97.9	98.5			100.5	101.9	99.7	99.8	99.3			98.2	97.9	99.1	99.5	99.8				
Mg#	55.1	55.3	54.0	54.4	56.1	0.7	55.0	78.9	78.4	78.9	79.2	79.2	0.3	78.9	81.5	81.5	81.3	81.4	81.3	0.1	81.4	Kdol 0.33	
															En 80.6	80.5	80.4	80.5	80.4	0.1	80.5	Kdpx 0.28	
															Wo 1.1	1.3	1.1	1.1	1.1	0.1	1.1		

ED-6HM	Melt							OL							Px								
K	1	2	3	4	5	Sigma	Ave	1	2	3	4	5	Sigma	Ave	1	2	3	4	5	Sigma	Ave		
1280																							
Na_2O	0.3	0.2	0.3	0.3	0.2	0.0																	
MgO	11.2	11.3	11.4	10.9	10.9	0.2		39.3	39.1	38.5	38.7	38.2	0.2		29.2	28.7	29.3	29.7	28.8	0.4			
Al_2O_3	7.9	8.0	8.4	8.5	8.5	0.3									0.4	0.3	0.6	0.5	0.3	0.1			
SiO_2	50.2	50.4	50.1	49.8	50.2	0.1		39.0	39.0	38.0	38.6	38.4	0.1		55.0	55.8	56.0	55.8	56.7	0.3			
CaO	7.9	7.9	7.7	8.1	8.1	0.2		0.3	0.2	0.2	0.2	0.3	0.0		0.8	1.0	1.0	0.8	1.1	0.1			
TiO_2	0.5	0.5	0.4	0.5	0.5	0.0																	
Cr_2O_3	0.4	0.4	0.3	0.4	0.3	0.0		0.8	1.0	0.4	0.4	0.3	0.2		0.5	0.5	0.4	0.8	0.4	0.1			
MnO	0.7	0.8	0.7	0.8	0.8	0.0		0.7	0.7	0.5	0.5	0.8	0.1		0.8	0.5	0.5	0.5	0.5	0.1			
FeO	19.3	19.7	19.2	19.0	19.3	0.2		21.8	21.5	21.5	22.0	22.0	0.3		12.9	13.8	13.1	12.8	13.1	0.3			
Total	98.4	99.0	98.8	98.2	98.7			101.5	101.4	99.2	100.4	99.8			99.8	100.4	100.8	100.3	100.7				
Mg#	50.7	50.8	51.4	50.8	50.1	0.4	50.7	76.4	76.4	76.1	75.8	75.8	0.3	76.1	80.2	79.0	80.0	80.8	79.7	0.8	79.9	Kdol 0.32	
															En 78.9	77.5	78.5	79.8	78.0	0.7	78.5	Kdpx 0.26	
															Wo 1.8	1.9	1.9	1.5	2.1	0.2	1.8		

ED-7HM	Melt							OL							Px								
DL	1	2	3	4	5	Sigma	Ave	1	2	3	4	5	Sigma	Ave	1	2	3	4	5	Sigma	Ave		
1250																							
Na_2O	0.2	0.3	0.3	0.2	0.3	0.1																	
MgO	9.8	10.1	10.1	10.2	10.7	0.2		39.1	38.1	38.4	38.2	38.6	0.2		29.0	28.2	29.5	28.2	30.5	1.0			
Al_2O_3	8.8	9.1	9.1	9.2	9.0	0.2									0.5	0.1	1.0	0.3	1.2	0.4			
SiO_2	50.1	50.3	50.6	50.4	51.6	0.2		39.6	38.2	38.3	38.4	38.8	0.2		54.8	55.5	54.1	55.1	54.9	0.1			
CaO	8.3	8.2	8.3	8.2	8.6	0.1		0.2	0.2	0.3	0.2	0.2	0.0		1.0	0.9	0.8	0.8	0.9	0.1			
TiO_2	0.5	0.4	0.4	0.4	0.4	0.0		0.1	0.1	0.1	0.1	0.1	0.0		0.1	0.2	0.1	0.1	0.1	0.0			
Cr_2O_3	0.1	0.2	0.1	0.1	0.1	0.0		0.1	0.1	0.1	0.1	0.2	0.0		0.4	0.3	0.3	0.2	0.1	0.1			
MnO	0.5	0.5	0.5	0.4	0.5	0.0		0.5	0.5	0.4	0.5	0.5	0.0		0.4	0.4	0.4	0.4	0.4	0.0			
FeO	18.4	18.3	18.8	18.5	19.2	0.1		22.9	21.8	21.6	22.8	22.7	0.3		12.6	14.0	11.3	13.7	10.3	1.4			
Total	96.4	97.4	98.2	97.5	100.4			102.3	98.9	99.2	100.3	100.9			98.6	99.5	97.3	98.9	98.4				
Mg#	48.7	49.5	49.0	49.5	49.9	0.4	49.3	75.3	75.7	76.0	74.9	75.2	0.4	75.4	80.5	78.2	82.3	78.6	84.1	2.2	80.7	Kdol 0.32	
															En 79.0	76.9	81.1	77.3	82.7	2.2	79.4	Kdpx 0.23	
															Wo 1.9	1.7	1.5	1.7	1.7	0.1	1.7		

ED-8HM	Melt							OL							Px						
DL	1	2	3	4	5	Sigma	Ave	1	2	3	4	5	Sigma	Ave	1	2	3	4	Sigma	Ave	
1220																					
Na_2O	0.2	0.3	0.2	0.5	0.2	0.1															
MgO	8.4	8.5	8.4	8.5	8.4	0.0		36.1	36.4	35.9	36.6	36.6	0.2		27.3	26.5	26.4	27.8	0.6		
Al_2O_3	10.5	10.6	10.2	10.2	9.9	0.2									0.2	0.5	0.3	0.0	0.2		
SiO_2	49.5	50.2	49.7	49.9	49.7	0.1		37.9	38.1	37.8	37.8	37.8	0.2		55.6	54.3	54.6	55.0	0.3		
CaO	9.6	9.6	9.5	9.7	9.6	0.1		0.3	0.3	0.2	0.3	0.3	0.0		1.5	1.5	1.6	1.5	0.1		
TiO_2	0.6	0.5	0.6	0.7	0.6	0.0		0.1	0.1	0.1	0.1	0.1	0.0		0.1	0.1	0.1	0.1	0.0		
Cr_2O_3	0.2	0.2	0.1	0.2	0.2	0.0		0.1	0.2	0.2	0.1	0.2	0.0		0.4	0.4	0.4	0.2	0.1		
MnO	0.4	0.4	0.4	0.4	0.4	0.0		0.4	0.5	0.5	0.4	0.5	0.0		0.5	0.3	0.4	0.4	0.0		
FeO	18.0	18.0	17.8	17.9	18.2	0.2		25.3	25.2	24.4	24.6	24.7	0.2		15.5	14.6	15.4	13.6	0.7		
Total	97.3	98.5	96.9	97.9	97.2			100.2	100.8	99.1	100.0	100.2			101.0	98.6	99.2	98.5			
Mg#	45.4	45.8	45.7	46.0	45.1	0.3	45.6	71.8	72.0	72.4	72.4	72.6	0.3	72.2	75.8	76.5	75.4	76.5	1.2	76.5	Kdol 0.32
															En 73.5	74.2	73.0	76.2	1.2	74.2	Kdpx 0.26
															Wo 2.8	3.0	3.2	2.9	0.2	3.0	

ED-9HM	Melt								OL								Px						
DL	1	2	3	4	5	6	Sigma	Ave	1	2	3	4	5	6	Sigma	Ave	1	2	3	4	Sigma	Ave	
1200																							
Na_2O	0.4	0.2	0.4	0.2	0.3	0.2	0.1																
MgO	7.2	7.4	7.3	7.5	7.5	8.1	0.3		34.4	34.9	35.4	34.2	34.5	35.3	0.3		27.3	26.5	27.3	29.1	1.0		
Al_2O_3	11.1	11.7	11.2	11.2	11.0	10.6	0.3										0.9	0.9	0.4	0.3	0.3		
SiO_2	49.5	50.9	49.6	50.2	50.5	49.1	0.2		36.7	37.7	38.5	38.6	36.5	37.7	0.2		56.5	53.8	55.0	55.4	0.6		
CaO	10.3	10.2	10.0	10.4	10.4	9.2	0.4		0.3	0.4	0.2	0.3	0.2	0.3	0.0		2.0	1.8	1.1	2.0	0.3		
TiO_2	0.7	0.6	0.7	0.6	0.6	0.5	0.1		0.1	0.1	0.1	0.1	0.1	0.1	0.0		0.1	0.1	0.1	0.1	0.0		
Cr_2O_3	0.1	0.1	0.1	0.1	0.1	0.1	0.0		0.1	0.1	0.2	0.1	0.1	0.2	0.0		0.2	0.3	0.1	0.1	0.1		
MnO	0.4	0.4	0.4	0.4	0.5	0.4	0.0		0.5	0.4	0.5	0.6	0.5	0.5	0.1		0.5	0.4	0.4	0.5	0.0		
FeO	18.3	18.3	18.3	19.2	19.0	19.4	0.4		27.8	27.6	28.0	25.8	26.6	26.6	0.4		13.9	15.6	14.2	12.2	1.3		
Total	97.9	98.9	97.9	99.8	100.1	97.8			100.0	101.2	102.9	99.0	98.5	100.6			101.4	99.4	98.9	99.6			
Mg#	41.2	41.9	41.7	41.0	41.2	42.7	0.6	41.6	68.6	69.3	69.3	69.4	69.8	70.3	0.5	69.5	77.8	75.1	77.4	80.9	2.1	77.8	Kdol 0.31
																	En 74.2	72.5	75.0	77.8	1.9	74.8	Kdpx 0.20
																	Wo 3.9	3.5	2.2	3.9	0.7	3.4	

ED-10HM	Melt							OL							Px						
DL	1	2	3	4	5	Sigma	Ave	1	2	3	4	5	Sigma	Ave	1	2	3	4	Sigma	Ave	
1180																					
Na_2O	0.2	0.4	0.2	0.5	0.5	0.1															
MgO	6.5	6.5	6.8	6.9	6.9	0.1		34.4	34.5	34.0	34.1	33.4	0.2		24.8	22.9	23.9	23.6	0.2		
Al_2O_3	12.3	12.2	12.3	12.3	12.2	0.2									0.5	0.9	0.6	0.9	0.2		
SiO_2	49.3	48.2	49.4	49.8	49.8	0.2		37.8	38.3	37.4	37.5	37.2	0.2		55.0	51.5	54.5	53.2	0.2		
CaO	10.5	10.2	10.7	10.6	10.8	0.1		0.4	0.4	0.4	0.3	0.3	0.0		2.5	2.6	3.2	2.7	0.3		
TiO_2	0.7	0.6	0.8	0.8	0.7	0.1		0.1	0.1	0.1	0.1	0.1	0.0		0.2	0.1	0.1	0.2	0.0		
Cr_2O_3	0.1	0.1	0.2	0.1	0.1	0.0		0.1	0.3	0.1	0.1	0.2	0.1		0.4	0.3	0.4	0.4	0.0		
MnO	0.4	0.4	0.4	0.4	0.4	0.0		0.6	0.5	0.5	0.5	0.6	0.0		0.5	0.5	0.6	0.5	0.1		
FeO	17.1	16.2	16.8	17.5	17.2	0.2		28.5	27.6	27.4	27.1	27.9	0.4		17.7	16.1	17.0	17.2	0.3		
Total	97.1	94.7	97.6	99.0	98.5			101.9	101.7	99.9	99.7	99.7			101.4	94.9	100.3	98.8			
Mg#	40.2	41.5	42.0	41.4	41.7	0.6	41.4	68.3	69.0	68.9	69.2	68.1	0.4	68.7	71.4	71.8	71.4	71.0	0.3	71.4	Kdol 0.32
															En 67.8	67.9	66.9	67.1	0.4	67.4	Kdpx 0.28
															Wo 4.9	5.4	6.4	5.5	0.5	5.6	